SSC-454

ULTIMATE STRENGTH AND OPTIMIZATION OF ALUMINUM EXTRUSIONS

SHIP STRUCTURE COMMITTEE
2008

Ship Structure Committee

RADM Brian M. Salerno
U. S. Coast Guard Assistant Commandant,
Assistant Commandant for Marine Safety, Security and Stewardship
Chairman, Ship Structure Committee

{Name}	Dr. Roger Basu
{Title}	Senior Vice President
Naval Sea Systems Command	American Bureau of Shipping
Mr. Joseph Byrne	Mr. William Nash
Director, Office of Ship Construction	Director General, Marine Safety,
Maritime Administration	Safety & Security
	Transport Canada
Mr. Kevin Baetsen	Dr. Neil Pegg
Director of Engineering	Group Leader - Structural Mechanics
Military Sealift Command	Defence Research & Development Canada - Atlantic

CONTRACTING OFFICER TECHNICAL REP.	**EXECUTIVE DIRECTOR**
Mr. Chao Lin / MARAD	Lieutenant Commander, Jason Smith
Mr. Glenn Ashe / ABS	U. S. Coast Guard
DRDC / USCG	

SHIP STRUCTURE SUB-COMMITTEE

AMERICAN BUREAU OF SHIPPING	DEFENCE RESEARCH & DEVELOPMENT CANADA ATLANTIC
Mr. Glenn Ashe	Dr. David Stredulinsky
Mr. Derek Novak	Mr. John Porter
Mr. Phil Rynn	
Mr. Balji Menon	

MARITIME ADMINISTRATION	MILITARY SEALIFT COMMAND
Mr. Chao Lin	Mr. Michael W. Touma
Mr. Carl Setterstrom	Mr. Paul Handler
Mr. Richard Sonnenschein	

ONR / NAVY/ NSWCCD	TRANSPORT CANADA
{Name}	Paul Denis Vallee
{Name}	
{Name}	
{Name}	

US COAST GUARD	SOCIETY OF NAVAL ARCHITECTS AND MARINE ENGINEERS
CDR Charles Rawson	Mr. Jaideep Sirkar
Mr. James Person	Mr. Al Rowen
Mr. Rubin Sheinberg	Mr. Norman Hammer

**Ship
Structure
Committee**

SSC – 454
SR – 1457

OCTOBER 3, 2008

ULTIMATE STRENGTH AND OPTIMIZATION OF ALUMINUM EXTRUSIONS

This report presents a design method to optimize aluminum extruded panels for use on high-speed vessels. Existing strength prediction methods for aluminum plates and panels are first reviewed, including structural response under a mix of in-plane and out-of-plane loading. These methods are then compared to available experimental test results, highlighting the need for improved prediction methods for out-of-plane responses and structural elements undergoing combined loading. Based on the review of existing methods, a strength approach is developed and coupled to a multi-objective genetic algorithm optimizer to form a design method.

Two example design problems are developed for a typical high-speed vessel, a vehicle deck location and a strength deck location. Three different types of extrusions – plate and stiffener, sandwich panels, and hat-shape stiffeners – are optimized for each location. The three different types of extrusions are compared through a series of Pareto frontiers, all three generally perform similarly. The optimizer design method proves practical, requiring only a few minutes to generate entire Pareto frontiers for a given design problem on a standard desktop PC. A list of recommendations for further research and potential extensions to the optimizer approach is presented and discussed. Complete details of the generated Pareto fronts are provided in an Appendix.

BRIAN M. SALERNO
Rear Admiral, U.S. Coast Guard
Chairman, Ship Structure Committee

Technical Report Documentation Page

1. Report No.	2. Government Accession No.	3. Recipient's Catalog No.
4. Title and Subtitle **Ultimate Strength and Optimization of Aluminum Extrusions**		5. Report Date
		6. Performing Organization Code
7. Author(s) **M. Collette, X. Wang, J. Li, J. Walters, T. Yen**		8. Performing Organization Report No. **SR-1457**
9. Performing Organization Name and Address **SAIC** **4321 Collington Road, Suite 250** **Bowie, MD 20716**		10. Work Unit No. (TRAIS)
		11. Contract or Grant No. **GS-23F-0107J/ HSCG23-07-F-MSE112**
12. Sponsoring Agency Name and Address **Ship Structure Committee** **U.S. Coast Guard (CG-5212/SSC)** **2100 Second Street SW** **Washington, D.C. 20593-0001**		13. Type of Report and Period Covered **Final Report**
		14. Sponsoring Agency Code **CG-5**

15. Supplementary Notes
Sponsored by the Ship Structure Committee. Jointly funded by its member agencies

16. Abstract
Recent large aluminum high-speed vessels have made use of custom extrusions to efficiently construct large flat structures including internal decks, wet decks, and side shell components. In this report, general methods for designing and optimizing such extrusions to minimize structural weight are investigated. Strength methods for aluminum plates and panels under in-plane and out-of-plane loads are reviewed, and are compared to the available experimental test data published in open literature. Good agreement was generally found for in-plane compressive strength of aluminum plates and panels. However, the current state-of-the-art methodology for assessing out-of-plane loading on plate components, and for plates and panels acting under combined loads, is not as advanced. Further research in these areas is recommended. A multi-objective optimizer using a genetic algorithm approach was developed; this optimizer was designed to quickly generate Pareto frontiers linking designs of minimum weight for a wide range of strength levels. An engineering approach to estimating the strength of arbitrary extrusions under combined in-plane and out-of-plane loading wad developed, and linked to the optimizer to create a complete design method. This method was used to develop Pareto frontiers for panels for a main vehicle deck and strength deck location on a nominal high-speed vessel for three different types of extruded panels – plate and stiffener combinations, sandwich panels, and hat-shaped stiffened panels. Finally, conclusions and recommendations for future research are presented. In general, all three types of panels performed well over a wide range of strengths, though the sandwich panel was slightly heavier than the other two for certain applications. This combination of an engineering strength estimation approach and the multi-objective genetic algorithm optimization approach proves to be practical for the design of such extrusions, with generation times for complete Pareto frontiers of a few minutes on a standard desktop PC.

17. Key Words **Aluminum, Extrusions, Buckling, Ultimate Strength, Optimization, Genetic Algorithms.**	18. Distribution Statement **Distribution unlimited, available from:** **National Technical Information Service** **Springfield, VA 22161** **(703) 487-4650**

19. Security Classif. (of this report) **Unclassified**	20. Security Classif. (of this page) **Unclassified**	21. No. of Pages	22. Price

CONVERSION FACTORS
(Approximate conversions to metric measures)

To convert from	to	Function	Value
LENGTH			
inches	meters	divide	39.3701
inches	millimeters	multiply by	25.4000
feet	meters	divide by	3.2808
VOLUME			
cubic feet	cubic meters	divide by	35.3149
cubic inches	cubic meters	divide by	61,024
SECTION MODULUS			
inches^2 feet^2	centimeters^2 meters^2	multiply by	1.9665
inches^2 feet^2	centimeters^3	multiply by	196.6448
inches^4	centimeters^3	multiply by	16.3871
MOMENT OF INERTIA			
inches^2 feet^2	centimeters^2 meters	divide by	1.6684
inches^2 feet^2	centimeters^4	multiply by	5993.73
inches^4	centimeters^4	multiply by	41.623
FORCE OR MASS			
long tons	tonne	multiply by	1.0160
long tons	kilograms	multiply by	1016.047
pounds	tonnes	divide by	2204.62
pounds	kilograms	divide by	2.2046
pounds	Newtons	multiply by	4.4482
PRESSURE OR STRESS			
pounds/inch^2	Newtons/meter^2 (Pascals)	multiply by	6894.757
kilo pounds/inch^2	mega Newtons/meter^2 (mega Pascals)	multiply by	6.8947
BENDING OR TORQUE			
foot tons	meter tons	divide by	3.2291
foot pounds	kilogram meters	divide by	7.23285
foot pounds	Newton meters	multiply by	1.35582
ENERGY			
foot pounds	Joules	multiply by	1.355826
STRESS INTENSITY			
kilo pound/inch^2 inch$^{\frac{1}{2}}$(ksi√in)	mega Newton MNm$^{3/2}$	multiply by	1.0998
J-INTEGRAL			
kilo pound/inch	Joules/mm^2	multiply by	0.1753
kilo pound/inch	kilo Joules/m^2	multiply by	175.3

Table of Contents

List of Illustrations

List of Tables

1 Introduction

1.1 Background to Aluminum Structural Extrusions

The current commercial and military interest in large high-speed vessels has resulted in the development of monohull, catamaran, and trimaran designs between 70m and 130m in length for both transportation and combat roles. In this design space, deadweight is restricted, and the vessel operates under a constant trade-off between cargo capacity, achievable speed, and achievable range quite unlike conventional displacement vessels. Given these restrictions, minimization of lightship weight, and hence structural weight, is of great significance in the design of the vessels. Most vessels in this category have been constructed out of aluminum to reduce structural weight. In addition to being a lighter material than steel, aluminum is marked by its ability to be extruded into custom profiles very economically. This ability gives the designer the freedom to replace conventional plate and welded-stiffener panels with extrusions where the plate thickness may be varied, or where the plate and stiffener construction may be replaced by a sandwich-type structures. Such extrusions can be used economically on large flat deck structures such as cargo and passenger decks, cross-decks for multi-hull vessels, and the side shell above the waterline. Such extrusions offer the possibility of weight savings, along with easier welding and reduced complexity of the resulting structure. A conventional panel and various types of extruded panels are shown in Figure 1. The conventional panel, constructed by welding stiffeners to a large, flat plate, is shown in the upper left-hand corner. On the upper right, an extruded panel is shown where the stiffener and attached plate is extruded as a single unit. Multiple such extrusions are then joined by butt-welds to form a panel. Other types of panels that have found favor include a hat-type stiffener, shown on the lower left of Figure 1, and a sandwich-type extrusion shown on the lower right.
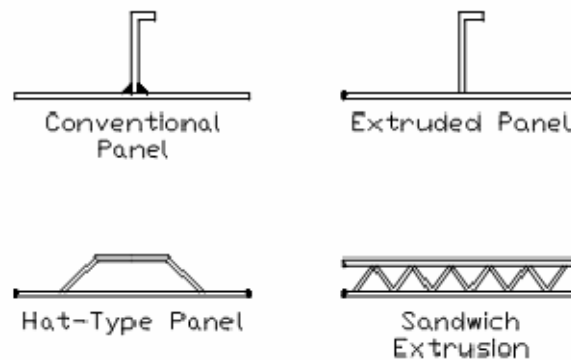
Figure 1: Aluminum Extrusions

To optimize the design of high-speed vessel structures, ultimate limit state design is the preferred approach. Using limit-state design to calculate the loads at which the structure will actually fail in service, a more rational risk assessment and comparisons of alternatives can be made in the optimization process. At the present time, ultimate strength methods are only available for conventional plate and welded stiffener panels; the more complex, yet potentially more efficient,

designs possible by extruded aluminum cannot easily be considered. This lack of tools and assessment techniques means that designers are restricted in the types of structures they can consider. Robust methods for performing such optimization are required if optimization is going to become a practical tool for use in design offices. The primary goal of this project is to demonstrate a procedure using existing ultimate strength techniques for plate and panel components that can address the strength prediction for novel extrusions. An optimization approach will then be developed to investigate if such optimization is practical. An additional goal is to determine whether any specific extruded profiles are preferable on a weight basis for certain structural applications. Such work requires careful consideration of the all potential failure modes of the extrusions. Some failure modes – such as local web buckling – may have been designed out of standard rolled shapes for steel vessels; thus, traditional steel-based strength approaches may not address them. Additionally, restrictions on the size and distribution of material throughout the extrusion need to be investigated to ensure that the resulting extrusion can be economically produced.

1.2   Introduction to Aluminum as a Material

As a structural material, aluminum alloys have noticeable differences from steel [1, 2]. A wide variety of aluminum alloy series are available for structural use; however, in the marine community, alloys of the 5xxx-series and 6xxx-series are primarily used. These alloys have good corrosion resistance, are weldable, and are economical to purchase. The 5xxx-series alloys are typically used in rolled plates and rarely encountered in complex extrusions, though Alcan does produce 5383 extruded stiffeners (without any attached plate) for marine use. These alloys are strain-hardened. The 6xxx-series alloys can be extruded much more easily and can form complex shapes with enclosed voids, such as the hat-shaped stiffener and sandwich panel shown in Figure 1. The 6xxx-series alloys are precipitation-hardened alloys that gain their strength via heat treatment. The material differences between the marine aluminum alloys in the 5xxx and 6xxx alloy series and steel alloys in terms of ultimate limit strength analysis (ignoring corrosion and fatigue mechanisms) can be briefly summarized as:

- The elastic moduli of the aluminum alloys are roughly 1/3 the elastic modulus of steel. Thus, an aluminum structure of similar geometry to a steel structure will be more susceptible to elastic buckling, and any strength methods or rules of thumb that do not explicitly consider the elastic modulus of the material developed for steel (such as limiting b/t ratios for plating) will not be conservative for aluminum.

- The shape of the aluminum stress-strain curve is generally more rounded than that of steel. Typically, no defined yield point can be identified in the material stress-strain curve and a 0.2% offset proof stress used in place of the yield stress. The 0.2% offset proof stress is defined as the stress where the plastic component of the strain is 0.2%. The 5xxx-series alloys have a particularly rounded stress-strain curve, and their local tangent modulus may fall significantly below the elastic modulus before the proof stress is reached. This indicates that these alloys may be more prone to buckling in the inelastic regime than equivalent steel or 6xxx-series alloy structures. As the 5xxx-series alloys are strain hardened, the proof stress is often higher in tension than compression, a fact often overlooked in marine structural analysis. The 6xxx-series generally has a stress-strain curve closer to the elastic perfectly-plastic assumption often used for steel structures, however, after the extrusion process the material may show a pronounced anisotropy, with

generally lower strength and ductility in samples taken at a right angle to the direction of extrusion.

- Both 5xxx and 6xxx series alloys become weaker in a local region near the weld when welded by fusion welding. This local weak region is known as the heat-affected zone (HAZ). For 5xxx-series alloys, the HAZ material is typically similar to anneal material. For the 6xxx-series, the HAZ is typically an over-aged region in terms of the precipitation hardening. This means that while the proof stress is reduced for both the 5xxx and 6xxx HAZ regions, the 6xxx series suffers a larger loss of material ultimate tension strength than the 5xxx-series alloys.

The differences in material stress-strain curves between the conventional elastic-plastic assumption for steel, and typical stress-strain curves for the 5xxx and 6xxx series alloys are shown in Figure 2. In this figure, the proof stress of the aluminum alloys and the yield stress of the steel alloys have all been set to 215 MPa, so only the difference in the curve shape will appear in the stress-strain curve. The reduced elastic modulus of both aluminum alloys, and the pre-proof stress softening of the 5xxx-series alloys are clearly visible.
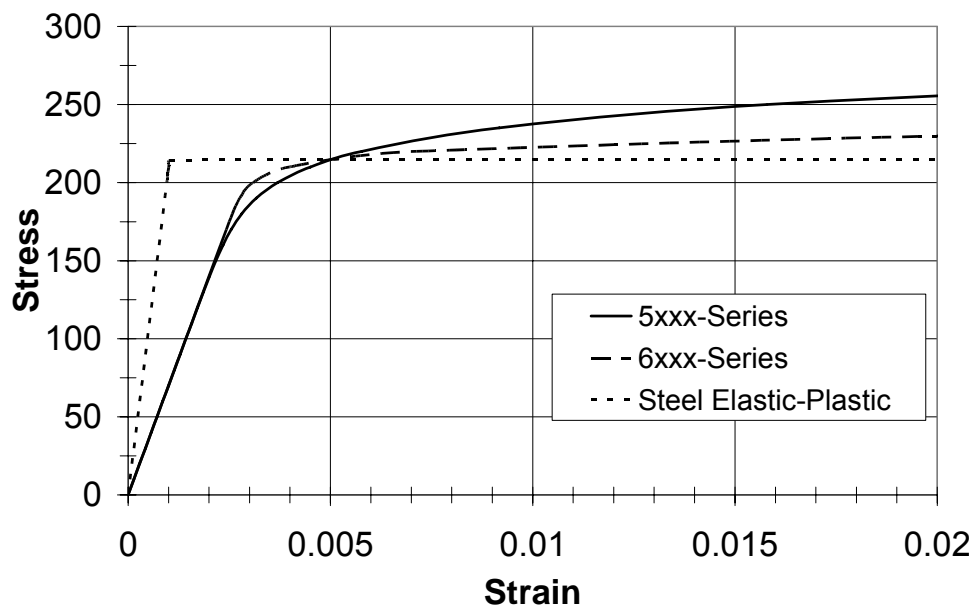
Figure 2: Hypothetical Stress-Strain Curves for Aluminum Alloys and Elastic Perfectly Plastic Steel

1.3   Approaches to Structural Design Optimization

The process of optimizing a structure is highly complex, with many trade-offs between weight, structural capacity, and cost. This is especially true if through-life costs are included in addition to build costs. Hughes [17] explored the structural optimization problem in some detail and provides background to the challenges of the optimization problem. In the current study, a more limited multi-objective optimization addressing structural weight and strength is explored. Even

within this reduced scope, however, the optimization problem is still difficult to solve mathematically. The relationship between weight and strength is complex, and there may be many local minima of structural weight that will be encountered before a truly global minima of weight for a given strength level is found. This type of problem is typically difficult to address with optimization techniques that use derivatives of the objective function to search for minima. When investigating the trade-offs between weight and structural strength, the problem is further complicated because the result will no longer be a single minima but, rather, a Pareto set consisting of designs where the strength can no longer be improved without a corresponding increase in weight. When plotted on an axis of structural strength vs. weight, this Pareto set will form a Pareto frontier, or a curve connecting designs that represent the maximum strength obtainable for a given weight. Researchers have tried many different approaches to determine the Pareto frontier for a given problem efficiently, with genetic algorithm approaches becoming more popular recently. These approaches typically trade some optimization speed – measured in the number of evaluations of the objective functions – for greater robustness and the ability to escape from local minima and eventually converge to a global minima. A similar approach has recently been demonstrated for steel laser-weld sandwich panels [3]. Such an approach is outlined in Section 3 and then applied to sample panel optimizations in Section 4 of this report.

1.4   Outline of the Present Study

The remainder of this report is divided into four sections. In Section 2, the existing methods for the strength of aluminum plate elements and stiffened panels are explored, and compared to available experimental test data. Load combinations and variable-thickness plates are also explored. Section 3 presents the background to multi-objective optimization with constraints, and explores genetic algorithm approaches to such optimization problems. An optimizer is developed, and tied to a structural strength and weight objective function developed from the methods explored in Section 2. This optimizer is then applied to four sample panel optimization problems in Section 4. Conclusions and recommendations for future work are presented in Section 5.

2 Strength of Aluminum Plates and Panels

2.1 Un-stiffened Plates

2.1.1 Introduction

Un-stiffened plates are the basic building blocks of most ship structures and, as such, accurate strength analysis of individual plate components is one of the key building blocks of general strength analysis techniques. This section explores simplified and numerical methods for predicting the strength of un-stiffened plates. Different types of loading are investigated, including uniaxial compression, lateral (out-of-plane) loading, and combined loading. Tension loading is typically compared to base material properties for ship structures, as structural tension response is largely assumed to follow the base material properties. This assumption is difficult to directly apply to welded aluminum structures where welds create variation in the material properties [1]. For each loading type, several methods are presented and compared to each other, and to experimental data where available. Of all the load types, uniaxial compression and the associated buckling and ultimate strengths has received the most research attention to date, as this loading mode directly influences overall panel compressive strength. Complete failure of individual plate components by lateral loading is rare. Usually the overall panel or grillage that the plate is a component of will fail before the individual components; hence allowable lateral loading is typically set by an allowable stress or allowable permanent set criteria in place of a direct collapse analysis. Both allowable stress and allowable permanent set criteria will be examined in this section. Combined load effects are typically investigated by interaction formulas, or by direct numerical simulations, and several proposals and suggestions will be examined for combined loads.

2.1.2 Uniaxial Compression

Uniaxial compression, as shown in Figure 3, consists of compressive loading in the plane of the plate. At sufficiently high load levels, such loading leads to compressive buckling and, finally, collapse of the plate element. In most ship structures, the plate elements are arranged so that the dominant compressive load is applied across the shorter side (*b* side in Figure 3), which typically results in a higher buckling stress than loading on the *a* side. The aspect ratio of the plate is defined as *a*/*b*, and values of three to five are common in conventional ship structures, with even higher values possible in aluminum extrusions.
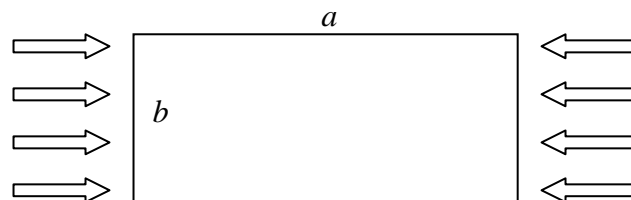
Figure 3: Uniaxial Plate Compression and Plate Dimensions

When investigating the strength of plates under uniaxial compressive loading, a useful non-dimensional measure of the plate's elastic stability is the plate slenderness ratio, or β, which is defined for aluminum in Equation 1, below. For purely elastic stability, plates with equal β will

perform similarly regardless of material, e.g. a steel plate and an aluminum plate with the same β ratio will have the same elastic stability properties. Thus, β, is a useful parameter for comparing designs, especially in cases such as aluminum extrusions where the individual plate elements may have very different dimensions than conventional steel plates.

$$\beta = \frac{b}{t}\sqrt{\frac{\sigma_{02}}{E}}$$
Equation 1

While the β ratio directly deals only with elastic buckling behavior, it is still a useful metric to classify the slenderness of plate elements. Typically, the compressive response of individual aluminum plate elements can be divided into three regions based on the β parameter of the plate:

- **Squash Region:** Plates with very low β values, typically < 1, tend not to buckle until after they have reached their proof stress in compression. Thus, these plates tend to fail initially by gross yielding of the material in the plate, which is termed a squash failure. Typically the proof stress of the material is taken as the ultimate strength in this region, though strain-hardening alloys may be able to sustain a slightly higher load.
- **Inelastic Buckling Region:** Plates of intermediate β values tend to fail by inelastic buckling, where the initial buckling of the plate occurs under a high enough stress that the additional bending stress in the buckled regions quickly leads to large-scale yielding and final collapse of the plate. In this region, the initial buckling strength and collapse strength are almost equal.
- **Elastic Buckling Region:** Slender plates with high β values initially tend to buckle elastically. Because the stress at buckling is typically well below the proof stress of the material, the plate is able to accept further loading in the buckled condition before large-scale yielding occurs. Such additional loading is termed post-buckling strength, and allows the collapse strength to be noticeably higher than the initial buckling strength.

Similar to column buckling in steel, initial out-of-plane (IOOP) imperfections and residual stresses from welding strongly impact the buckling strength of plates, especially at lower slenderness ratios. An additional complication for aluminum plates is that welding at the plate boundary results in localized HAZ with lower material strengths than the rest of the plate. The plate boundaries are typically the most effective regions for carrying in-plane loads, and welding in these regions can noticeably reduce the plate's effectiveness.

In the remainder of Section 2.1.2, experimental uniaxial compressive collapse data is reviewed, and then several simplified strength methods and numeric methods are applied to the experimental data sets, and their performance is compared.

2.1.2.1 Experimental Data

There are two primary public-domain sources of uniaxial strength data for aluminum plates in compression: a series of 58 plates in aerospace alloys 2024, 2014, and 7075 in the T3 and T6 tempers reported by Anderson and Anderson [4], and a series of 76 plates in the civil and marine

alloys 5083 and 6082 tested in the United Kingdom by Mofflin [5] in the O, F, and TF (roughly corresponding to the modern T6) tempers. The plates tested by Anderson and Anderson were made of thin sheet material, normally 1.59mm thick, and were long enough for 5 buckling waves or more to form over the length of the plates. The test program covered b/t ratios between 14.6 and 58.2, and non-dimensional slenderness, β, values between 1.1 and 4.84. Both the initial bucking strength and the collapse strength were measured. The initial out-of-plane imperfections of these panels were not measured, nor were any of the plates welded. The alloys used represent aerospace alloys that are typically heat-treated to achieve the high, un-welded strength that is beneficial for riveted aerospace structures. Several of the alloys in this data set had proof stress in excess of 400 MPa, much higher than typical marine alloys. Compressive material properties were measured. Thus, the test results of Anderson and Anderson are useful for investigating how strength methods apply to aluminum plates in general, but do not represent typical aluminum vessel structures.

The test results by Mofflin are generally similar to plates commonly encountered in aluminum vessels. These plates were all approximately 6mm thick, and were tested with an aspect ratio of 4, with compressive displacements applied along the short edges (*b* side in Figure 3) of the plate. Two levels of initial out-of-plane deformations were introduced into the plates, with maximum values of roughly 0.001 times the plate width for small deformations, and 0.005 times the plate width for large deformations, although in some cases the achieved deformations differed significantly from the target deformation. Mofflin simulated the effects of welding on the plates by making TIG passes along the long, unloaded edges of certain plates without depositing weld metal. Two levels of welding were used in the study, defined as "light" and "heavy", with heat inputs roughly corresponding to MIG fillet welds of 3mm and 4mm leg lengths, respectively. Of the total of 76 plates tested by Mofflin, 66 were either un-welded or had welds simulated in this fashion. A further 10 plates had MIG welds made in the middle of the plate, perpendicular to the applied loading; however, these plates were not investigated in the current study. The test program covered b/t ratios between 20 and 85, and non-dimensional slenderness ratio, β, values between 0.93 and 5.41. Compressive material properties were measured and used for the definition of β. Thus, the Mofflin test program covers the materials, tempers, and the range of dimensions for plates likely to be encountered in marine structures.

The plate strengths observed in the two experimental programs are plotted below against the non-dimensional slenderness ratio, β, for non-welded plates in Figure 4, and for welded plates in Figure 5, non-dimensionalized by the proof stress of the base material. In each figure, the classical elastic buckling stress is also included on the plot in a heavy dark line. This stress is given by:

$$\sigma_{Elastic} = k \frac{\pi^2 E}{12(1-v^2)} \left(\frac{t}{b} \right)^2 \qquad \textbf{Equation 2}$$

The coefficient k is taken as 4.0 for long, simply-supported plates. The elastic buckling stress is limited to the proof stress of the material in the plots. Figure 4 below shows that the aluminum plates display similar buckling characteristics to steel plates. On the left side of the curve, the buckling strength for stocky plates approaches the proof stress of the material, indicating that plate failure originates by gross yielding. As the slenderness increases, the plate strength drops

below both the proof strength and the predicted elastic strength. This region corresponds to inelastic initial buckling. As slenderness further increases, the experimentally-observed strengths cross the elastic buckling line and then rise above it, indicating that the plates develop post-buckling strength in this region after initially elastically buckling in compression. In the inelastic region, there appears to be a distinction between the different alloy types, with the heat-treated alloys from the 2xxx, 6xxx, and 7xxx series falling above the strain-hardened 5xxx alloys. Figure 5 shows that welding makes a general strength reduction but does not change the overall shape of the strength curve. Welding seems to have the largest impact in the inelastic region. It is important to note that none of the current experimental results had welds along the short, loaded edges of the plate (*a* side in Figure 3). Such welds could further reduce the strength of the plate, especially in the inelastic buckling region, where the average axial stress in the plate may exceed the proof strength.
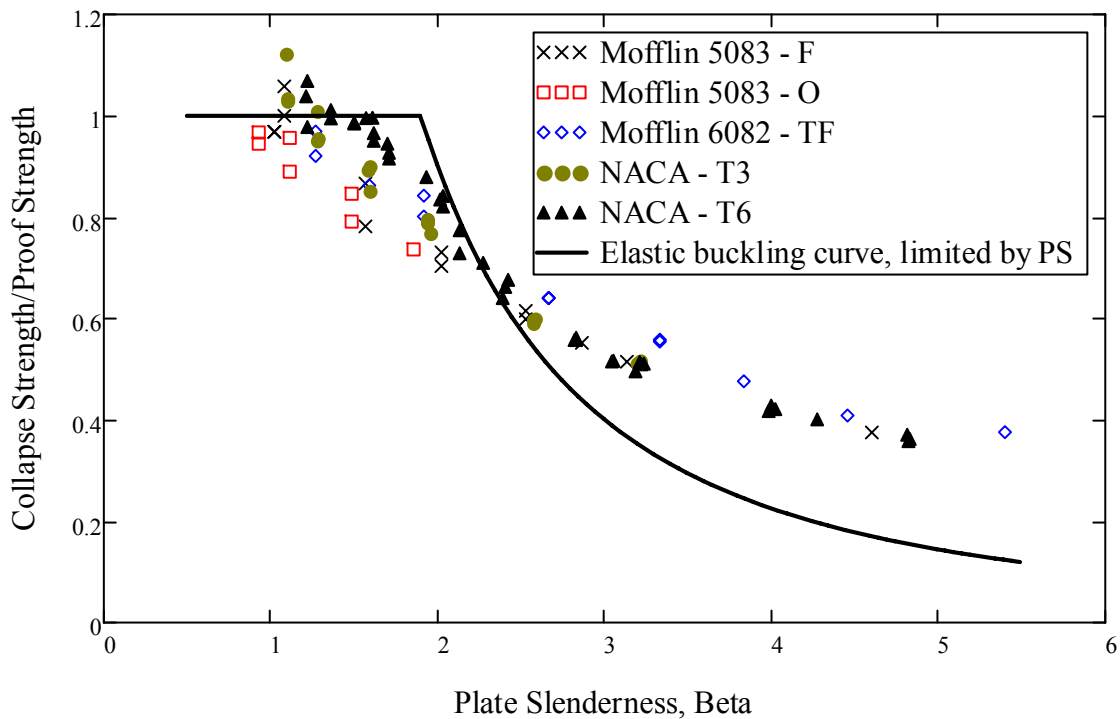
Figure 4: Comparison of Experimental Uniaxial Compression Strength: Non-Weld Plate by Alloy

This experimental data base of plate tests will now be used to validate a series of plate-strength equations.
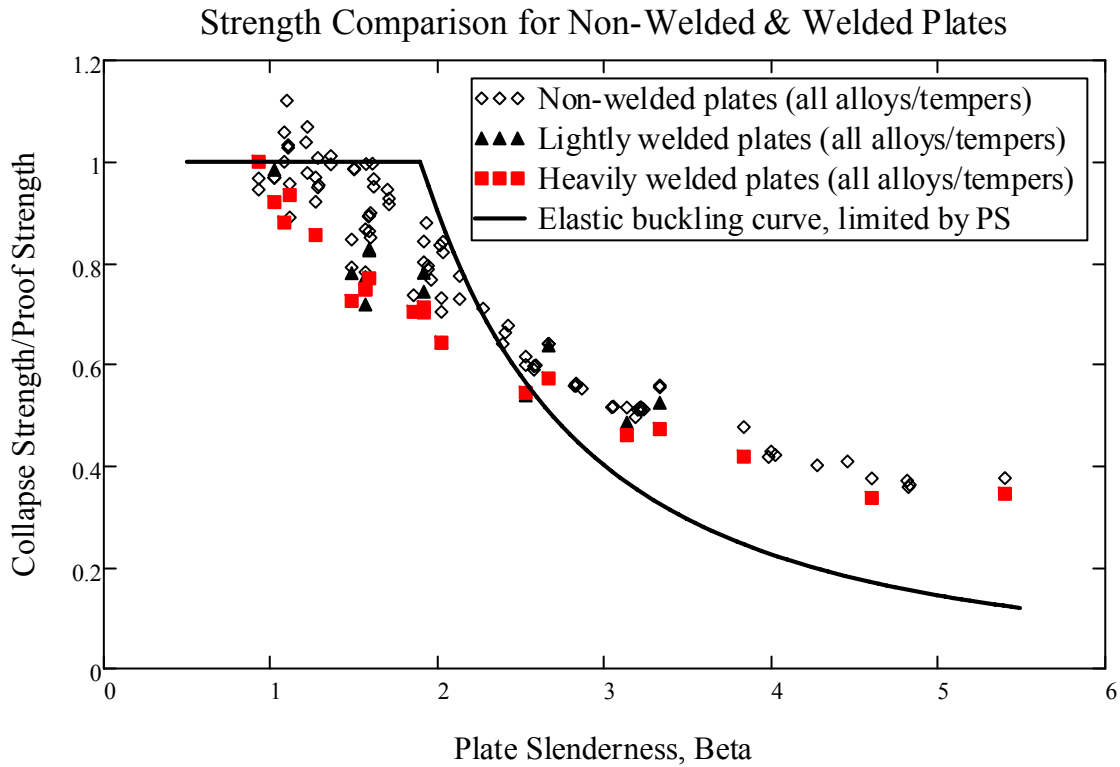
Figure 5: Comparison of Experimental Uniaxial Compression Strength: Welded Plates

2.1.2.2 U.S. Navy DDS 100-4/Faulkner Method

The U.S. Navy Design Data Sheet DDS 100-4[6] proposes a simple method for estimating the buckling strength of steel plates, based on the non-dimensional slenderness parameter, β, alone. The formula was originally given in terms of the plate yield strength. Replacing this with the 0.2% offset proof strength for aluminum alloys yields:

$$\frac{\sigma_U}{\sigma_{02}} = \frac{2.25}{\beta} - \frac{1.25}{\beta^2}, \beta > 1.25$$

$$\frac{\sigma_U}{\sigma_{02}} = 1, \beta \leq 1.25$$

Equation 3

This is basically a two-zone buckling model, with squash-type failures assumed for stocky plates with β < 1.25, and a single quadratic relationship handling inelastic and elastic buckling. Faulkner [7] further reviewed steel plate test data, and proposes a slightly lower strength formula following the same pattern as the DDS-100-4:

$$\frac{\sigma_U}{\sigma_{02}} = \frac{2}{\beta} - \frac{1}{\beta^2}, \beta > 1$$

Equation 4

$$\frac{\sigma_U}{\sigma_{02}} = 1, \beta \leq 1$$

Both of these methods rely on steel test data for the coefficients of the equations, which has questionable applicability to aluminum. Neither of these methods is alloy-specific, so the differences between the heat-treated and strain-hardened alloys are not reflected in the formulae. Nor can either of the methods address the weaker HAZ around welds in aluminum. Where the properties of welds at the edge of the panel are known, and the tensile and compressive residual stresses in the plate can be estimated, Faulkner [7] proposed an extension to this method to be able to include the weakening effect of residual stresses. In the current study, this enhancement is not included, as the different material properties in the HAZ near the welds make estimating the parameters of the residual stress model difficult. For the Mofflin data set, both the DDS 100-4 and the Faulkner method were compared to non-welded and welded plates, as shown in Figure 6 and Figure 7, respectively. In these figures, the actual and predicted failure stresses are compared. Both are non-dimensionalized by the 0.2% offset proof stress of the plate material.
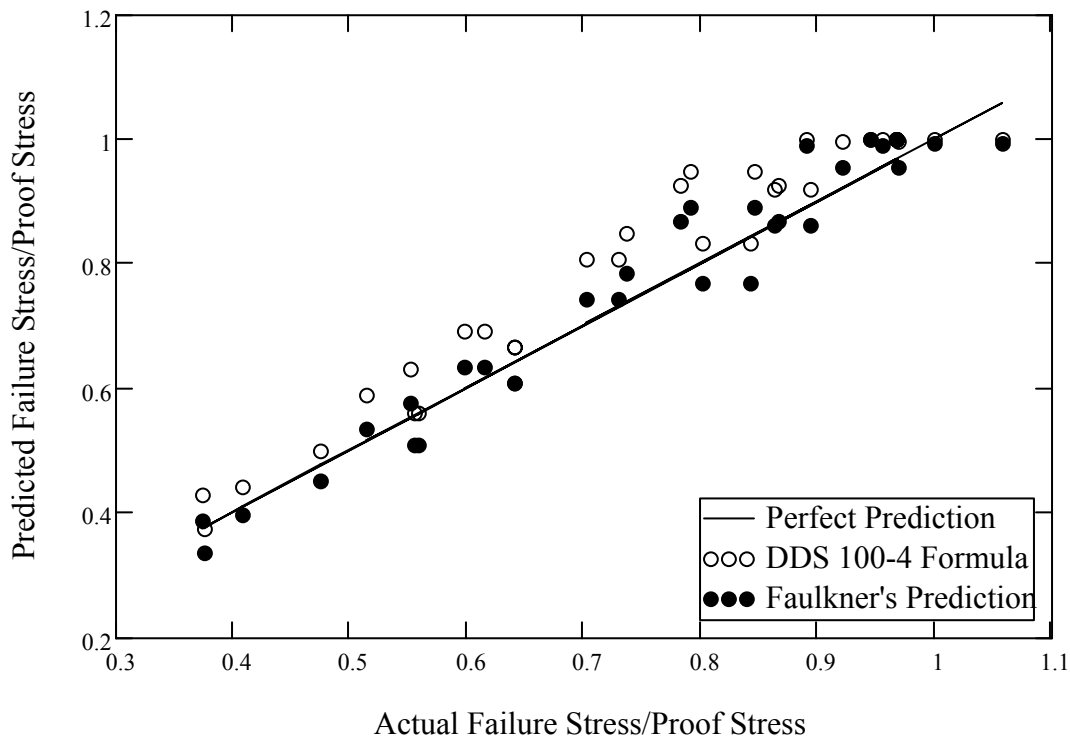
Figure 6: DDS 100-4 and Faulkner Method, Non-Welded Mofflin Plates, All Alloys

For the non-welded Mofflin plates, both methods perform consistently over a wide range of non-dimensionalized strength. The bias of each method is defined as the predicted strength divided by the experimentally-observed strength of each plate:

$$Bias = \frac{\text{Predicted Strength}}{\text{Experimental Strength}}$$

Equation 5

Thus, a bias of 1.0 indicates a perfect prediction, a bias of < 1.0 indicates a conservative prediction, and a bias of > 1.0 indicates a non-conservative prediction. Both the mean (average) bias and the coefficient of variation (COV) of the bias were tracked, with the COV defined as the standard deviation of the bias value divided by the mean of the bias value. For the non-welded Mofflin plates, the DDS 100-4 method had a mean bias of 1.07, with a COV of 6%, while the Faulkner method had a mean bias of 1.01, with a COV of 6%, showing that the more pessimistic predictions of the Faulkner approach are closer to reality.
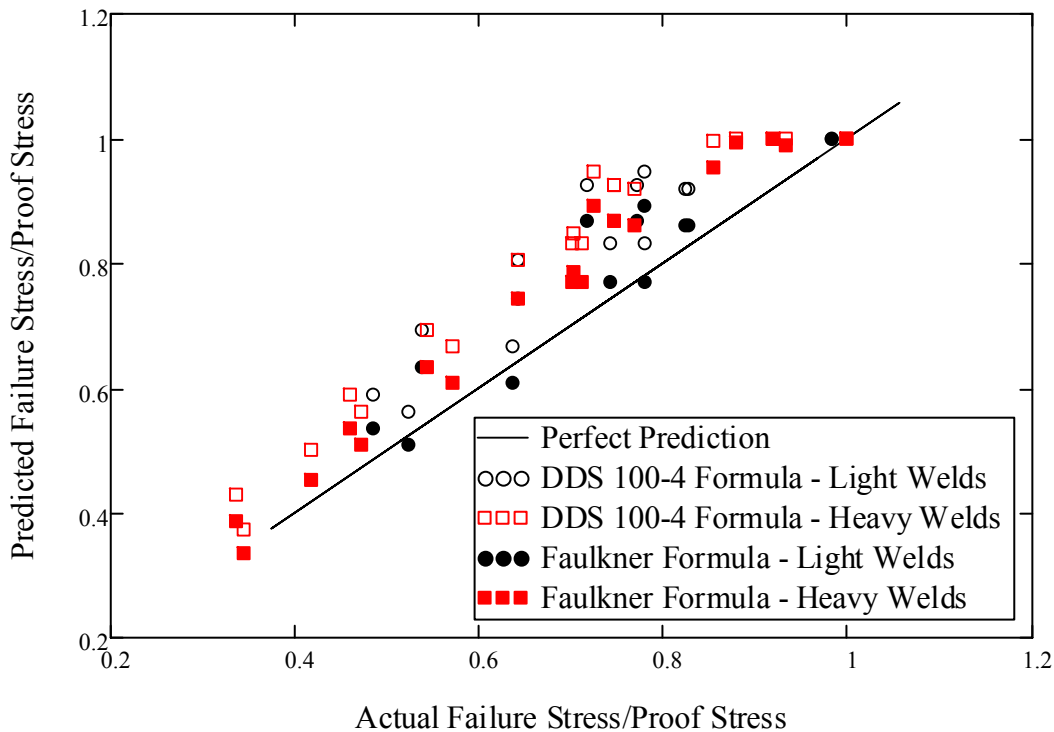
Figure 7: DDS 100-4 and Faulkner Method, Welded Mofflin Plates, All Alloys

For the welded plates, both methods are optimistic compared to the experimental data, increasingly so for the plates with high failure stresses, where the weakening effect of the HAZ is more pronounced. The mean bias for the DDS 100-4 method was 1.15 for the light welds and 1.19 for the heavy welds, with COVs of 8% for the light welds and 7% for heavy welds. For the Faulkner method, the mean bias was 1.07 for the light welds and 1.11 for the heavy welds, with COVs of 7% and 5%, respectively. For comparison purposes, the application of the DDS 100-4 method and the Faulkner method were repeated for the welded plates, using the estimated proof strength in the HAZ in place of the base metal proof stress in the formula. For the three different alloys, the following estimates were made of the HAZ proof strength:

- **6082-TF**: The HAZ strength was estimated as 50% of the base metal proof strength, based on limited measurements by Mofflin.

- **5083-M**: These plates displayed a wide variety of initial strengths; in all cases it was assumed that the HAZ achieved the grade-minimum strength of 125 MPa for annealed 5083.
- **5083-O**: No reduction in strength was assumed for the plates Mofflin annealed during the study. It is worth noting that some of these plates had strengths as low as 91 MPa, which is below the grade minimum.

The results of this comparison are shown in Figure 8. As can be clearly seen, for most of the plates this approach is far too conservative, with strengths often under-predicted by 50% or more. Interestingly, for some of the stockier plates the methods are still optimistic. These plates are believed to be the annealed or low-strength 5083 plates, where the welded and base properties are not significantly different. These over-predictions may be evidence of significant residual stresses in the plates that is lowering their strength capacity independently of the weakening effects of the HAZ. However, using the welded material strength for general collapse is clearly not an appropriate approach.
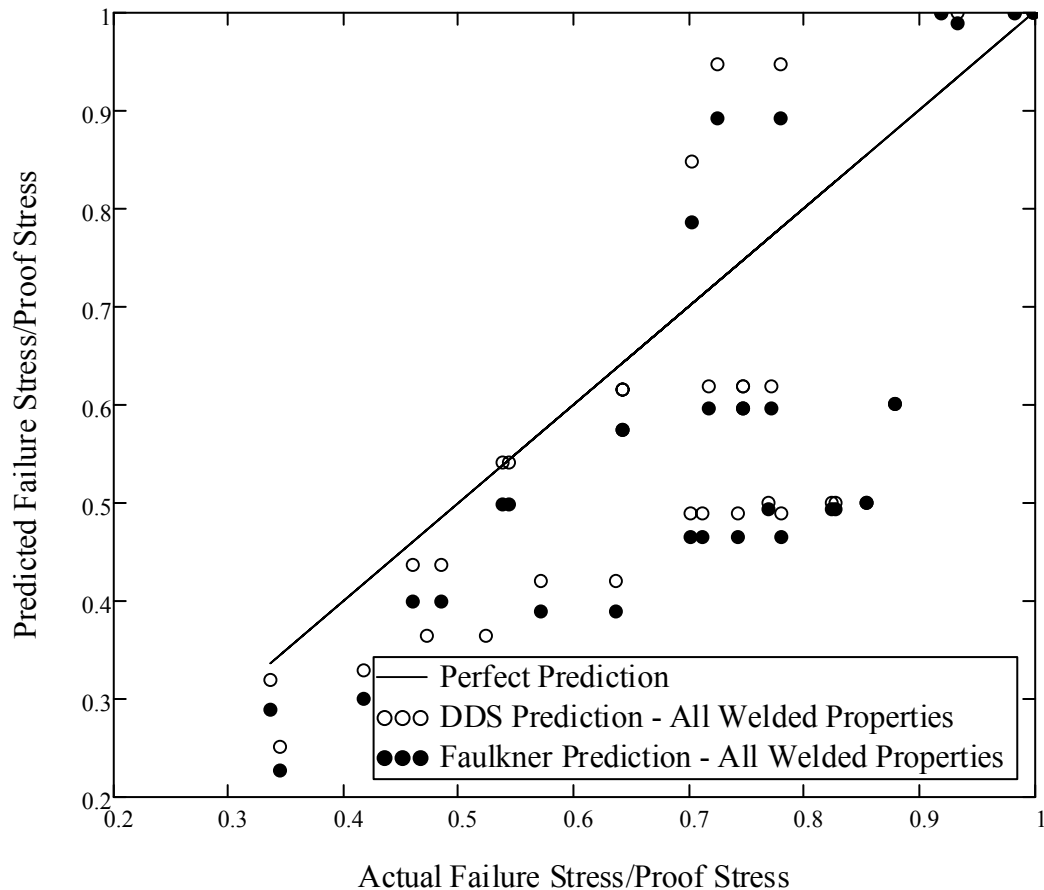
Figure 8: DDS 100-4 and Faulkner Method for Welded Mofflin Plates with Welded Material Properties

A similar comparison was made to the NACA plate data, which is composed of only non-welded plates, and is shown in Figure 9. For these plates, the DDS 100-4 method appears to be a better fit for the stockier plates, which reach a high proportion of the base metal proof stress before

failing. This may be a result of the NACA plates having generally smaller initial imperfections than the Mofflin data set; however, the initial distortion data for the NACA plates is not available so this can not be confirmed. In the lower strength ranges, the Faulkner approach appears superior to that of the DDS 100-4. For this data set, the mean bias of the DDS 100-4 method was 1.05, with a COV of 8%, and for the Faulkner method was 0.97, with a COV of 6%.
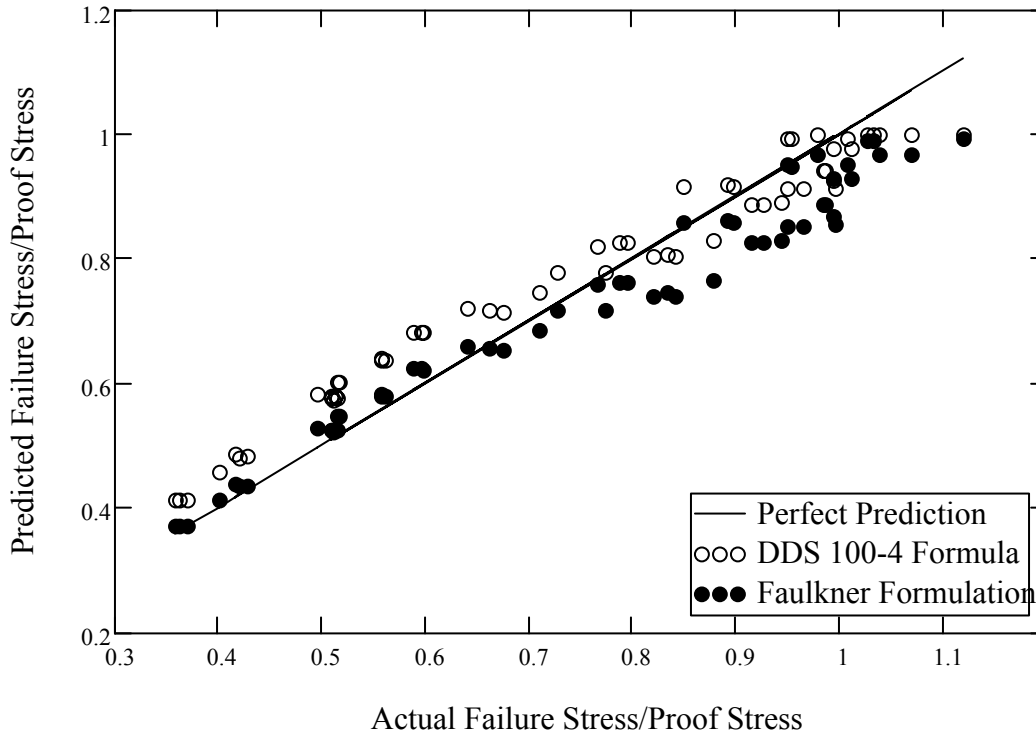
Figure 9: DDS 100-4 and Faulkner Method for NACA Plates, All Alloys

Overall, the DDS 100-4 and Faulkner methods both performed generally well for non-welded aluminum plates; however, their predictions are not reliable for welded plates. Simply replacing the base material strength with the welded material strength is not sufficient to achieve good predictions for the welded plates.

2.1.2.3 Wang et al. Method

The general approach taken by DDS 100-4 and Faulkner was further extended by Wang et al. [8] so that the effects of welds could be included in the strength calculations. The basic formulation follows that of Faulkner, but an additional factor, ψ, is applied to the definition of β, the plate slenderness:

$$\frac{\sigma_U}{\sigma_{02}} = \frac{2}{\bar{\beta}} - \frac{1}{\bar{\beta}^2}, \bar{\beta} > 1.00$$

$$\frac{\sigma_U}{\sigma_{02}} = 1, \bar{\beta} \leq 1.00 \qquad\qquad \textbf{Equation 6}$$

$$\bar{\beta} = \frac{1}{\psi} \frac{b}{t} \sqrt{\frac{\sigma_{02}}{E}}$$

The factor, ψ, is defined in terms of the plate slenderness and the strength reduction in the HAZ, where σ_{02W} is the proof stress in the weld HAZ:

$$\eta = \frac{\sigma_{02W}}{\sigma_{02}}$$

$$\psi = 1, \ \eta \geq 1 - 0.1\sqrt{\beta} \qquad\qquad \textbf{Equation 7}$$

$$\psi = 1.142 - \frac{1.42}{\sqrt{\beta}}(1-\eta), \ \eta < 1 - 0.1\sqrt{\beta}$$

This approach increases the effective value of β in the Faulkner formulation as the plate becomes stockier, and where there is a greater reduction in the HAZ, both situations where the presence of the weaker HAZ can significantly reduce the plate strength. In cases where the plate is slender enough that the failure stress is likely to be below even the reduced strength in the HAZ, the factor, ψ, is kept at 1.0. In deriving this formula, Wang et al. state that the HAZ breadth was assumed to be 3 times the plate thickness for plates less than or equal to 7.5mm in thickness, and 20mm plus one-third the plate thickness for thicker plates. The derivation of this method appears to be mainly based on 5xxx-series alloys. The proposed formula was validated against 132 plate buckling collapse simulations with non-linear finite elements, covering a range of β from 1 - 4 and HAZ with strengths between 40% and 100% of the base material. Initial imperfections were added in a multi-mode sinusoidal pattern with maximum amplitude of 0.09 times the plate breadth. Residual stresses were not included.

The results of the Wang et al. method are shown below for the Mofflin plates, plotted by weld type (Figure 10) and alloy type (Figure 11). In general, for the 5xxx-series plates, which the method was designed for, it performs excellently. For the welded 6xxx-series plates, the method is conservative; these plates tend to have slightly higher inelastic buckling strength, as the 6xxx-series alloys tend to have a higher proportional limit than the 5xxx-series alloys. Another reason for the conservatism may be the difference between the welding assumed in the Wang et al. method, which was applied to all four plate edges, and the welding in the Mofflin method, which was only applied to the two, long, unloaded edges. This difference is likely to significantly reduce the predicted strength. Including the 6xxx-series results, this method had a mean bias of 0.96 for all of the Mofflin data, and a bias COV of 12.3%. However, the results for the 5083-F plates, which correspond most closely to the plates used in the development of this model, are notably better, with a 1.01 bias and a COV of only 5%.

The Wang et al. method was also applied to the aerospace alloys in the NACA data set. Here, the method gave generally very good results, with some conservatism for plates that obtain over

14

80% of their base material proof stress in compression. These alloys are very different from the 5xxx-series alloys used in the development of the method. For the NACA data set, the overall bias was 0.97, with a COV of 6%. These results are shown in Figure 12. Including all the Mofflin alloys and the NACA data, the Wang et al. method had an overall bias of 0.97 and a COV of 10%.
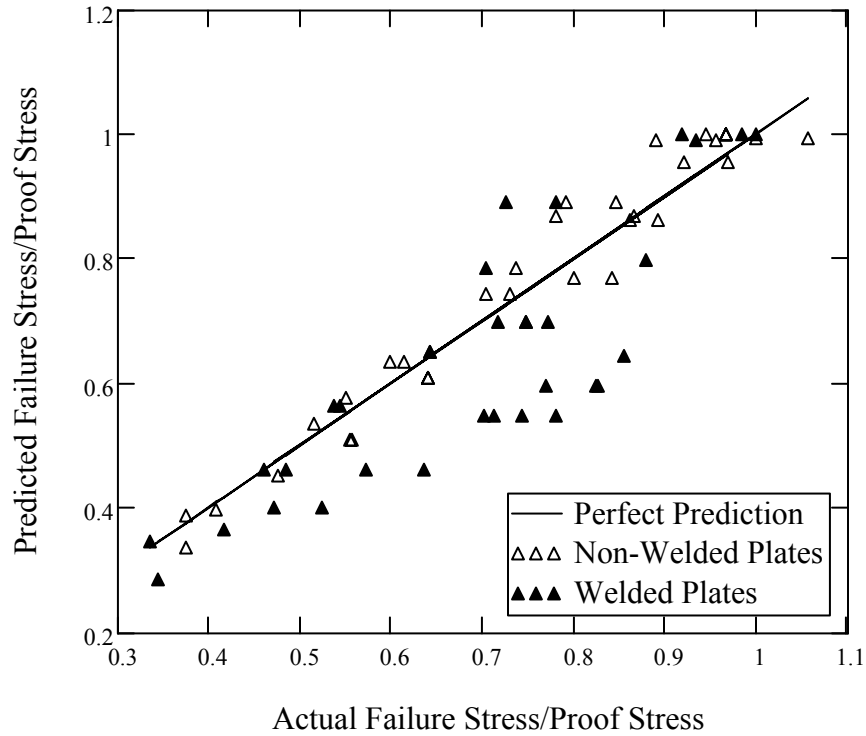
Figure 10: Wang et al. Approach for Mofflin Plates
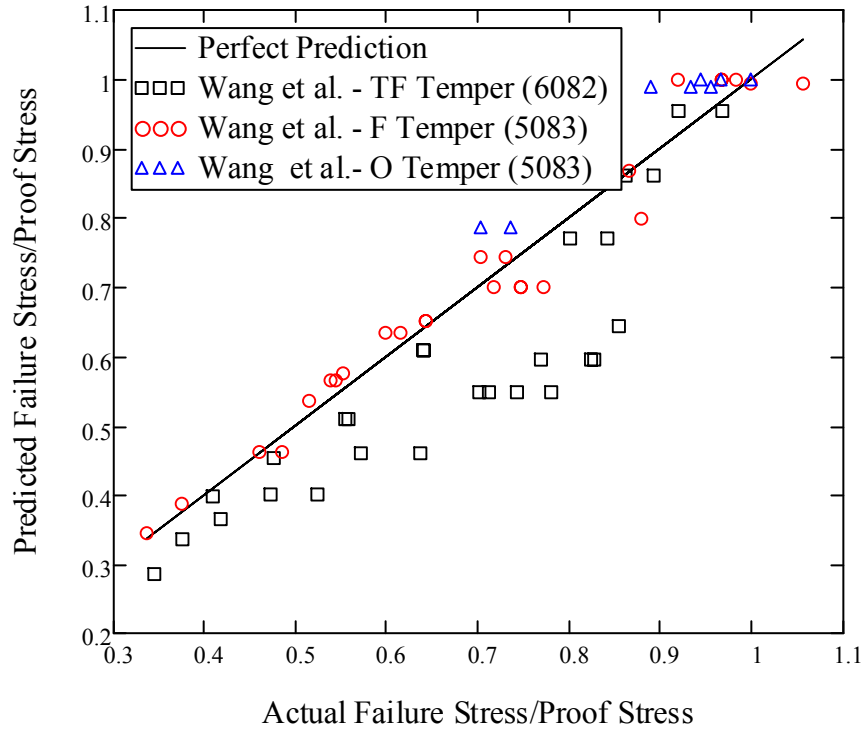
Figure 11: Wang et al. Approach for Mofflin Plates – Plotted by Temper
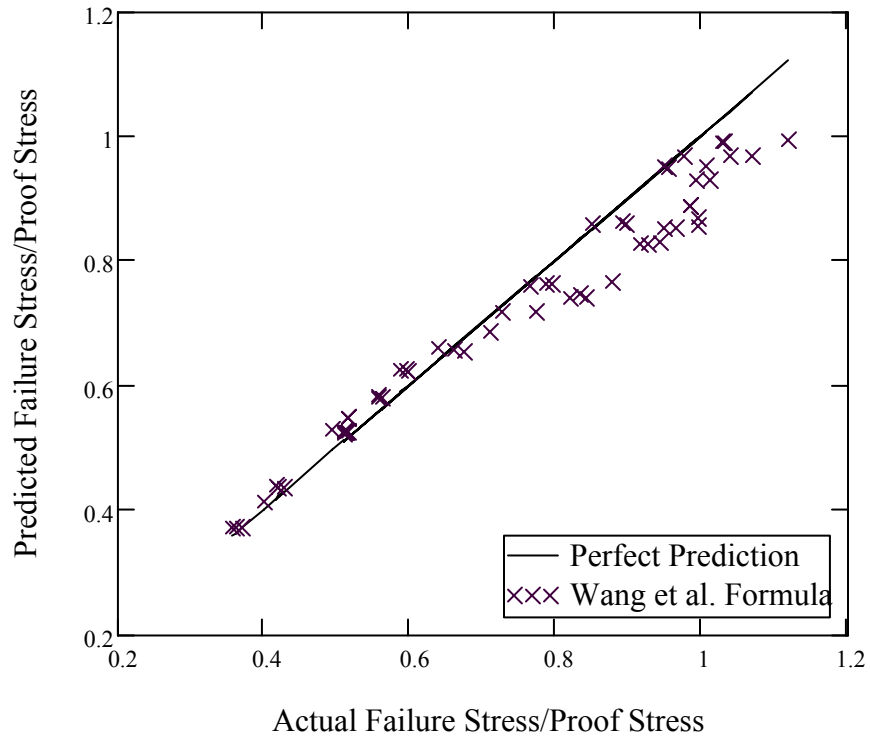
Figure 12: Wang et al. Approach for NACA Plates – All Tempers

2.1.2.4 Paik and Duran Method

Paik and Duran [10] formulated a slightly different regression equation from a parametric series of finite element models. Using the DNV material minimums for 5383-H116, Paik and Duran constructed a series of 23 finite element models covering a range of β of 0.54-5.34. All plates had a HAZ equal to three times the plate thickness, which itself ranged from 4.2mm to 40mm. The material proof strength in the HAZ was assumed to be 70% of the base material strength for every plate. No residual stresses were included in the finite element model. Sinusoidal initial imperfections were used, with maximum amplitude of 0.009 times the plate breadth. Paik and Duran noted that the slender plates generally deformed similar to steel plates as they buckled, but the stockier plates tended to have larger, localized deformations near the HAZ at the loaded ends. Based on the finite element studies, Paik and Duran proposed the following plate compressive ultimate strength model, where the buckling behavior is fitted by two piecewise linear regression equations after the squash region.

$$\frac{\sigma_U}{\sigma_{02}'} = 1.0, \quad \beta' \leq 0.46$$

$$\frac{\sigma_U}{\sigma_{02}'} = -0.215\beta' + 1.1, \quad 0.46 \leq \beta' \leq 2.2 \qquad \textbf{Equation 8}$$

$$\frac{\sigma_U}{\sigma_{02}'} = -0.083\beta' + 0.81 \quad \beta' > 2.2$$

Where the properties σ_{02}' and β' can be calculated from the volume-averaged material properties of the plate, including the HAZ and the base plate:

$$\sigma_{02}' = \frac{P_P}{ab}$$

$$P_P = (a - 2b_{HAZ})(b - 2b_{HAZ})\sigma_{02} +$$
$$2[ab_{HAZ} + (b - 2b_{HAZ})b_{HAZ}]\sigma_{02W} \qquad \textbf{Equation 9}$$

$$\beta' = \frac{b}{t}\sqrt{\frac{\sigma_{02}'}{E}}$$

Similar to the Wang et al. model, the Paik and Duran model is based on finite element models of 5xxx-series alloys, so its applicability to the more commonly-used 6xxx-series extrusions is not known. Additionally, the HAZ was kept at three times the plate thickness regardless of the plate thickness, and the HAZ strength was kept at 70% of the base material strength. This results in a model that is highly tuned to 5383 and similar 5xxx alloys, such as 5083 and 5456 in the –H116 temper, but may not perform well for other alloys. The results for the Mofflin plates are plotted in Figure 13 by temper, as the Wang et al. results were in Figure 11 previously. In performing this calculation, Paik and Duran's suggestion that the HAZ breadth be taken as *3t* was used. Similar trends can be seen to the Wang et al. results, with the 6082-TF plates generally forming the lower (most conservative) bound of prediction, though the results are more tightly grouped across alloy and temper than those from the Wang et al. theory. The mean bias is 0.96 with a

COV of 10% for the Mofflin data set, which is similar again to the Wang et al. theory. The Paik and Duran data appears to become conservative for the stockier plates that fail at roughly 75% of the base material. One reason for the conservatism in this region could be a larger initial imperfection assumed by Paik and Duran (0.009b) than what Mofflin used in his experiments (0.001b-0.005b targeted range). However, the Paik and Duran data does not include residual stresses, while the Mofflin experimental plates do have residual stresses, which would be expected to push the error the other way.

The Paik and Duran method was also applied to the NACA plates, as shown in Figure 14. For these plates, the Paik and Duran method was very conservative in the inelastic region. This is most likely a result of the regression formula not including any plates without a HAZ, as none of the NACA plates were welded. However, when the failure stress was less than 60% of the base material strength, the method performed quite well. For the NACA plates, the Paik and Duran method had a bias of 0.92, with a COV of 14%. Overall, for all the plate data, the Paik and Duran method had a bias of 0.94, with a COV of 12%, though these numbers are skewed by the relatively poor performance of the method on the non-welded NACA panels.
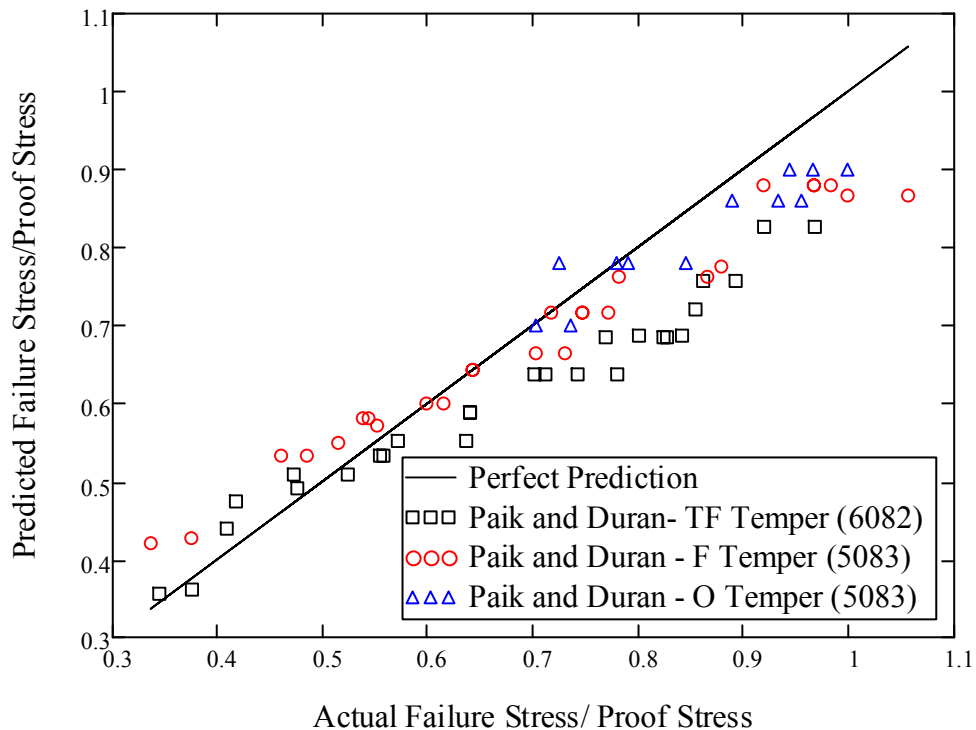
Figure 13: Paik and Duran Approach for Mofflin Plates – Plotted by Temper
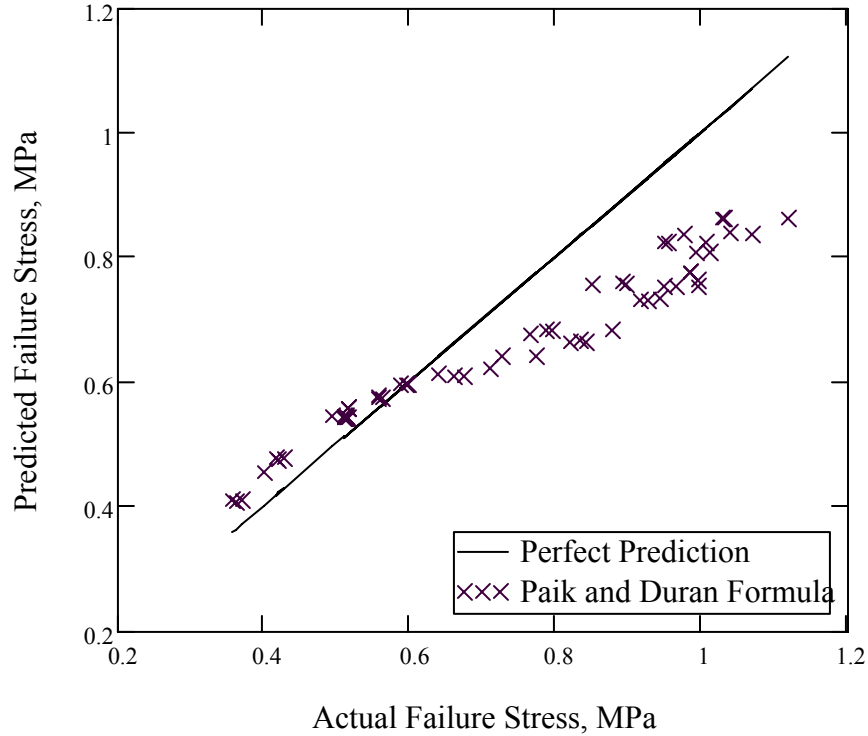
Figure 14: Paik and Duran Approach for NACA Plates – All Tempers

2.1.2.5 Kristensen Method

Kristensen [12] also formulated a regression model for compressive plate strength based on a series of finite element models. Kristensen's approach differed slightly from the approaches of Wang et al. and Paik and Duran in that a very wide range of plates were simulated, and then a regression equation was fitted to the lower-bound of the simulated data. Kristensen's simulation included three types of alloys, 5083-O, 5083-F, and 6082-T6, all modeled on Mofflin's experimental materials. Kristensen's simulations covered plate aspect ratios (or the plate length divided by the plate breadth) between one and five, and β ratios between one and five. Different HAZ patterns were explored, including welds in the center of the plate, as is common when joining extruded integral plate-stiffener units together. Initial deformations similar to those used by Wang et al. and Paik and Duran were used, with a maximum initial deformation of 0.005b. Kristensen proposed two formulas, one for non-welded plates, and one for welded plates with a HAZ on 25mm breadth, and strength half that of the base material. Kristensen also provided formulas for transverse compression, biaxial compression, and different HAZ strengths and widths, some of which are explored later. Kristensen proposed a single model for all types of buckling failures, squashing, inelastic buckling, and elastic buckling. For the non-welded plates, the regression formula proposed by Kristensen was:

$$\frac{\sigma_U}{\sigma_{elpl}} = 1.562 - 1.426 \exp\left(-0.9403 \beta^{-0.8616}\right)$$ **Equation 10**

Where Kristensen used the stress at which the elastic and plastic components of strain are equal, σ_{elpl}, as a non-dimensional term in place of the more conventional 0.2% offset proof stress. This term can be determined from Ramberg-Osgood stress-strain curves as follows:

19

$$\sigma_{elpl} = \sigma_{0.2}^{\frac{n}{n-1}} \left(0.002E\right)^{\frac{1}{1-n}}$$

Equation 11

For welded plates, with 25mm HAZ and HAZ strength equal to 50% of the base material strength, Kristensen proposed the following formula:

$$\frac{\sigma_U}{\sigma_{elpl}} = 0.7495 - 0.7036 \exp\left(-3.387\beta^{-1.224}\right)$$

Equation 12

In generating this formula, Kristensen noted that the plates with an aspect ratio of 1.0 gave the lowest ultimate strength for welded plates, and were used for this formula. However, these plates would be very atypical of plates used in marine applications, which typically have an aspect ratio between 3.0 and 5.0. For plates with an aspect ratio of 1.0, Kristensen noted the traditional (plate edges) and extrusion (short edges plus plate centerline) HAZ patterns had very similar ultimate strengths. In general, across all aspect ratios, Kristensen noted that when the short, loaded edges of the plate were welded, there was not a large difference in axial strength between plates welded on the longitudinal edges (conventional construction) and in the middle of the plate (extrusion construction). When the short, loaded edges were not welded, a large difference was noted between conventional and extrusion construction.

The Kristensen formulation was applied to the Mofflin data set, and the results are plotted by weld type in Figure 15, and by alloy type in Figure 16. The results indicate that the non-welded formulation performed excellently, while the welded formulation was generally conservative. This conservatism in the welded formulation is probably a combined result of the relatively broad (25mm) HAZ assumed by Kristensen for these plates, which were only 6mm thick, the high level of material strength reduction (50%) in the HAZ, and the fact that the HAZ was assumed to be on the short, loaded edges as well as the long edges in Kristensen's regression formula. In the experimental result, the short, loaded edges were not welded. This, plus the low aspect ratio of the plates used to generate the welded model, gave it some conservatism. If the HAZ extent is known, Kristensen's more detailed strength model could be used; however, this would not correct for the low aspect ratio or the HAZ on the short, loaded edges of the plate. For all the Mofflin plates, the Kristensen formula gave an overall bias of 0.94, with a COV of 11%.
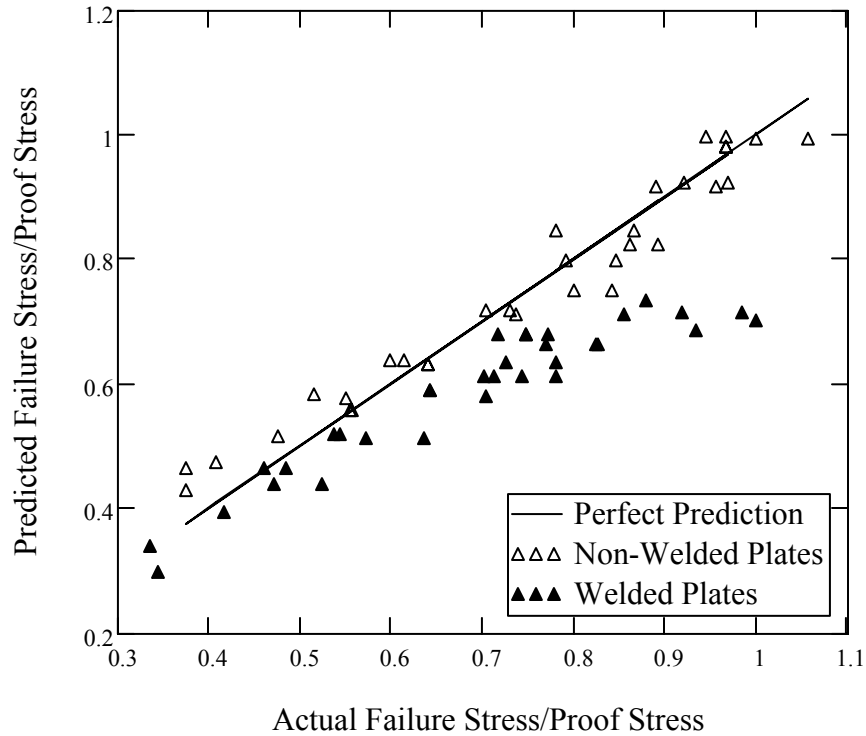
Figure 15: Kristensen Approach for Mofflin Plates

The Kristensen method was also applied to the NACA plates, all of which are un-welded. The results are shown in Figure 17. The formula provides accurate if slightly conservative predictions for the plates with average failure stresses above roughly 65% of the material yield stress, but is optimistic for the more slender plates. However, none of the aerospace alloys used in the NACA test were used in Kristensen's parametric finite element study, so this is not terribly surprising. The overall bias for the NACA test data set was 1.05, with a COV of 13%. The overall bias for the Kristensen method was 0.99, with a COV of 12%.
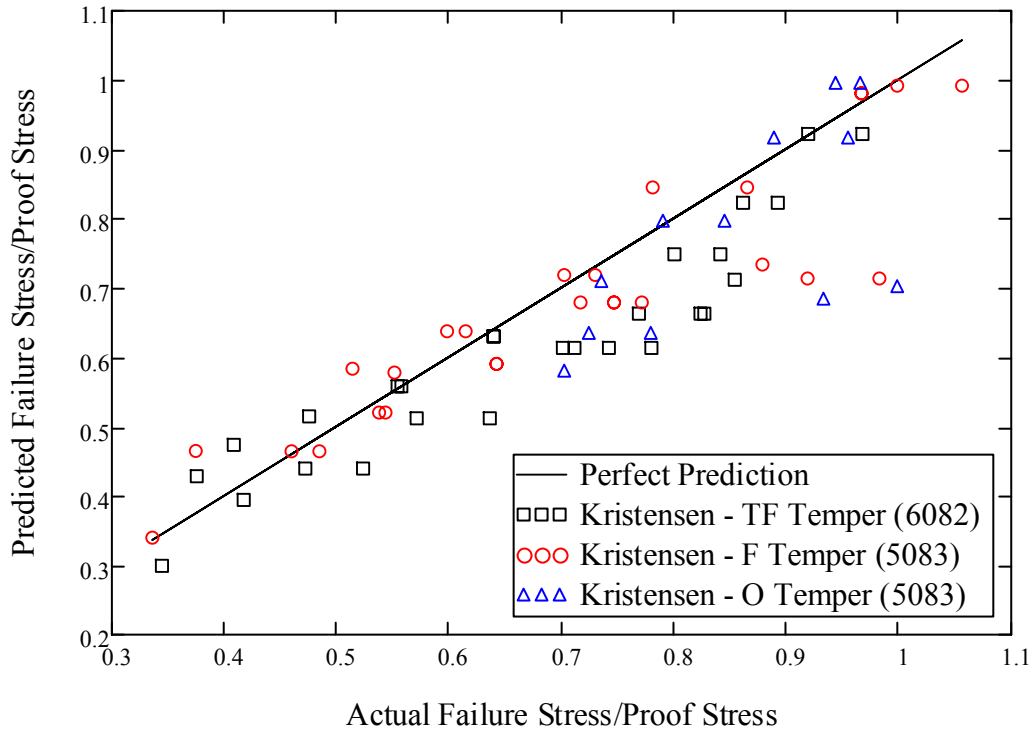
Figure 16: Kristensen Approach for Mofflin Plates – Plotted by Temper
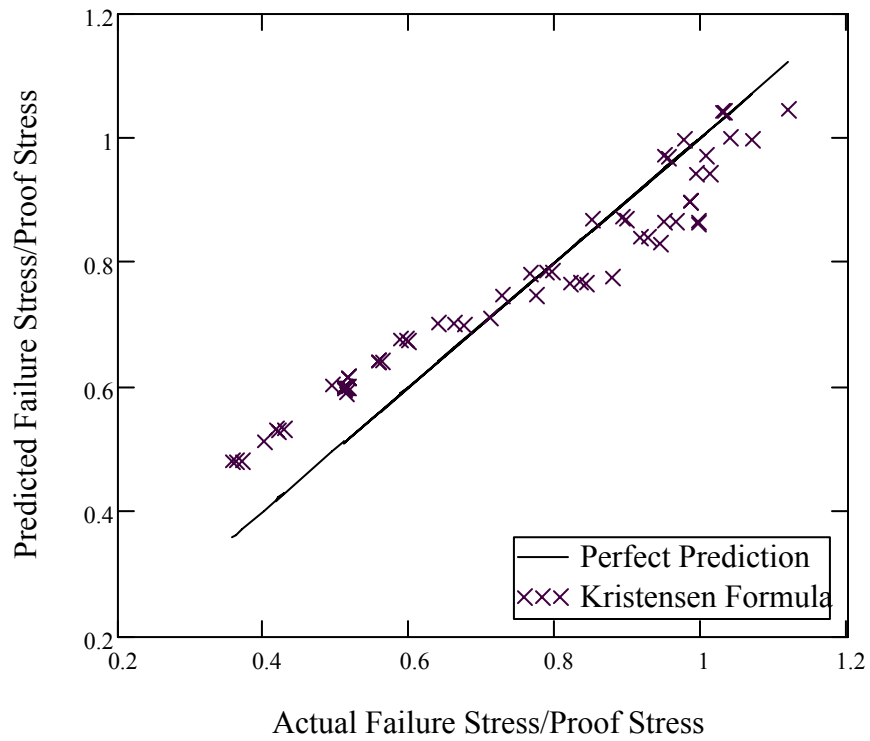
Figure 17: Kristensen Approach for NACA Plates

2.1.2.6 Aluminum Association

The U.S. Aluminum Association has published formulas for uniaxial compressive collapse of plates in its *Specification for Aluminum Structures* as part of the *Aluminum Design Manual* [13]. The approach taken by the Aluminum Association is based in part on an analysis of buckling of aluminum plates and columns – including the NACA data used here as a validation set. Therefore, good agreement is to be expected with the NACA set. In this approach, the buckling performance of the structure is divided into three regions, a squash compressive collapse region for very stocky members that can reach the material proof strength in compression, an inelastic buckling region where a linear relationship between element slenderness and buckling strength is proposed, and an elastic buckling region at the higher slenderness. For plates buckling in isolation, the Aluminum Association allows the recognition of post-buckling strength in the elastic region. Thus, the Aluminum Association approach is an alternative to traditional buckling formulations, such as the Johnston-Ostenfeld or Perry Robertson approaches, which link elastic buckling behavior and compressive collapse with different simplified relationships through the inelastic region. The Aluminum Association approach calculates a plate slenderness, *S*, which is equal to the plate *b/t* ratio, and divides the buckling region into three zones by slenderness constants, S_1 and S_2, which are based on the type of plate and edge supports. Additionally, there is a series of material-specific coefficients, *k*, k_2, B_P, and D_P which change based on the material properties and alloy type. The material coefficients are tabulated for common materials in the *Aluminum Design Manual* [13]. The general form of the method is given below, without any of the safety factors that would be applied when assessing compliance with the design code:

$$\sigma_U = \sigma_{02} \quad S < S_1$$

$$\sigma_U = B_P - D_P \left(k \frac{b}{t} \right) \quad S_1 \le S \le S_2$$

$$\sigma_U = \frac{k_2 \sqrt{B_P E}}{k \dfrac{b}{t}} \quad S > S_2$$

Equation 13

The reduced strength in the HAZ near welds must be accounted for when more than 15% of the cross-sectional area is welded. This is done by calculating the strength of an un-welded component and an all-HAZ material component, and interpolating between the two strengths based on the amount of the cross-sectional area that is welded. The method was applied to the Mofflin data set, and the results are shown in Figure 18, sorted by alloy. The results from the Aluminum Association formulation were quite good, with no clear bias towards one type of material or welded/non-welded specimens. The overall bias was 1.01 for the entire Mofflin data set, with a COV of 8%.
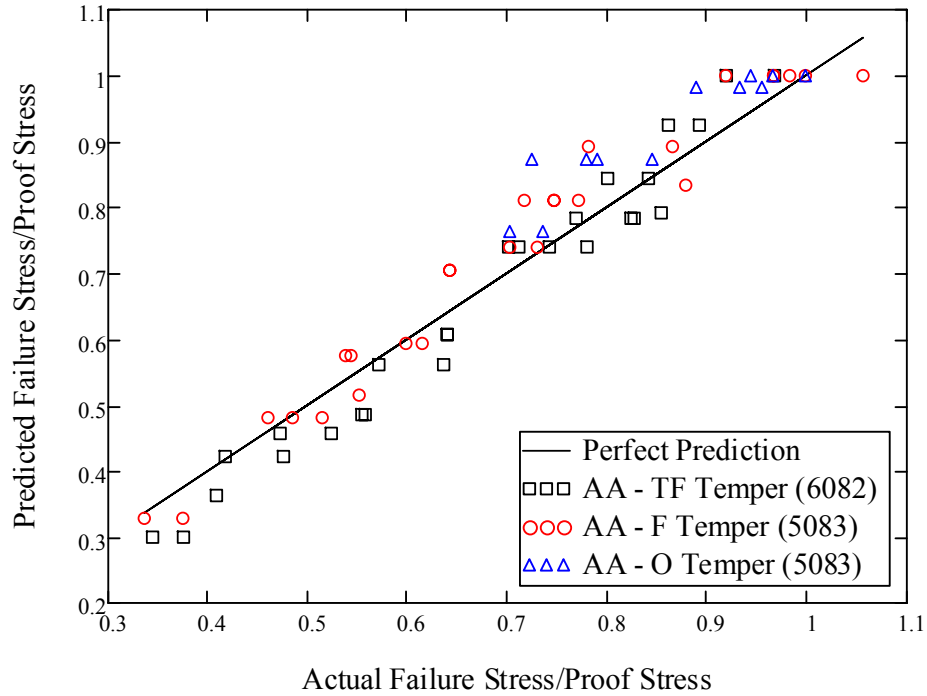
Figure 18: Aluminum Association Approach for Mofflin Plates

The method was also applied to the NACA data set, although, as stated above, this data set was used in part to develop the coefficients, so good agreement is expected. The results are shown in Figure 19, with very good agreement. There is a little bit of flattening out of the predicted strength at the 0.2% offset proof stress of the base material, which is the maximum strength allowed under the Aluminum Association method, while some of the very stocky experimental plates achieved average compressive failure stresses above the material proof stress. For this data set, the overall bias was 1.0 and the COV was 4%, and for both data sets the mean bias was 1.0, with a COV of 6%.
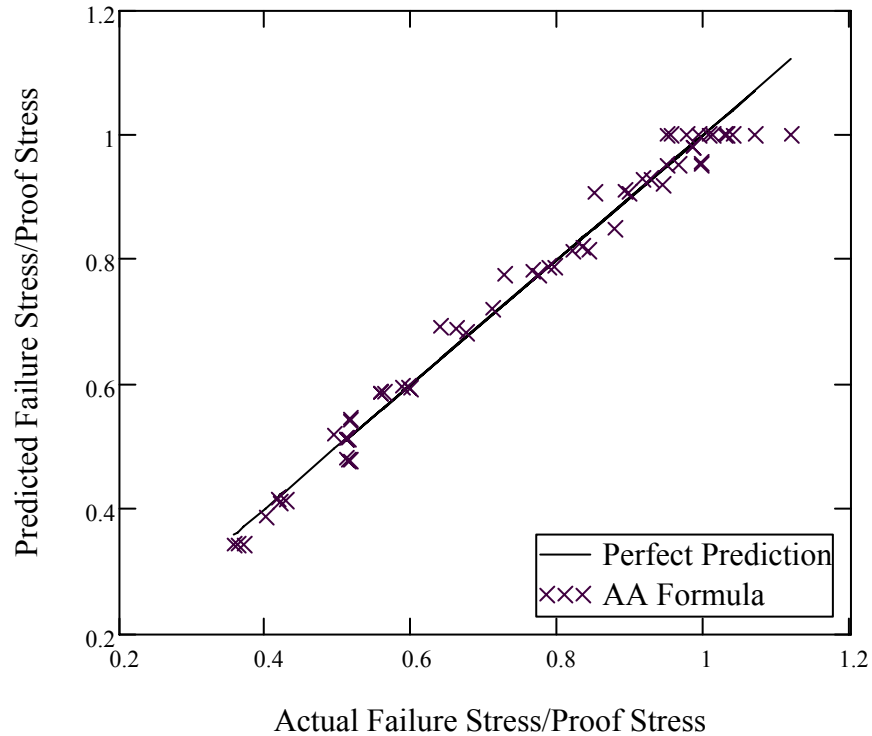
Figure 19: Aluminum Association Approach for Mofflin Plates

2.1.2.7 Eurocode 9

The European Committee for Standardisation (CEN) has developed a series of model building codes, designed to eventually replace national building codes in the European Union. Eurocode 9 [14] EN 1999, deals with the design of aluminum structures, and contains formulations for the ultimate strength of plates. Similar to the Aluminum Association formulation, the Eurocode method specifies partial safety factors for use in civil engineering application. For clarity, these factors have been removed from the presentation below. The Eurocode 9 formulation divides the buckling problem into two regions: stocky plates that fail essentially by squashing, reaching the material's full proof stress; or plates that buckle either inelastically or elastically (potentially with some post-buckling strength). A single quadratic-type relationship is used to handle both inelastic and elastic buckling, via an effective thickness approach. In this approach, the actual thickness of the plate is replaced by an effective thickness; calculated based on slenderness ratio and three coefficients, C_1, C_2, and C_3, which change with alloy type, edge supports, and whether the plate is welded or non-welded. The general form of the formula is given below:

$$\frac{\sigma_U}{\sigma_{02}} = \frac{a_{Net}}{a_{Orig}}$$

$$a_{Net} = bt_e$$

$$a_{Orig} = bt$$

$$\frac{t_e}{t} = 1, \quad \frac{\beta_{EC9}}{\varepsilon} \leq C_1$$

$$\frac{t_e}{t} = \frac{C_2}{\dfrac{\beta_{EC9}}{\varepsilon}} - \frac{C_3}{\left(\dfrac{\beta_{EC9}}{\varepsilon}\right)^2}, \quad \frac{\beta_{EC9}}{\varepsilon} > C_1 \qquad \textbf{Equation 14}$$

$$\beta_{EC9} = \frac{b}{t}$$

$$\varepsilon = \sqrt{\frac{250 MPa}{\sigma_{02}}}$$

Welding is accounted for by further reducing the effective thickness in the welded regions by a ratio of the base material and welded material strength. If this reduction is larger than the reduction for buckling specified in Equation 14, the weld reduction is used in place of the buckling reduction for the areas of the plate that are welded when calculating a_{Net}. The strength of the plate is then calculated as shown in Equation 14. If the welding thickness reduction is less than the buckling reduction, the effects of welding may be ignored. The results of applying the Eurocode 9 formulation to the Mofflin data set (both welded and non-welded) are shown in Figure 20, with generally excellent agreement seen throughout. The overall bias of the method was 0.97, with a COV of 6%. Agreement is largely the same regardless of slenderness of the plate or alloy.

The method was applied to the NACA plate data as well, as shown in Figure 21. Here a general conservative trend is seen towards the stockier plates, with higher failure stresses as a percentage of the base material strength. It is possible that being civil-engineering oriented, the material coefficients in the Eurocode are not as well tuned to the aerospace alloys, whereas the Aluminum Association formula uses the aerospace data in its derivation. The mean bias for these tests was 0.95, with a COV of 5%. Overall, the Eurocode 9 method had a mean bias of 0.96 and a COV of 6%.
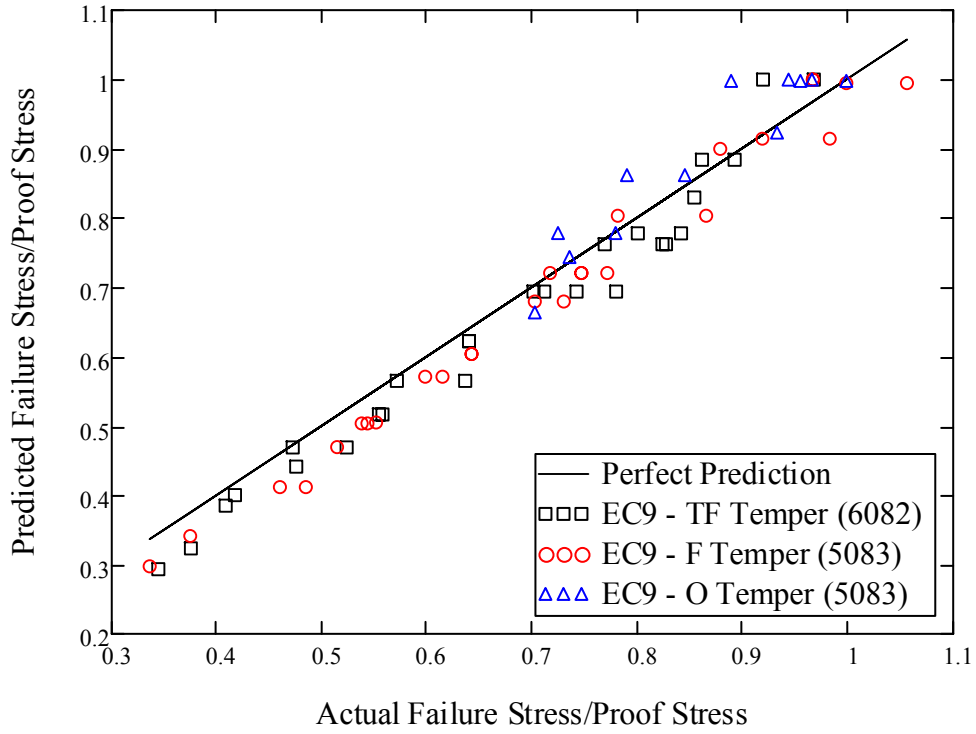
Figure 20: Eurocode 9 Approach for Mofflin Plates
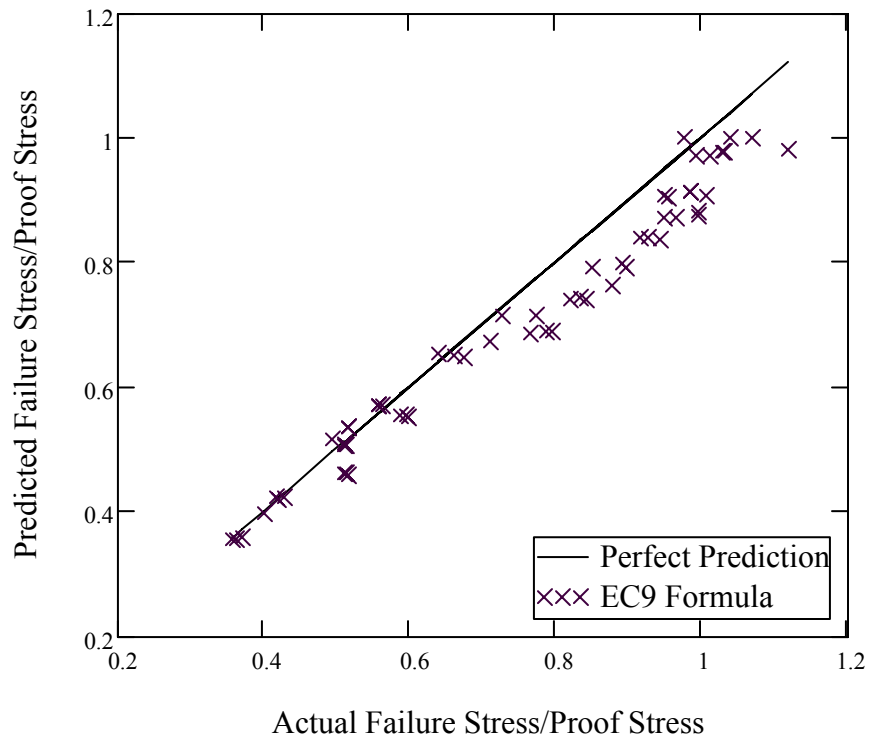
Figure 21: Eurocode 9 Approach for NACA Plates

2.1.2.8 Summary of Simplified Uniaxial Plate Strengths

Overall, the simplified uniaxial plate strength methods performed well. As expected, the limits of the experimental results used to develop the regression equations need to be respected. In all cases, methods that assumed welds on the short, unloaded edges, such as the Paik and Duran method, were notably conservative on the non-welded NACA data sets.   In general, most extrusions will have at least partial welding on the short transverse ends; however, it is possible that some plate components of the extrusions will be entirely non-welded, and also possible that many plate components will only have welds on the short, transverse ends and no welds on the longer, longitudinal sides. The civil engineering formulations seemed most adapt at handling a wide variety in the welding conditions of various plates. The overall performance is summarized in Table 1.

Table 1: Summary of Plate Methods

Method	Mofflin Plates		NACA Plates		Overall	
	Bias	*COV*	*Bias*	*COV*	*Bias*	*COV*
DDS 100-4	1.12	8%	1.05	8%	1.09	8.6%
Faulkner	1.05	7.4%	0.97	6%	1.02	8%
Wang et al.	0.96	12.3%	0.97	6%	0.97	10%
Paik and Duran	0.96	10%	0.92	14%	0.94	12%
Kristensen	0.94	11%	1.05	13%	0.99	12%
Aluminum Association	1.01	8%	1.0	4%	1.00	6%
Eurocode 9	0.97	6%	0.95	5%	0.96	6%

Another observation from the test data is that all the methods seemed to have a large bias at lower plate slenderness ratios. In this region, the ultimate strength is determined by inelastic buckling. The increased error in the inelastic buckling region may be, in part, a result of the different assumptions about welding in the methods and the experimental data, specifically the lack of welds on the short, transverse loaded edges in the experiment. As can be seen from Figure 5, in this region the welds have the largest impact on plate strength, and any discrepancy in the weld models is likely to have the largest impact in this region. To further investigate this potential difference in prediction bias, both experimental data sets for each method were combined and then split into two halves, one where the experimental failure stress was less than 65% of the base material proof stress, the other where it was higher. The bias and COV of the bias was calculated for each half of the split data set for each method, and is shown in Table 2. The larger error in the methods that assume welding on all four edges of the panel is clear from this table. It is difficult to establish other clear patterns from the data in this table; however, it is clear that the two civil engineering formulations work very well for either range.

Table 2: Bias by Failure Stress

Method	Failure Stress < 65% of σ_{02}		Failure Stress > 65% of σ_{02}		Overall	
	Bias	COV	Bias	COV	Bias	COV
DDS 100-4	1.14	6.0%	1.05	8.8%	1.09	8.6%
Faulkner	1.04	6.2%	1.00	8.7%	1.02	8%
Wang et al.	0.99	8.3%	0.95	10.7%	0.97	10%
Paik and Duran	1.05	7.0%	0.87	7.7%	0.94	12%
Kristensen	1.09	12.2%	0.93	8.8%	0.99	12%
Aluminum Association	0.97	7.0%	1.02	5.2%	1.00	6%
Eurocode 9	0.95	5.3%	0.96	6%	0.96	6%

2.1.2.9 Finite Element Analysis of Variable Thickness Plates

As no experimental results were found for compression of plates with variable plate thickness, finite element simulations were used to investigate the strength properties of these plates. The first step in doing so was to validate the finite element modeling approach against the experimental plate data from Mofflin. The finite element program CalculiX (Dhondt [15]) was selected for use in this project. In order to develop a validated finite element modeling approach, the load-shortening curves observed by Mofflin during his experiments were initially replicated. The initial imperfections introduced to the plates by Mofflin were replicated in the initial mesh of the finite element model. Mofflin introduced a central "bump" in the middle third of the panel by striking the plate with an indenter. In the finite element model, this "bump" was simulated by a circular depression at about the plate's center. A cosine function was used to compute the spatial variation of the depth of the depression as a function of the maximum indentation. It is likely that Mofflin's deformation procedure also resulted in residual stresses in the plate; however, these stresses were not measured during the experiment and were not included in the finite element model. The finite element model of the plate was assumed to be free to slide in the plane of the plate, with the long, unloaded edges constrained from deforming out-of-plane but not constrained to remain straight in-plane. This corresponds to the experimental support set-up used by Mofflin. Mofflin's material compression test results were used to model the material's plastic behavior via CalculiX's DEFORMATION PLASTICITY material option. The plate was meshed with 8-node reduced-integration shell elements, which are expanded into three-dimensional elements within the CalculiX solver. The number of elements was varied, however, convergences was achieved when 10 elements were used across the short, loaded edges of the plate and 40 elements used along the long edges of the plate. This keeps each element square and with a reasonable thickness-to-width ratio. In general, very good agreement between the FEA simulation and experimental results were obtained. In total, 20 non-welded Mofflin plates were investigated by FEA, covering b/t ratios of 20 to 50. Overall, the FEA approach had a mean bias of 1.01 for these panels and a COV of 8%. In general, the load-shortening curves also agreed well with the FEA and experimental results, as shown in Figure 22 and Figure 23 below, though in some instance the slope was not always perfectly predicted.
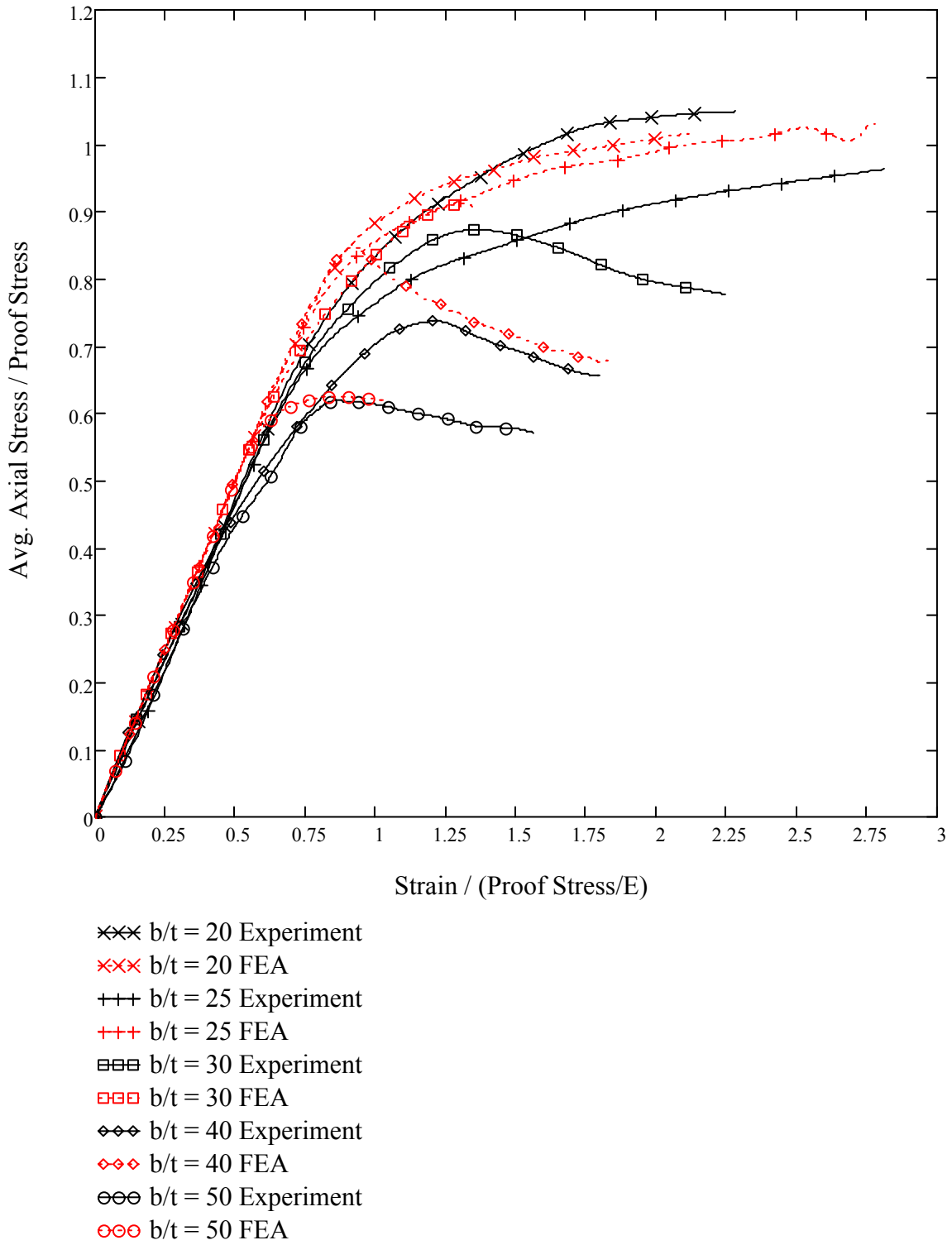
Figure 22: Comparison of Experimental and FEA Results for 5083-M Plates with Small Initial Out-of-Plane Deformations
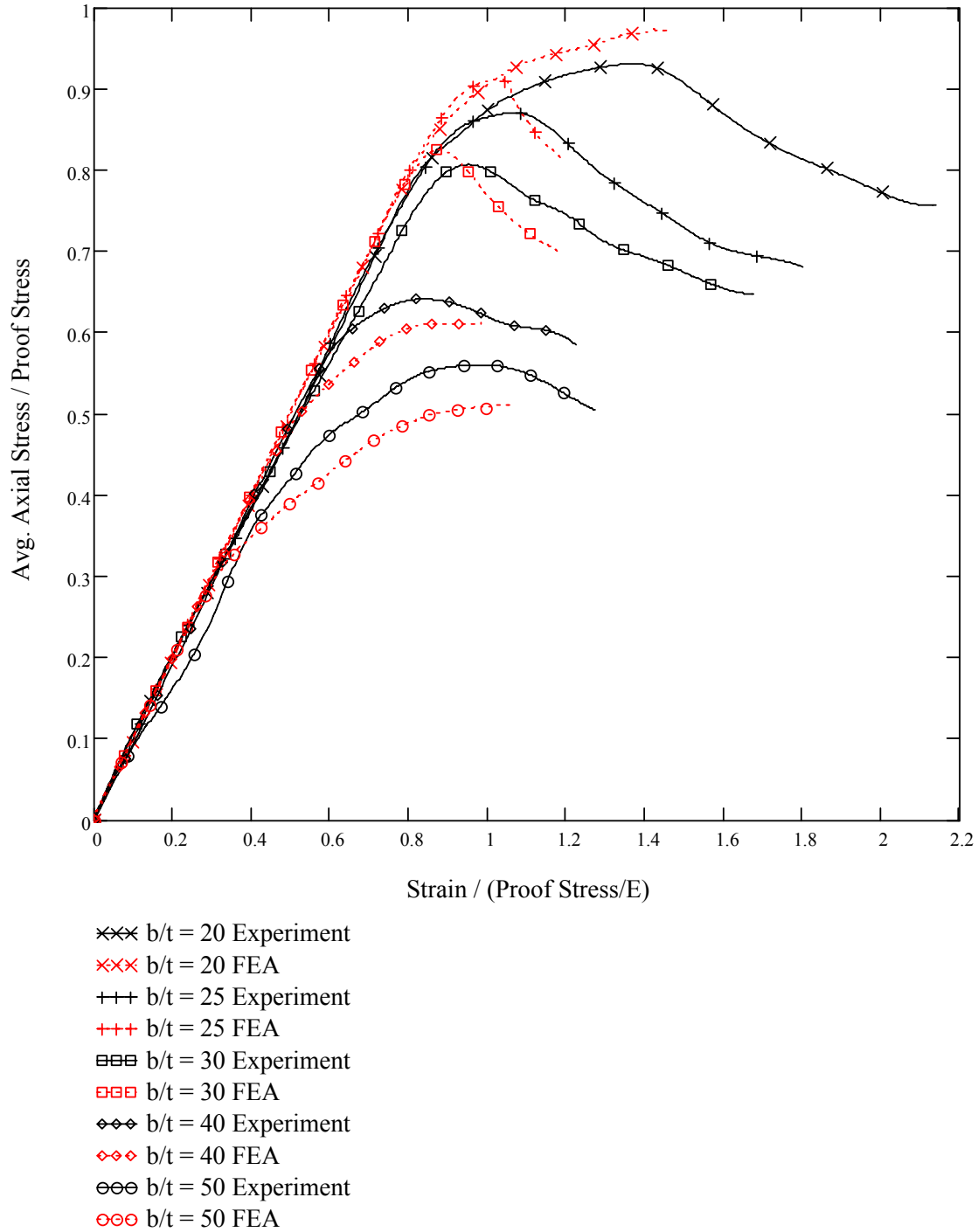
Figure 23: Comparison of Experimental and FEA Results for 6082-T6 Plates with Large Initial Out-of-Plane Deformations

With confidence in the finite element modeling parameters, the compression of variable thickness plates was studied using the CalculiX software. A plate with an average thickness of 5mm was used, made out of 6082-T6 with a yield strength of 262 MPa, an elastic modulus of 70000 MPa, and a Ramberg-Osgood exponent of 25. Plate breadths were selected so that plate

slenderness ratios, β, of 2, 3, and 4 were achieved, which corresponded to b/t ratios of 33, 49 and 65, respectively. Sinusoidal initial imperfections were introduced into the mesh for these plates. Unlike the Mofflin "indenter" deformations, these imperfections followed the lowest buckling mode of the plate, with uniform thickness and a maximum amplitude of 0.005 times the plate breadth. Two different thickness variations were made. In the first, the plates were made thicker in the middle of the plate; in the second, the edges of the plates were made thicker. The corresponding cross-sections of the plate are shown in Figure 24, and the numeric values of thickness are given in Table 3. In all cases, the thickness variation was linear, from the edge of the plate to the middle of the plate, and the average thickness – and thus the weight – of the plates remained the same.
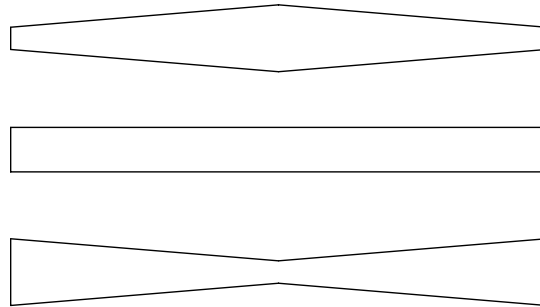
Figure 24: Cross-Sections of Variable Thickness Plates

Table 3: Plate Thicknesses Investigated

Case	T_{EDGE}	T_{MIDDLE}
1	6.66mm	3.33mm
2	5.71mm	4.29mm
3	5.00mm	5.00mm
4	4.29mm	5.71mm
5	3.33mm	6.66mm

The compressive stress-strain curves of variable thickness plates predicted by the finite element simulation are shown in Figure 25, Figure 26, and Figure 27. The results indicate that variable thickness plates do offer strength improvement at the same weight as constant-thickness plates, but primarily for slender plates in the post-elastic buckling region. The results for the β=2 plate shown in Figure 25 show negligible strengthening for a fairly stocky plate where the initial buckling is inelastic. For the β=3 and 4 plates, the plates with thicker edges appear to become stronger than the uniform thickness plates once the elastic buckling stress (shown as the heavy dashed line in Figure 26 Figure 27) is reached.
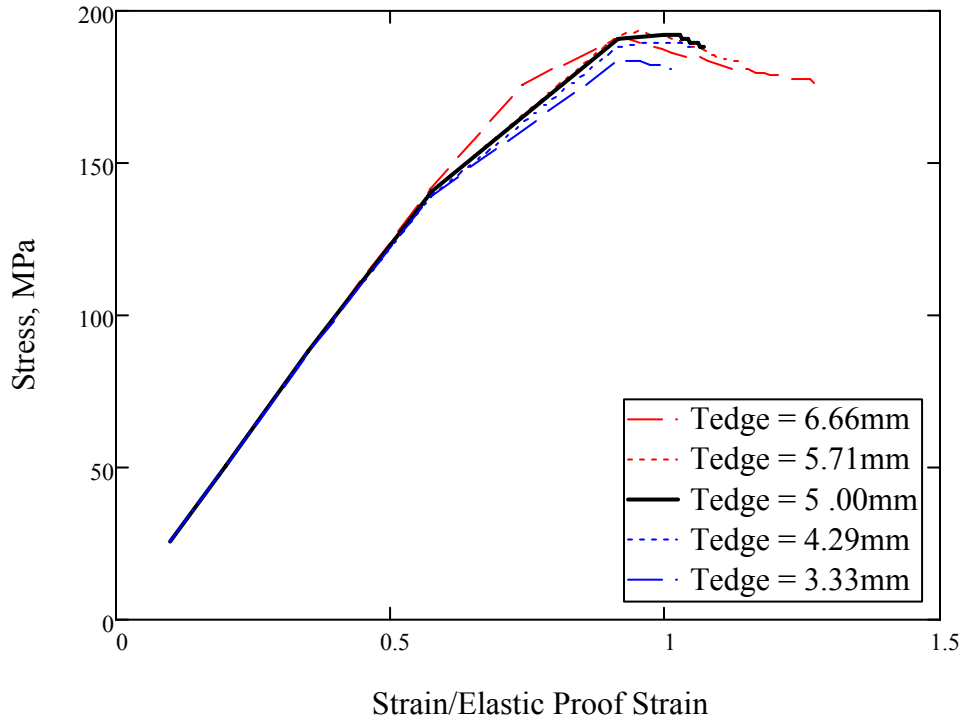
Figure 25: Compressive Stress-Strain Curves of β=2, b/t=33 with Variable Thickness
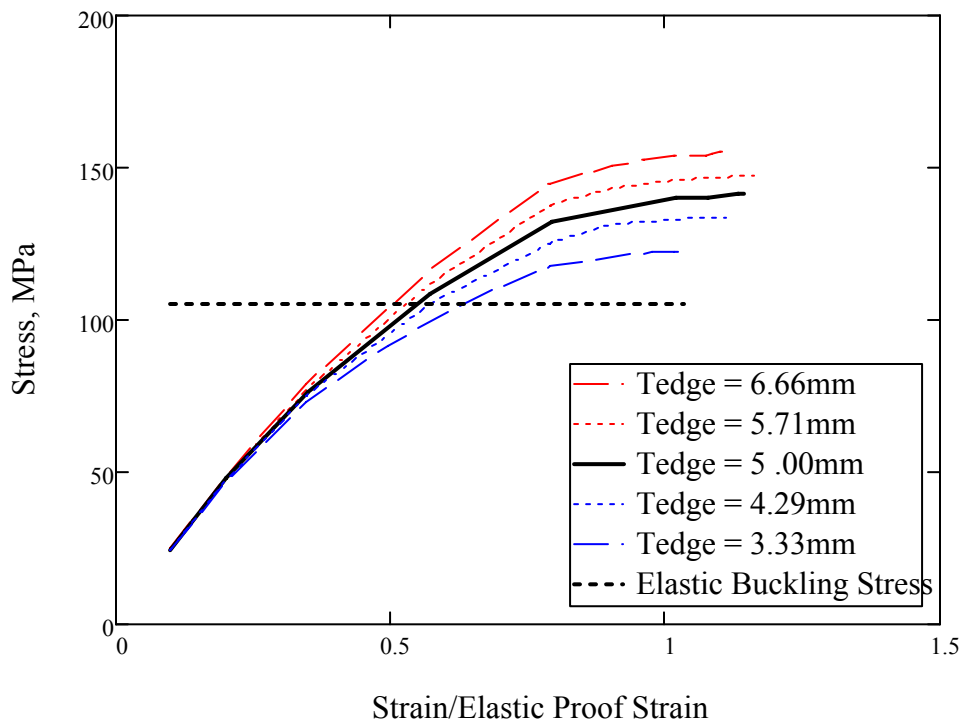
Figure 26: Compressive Stress-Strain Curves of β=3, b/t=49 with Variable Thickness
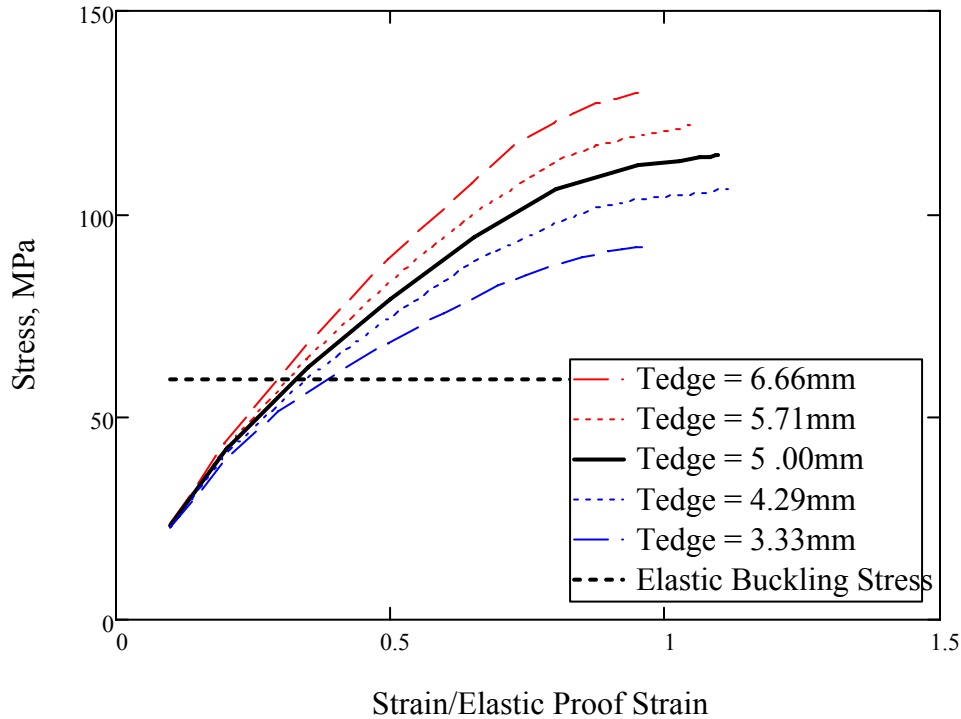
Figure 27: Compressive Stress-Strain Curves of β=4, b/t=65 with Variable Thickness

These figures also show that the compressive stress-strain curve for the plates with the thicker middle region falls below the stress–strain curve for the uniform-thickness plate in this range. For slender plates that buckle elastically before reaching their peak compressive strength, the effective axial strain distribution is theorized to shift so that the portions of the plate adjacent to the supported edge carry an increased portion of the compressive load. This is consistent with the finite element results, which show that slender plates with thicker edges do have a higher compressive strength.

The increase in strength obtainable from using variable thickness plates is potentially interesting to structural design. However, it appears to apply mainly to slender plates that do not achieve a high percentage of the base material strength in compression and, as such, are unlikely to be used in applications where compressive strength is critical. Additionally, within the scope of this project, it was not possible to investigate the performance of variable thickness plates under additional load components, such as lateral pressure or transverse compression. The plates in this study had ideal edge supports, with out-of-plane deformation rigidly constrained along the long edges of the plate. In real ship structures, such plates are likely to be supported by stiffeners, which may not provide edge support as rigid. However, using variable-thickness plate elements in extrusions may yield further weight savings in certain situations, and further investigation of this area is certainly of interest.

2.1.3 Lateral Loading

In addition to carrying in-plane loads, plate elements are often loaded laterally, either by sea pressures acting on the outside of the hull, or because of internal loads from vehicles and accommodation spaces. Unlike compressive collapse, where a plate ceases to be able to support

increases in in-plane loads, true collapse of plate components from lateral loads is difficult to achieve and often occurs only after very large out-of-plane deformations have taken place. Thus, in formulating limit states for plates under lateral loading, it is customary to either specify a level of out-of-plane deformation that will be considered failure, or to limit the working stress in the plate to a certain percentage of the yield stress. These two approaches are known as the permanent set approach and the allowable stress approach, respectively. Both types of approach are reviewed in this study, and methods that implement both approaches are presented and compared. Unfortunately, no experimental results for marine aluminum plates undergoing lateral loads were found, so validation of these approaches is not currently possible.

2.1.3.1 Approaches based on permanent set

Recent limit-state design for lateral loading on plate elements has favored methods that aim to limit the permanent set of plating, or the out-of-plane deformation that remains after the lateral load is removed. Limits on permanent set can be set based on fairness requirements, the need to keep decks smooth for personal and vehicle access, or other design requirements. As exact calculation of the plastic deformation of plates under lateral load, and the resulting "spring back" after load removal is difficult, most permanent set methods use simplified approaches. In this section, both yield-line theory and a method proposed by Hughes are reviewed [17]. Both of these methods were originally developed for steel structures, so their applicability to aluminum is untested. In this regard, the most problematic shortcoming is the inability to consider the weaker HAZ region, which may be located either at the plate edge or, as is common in structural extrusions, down the plate centerline. For welded plates, at the time being the conservative approach is to assume that the entire plate consists of HAZ material.

Yield-line theory (YLT) is a rigid-plastic simplification of the plate large-deflection problem. It was originally developed for concrete slabs in civil engineering [17], but has been extended to ship structures by several authors [17, 18]. In YLT, all elastic deformation are ignored, the plate edges are assumed to be pinned such that large membrane stress can develop in the plate, and a plastic collapse mechanism comprising several yield lines, as shown in Figure 28, is assumed to govern the collapse process. Hughes [17] has shown that these assumptions are best met for slender plates, but, for the majority of plates in conventional steel ships, the assumptions may lead to over-predictions of the load required for a given permanent set, especially when the permanent set is small in comparison to the plate thickness.
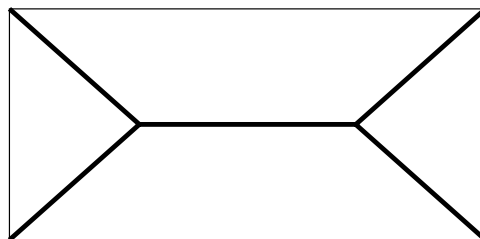
Figure 28: Collapse Yield Lines (Heavy Lines) assumed in YLT

For plates where the edges can be idealized as clamped, the relationship between permanent set and applied pressure is given by Equation 15, which is taken from Kmiecik [18]. In this equation, the uniaxial yield stress is used, although Hughes [17] has extended this to include the multi-axis stress state at the yield lines, resulting in higher strength. While clamped edge

conditions are not appropriate for in-plane loads, when all plate elements forming the shell of grillage are equally loaded laterally (as may be the case with shell plating or a deck undergoing uniform load), the clamped edge assumption is reasonable. For specific vehicle wheel load (patches), simply-supported edges would be a better assumption, and similar formulas for YLT collapse are available in the literature [17, 18].

$$\frac{p}{p_c} = 1 + \frac{w_0^2}{3t^2}\left(\frac{\zeta_0 + (3 - 2\zeta_0)^2}{3 - \zeta_0}\right) if \frac{w_0}{t} \leq 1$$

$$\frac{p}{p_c} = \frac{2w_0}{t}\left(1 + \frac{\zeta_0(2 - \zeta_0)}{3 - \zeta_0}\left[\frac{t^2}{3w_0^2} - 1\right]\right) if \frac{w_0}{t} > 1$$

Where :

$$\alpha = \frac{a}{b}$$

Equation 15

$$\zeta_0 = \frac{\sqrt{3 + \frac{1}{\alpha^2}} - \frac{1}{\alpha}}{\alpha}$$

$$p_c = \frac{12\sigma_y t^2}{b^2\left(\sqrt{3 + \frac{1}{\alpha^2}} - \frac{1}{\alpha}\right)^2}$$

Given the shortcomings of the YLT for stockier plates that are more typical of ship structures, Hughes formulated an alternative methodology for estimating the permanent set of steel plates typical of ship structures [17]. This approach is a semi-empirical expression that extends the edge-hinge forming load for an infinitely long plate, with correction terms for finite aspect ratios and for the experimental shape of the load – the permanent set curve. This approach also assumes that the edges of the plate are free to move-in plane, so that large membrane stresses do not exist. This is more conservative than YLT, and more likely to be the situation in typical vessel structures. Hughes compared his method to several experimental curves, with very good agreement for stockier plates ($\beta < 2$), and conservative predictions for more slender plates where YLT gives optimistic predictions. The implementation of Hughes' method is lengthy, and readers are referred to Hughes' book for details and formulations [17].

2.1.3.2 Approaches based on allowable stress

Given the complexities of estimating permanent set in ship-type plates, many design approaches still rely on allowable-stress formulations. These formulations generally assume elastic behavior, and limit the working stress in the plate under lateral load to a fraction of yield or some value of plastic strain. Often these methods also include empirical coefficients based on experience in service, and corrective terms for plates of finite aspect ratios. Two such methods will be reviewed in this section; a U.S. Navy strength formula recently extended to aluminum plates by Sielski [20]; and a method utilized in the current American Bureau of Shipping *Guide for Building and Classing High Speed Naval Craft - 2007* [21] (ABS HSNC *Guide*).

Sielski [20] presents the U.S. Navy plating design equation for plates undergoing lateral loads in Equation 16, where *b* and *t* are, respectively, the plate breadth and thickness; *C* is a material-specific allowable stress coefficient that has given values for either no permanent set, some permanent set, or a high level of permanent set; *k* is an aspect ratio correction factor; and *h* is lateral load pressure, expressed in feet of water.

$$\frac{b}{t} \le \frac{C}{k\sqrt{h}}$$

Equation 16

The value of *C* varies with the location of the plating on the vessel, with some locations requiring work stresses low enough that no permanent set occurs, and others allowing some permanent set. Sielski [20] explored the derivation of the values of C, and proposed the following values for 6082-T6:

Table 4: Proposed C-Coefficients for 6082-T6 Material (after Sielski [20])

Condition	C
No set	277
Some set	472
More set	604

The ABS HSNC *Guide* [21] specifies a similar allowable-stress formulation, relating allowable material stress (σ_a) to required thickness for a given plate breadth and loading, *p*. Note that the constant 1000 in the formula is a unit-conversion constant, as the rules specify lateral pressures in kN/m^2 while the allowable stress is in MPa. As with the U.S. Navy formula, *k* is an aspect ratio coefficient. As can be seen, the formula is basically the same relation as the U.S. Navy formula, but with different coefficients and an explicit allowable stress (where the U.S. Navy approach includes the allowable stress in the coefficient *C*). In this work, the allowable stress was set at 60% of the base material yield strength, which corresponds to plates subjected to general deck loads in the ABS HSNC Guide.

$$t = b\sqrt{\frac{pk}{1000\sigma_a}}$$

Equation 17

2.1.3.3 Comparison of Methods

The permanent set and allowable stress approaches were compared for two 300mm width 6082-T6 plates with nominal yield strength of 260 MPa. One plate was 5mm thick, the other was 8mm thick. The resulting curves of load vs. set are shown in Figure 29 and Figure 30. In these figures, the allowable stress results are plotted as dashed horizontal lines, as these approaches do not correspond to any specific level of allowable set. In addition to the YLT presented in Equation 15, the modified YLT with a multi-axis yield criteria proposed by Hughes [17] was

included in the comparison. This method is slightly more optimistic than the YLT based on uniaxial yield stress. Both figures show similar behavior, with higher pressures allowed by the permanent set method, and the YLT becoming increasingly optimistic compared to the other methods, especially as the allowable set increases. In this high-set range, the lack of membrane stresses in the Hughes formulation, and the allowable stress formulations, may make them overly-conservative. The ABS allowable stress method and the U.S. Navy "No Set" pressures are very close for both plates; however, the results for allowable permanent sets between 0.5 and 1.0 times the plate thickness are discouraging, as the agreement between methods is quite poor. The U.S. Navy methods which allow some or more set fall below the YLT and Hughes method, which in turn have significant disagreements (though perhaps expected given the assumptions of YLT) for this range of set values. For strength decks, where in-plane loading concerns (and load combinations) will restrict allowable out-of-plane set, either the ABS formula or the U.S. Navy formula for "No Set" seems appropriate. For decks where some set can be tolerated, it is difficult to recommend an approach based on this comparison. The situation becomes more complex if the plate has one or more welded boundaries. Currently, the only demonstrably safe approach to designing such a plate is to assume that the entire plate consists of welded material.
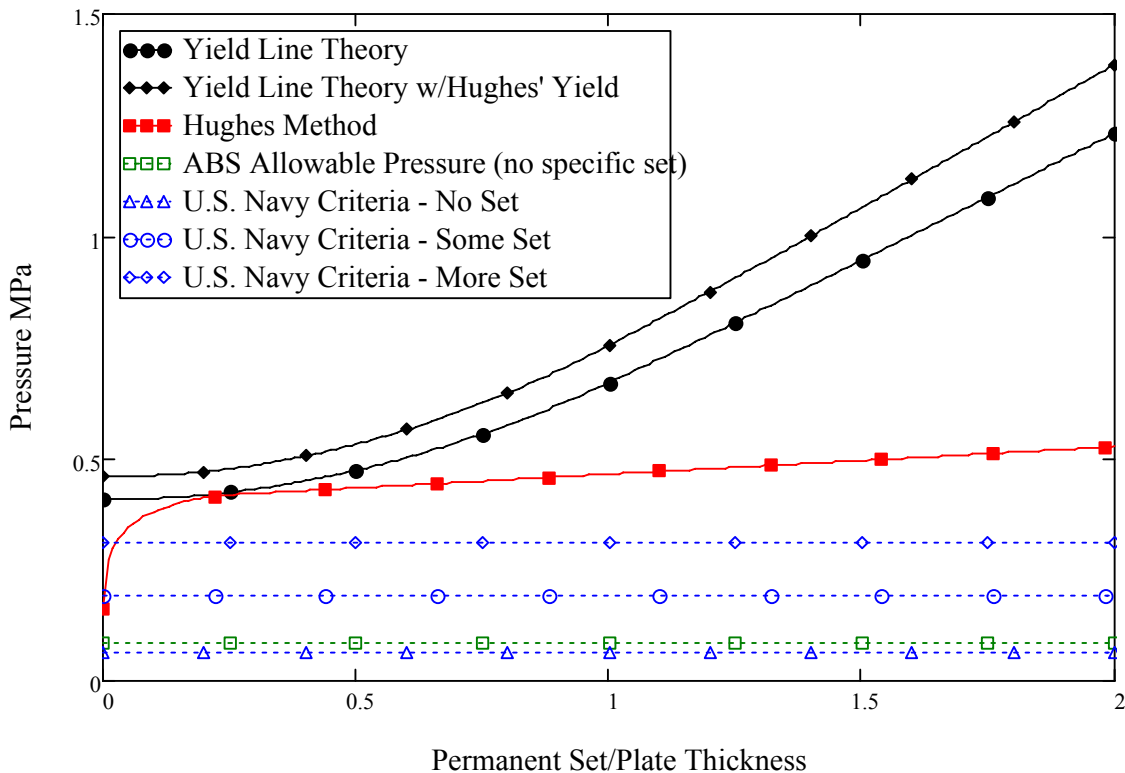
Figure 29: Comparison of Lateral Pressure Approaches for Long Plate with b=300mm, t=5mm

2.1.4 Load Combination

In many situations, plate elements of vessels are loaded in more than one direction at once. In principle, such plates may undergo longitudinal and transverse compression, lateral loading, and in-plane shear loading. In general, analytic formulas for the effect of load combination on ultimate strength are not available, especially where inelastic behavior is involved. Empirical interaction equations are typically used in place of analytic approaches when investigating the

strength of the plate elements under combined loads. Given the problem description for the current project, interaction equations were sought for combined in-plane loads, which will be used in the optimization project.
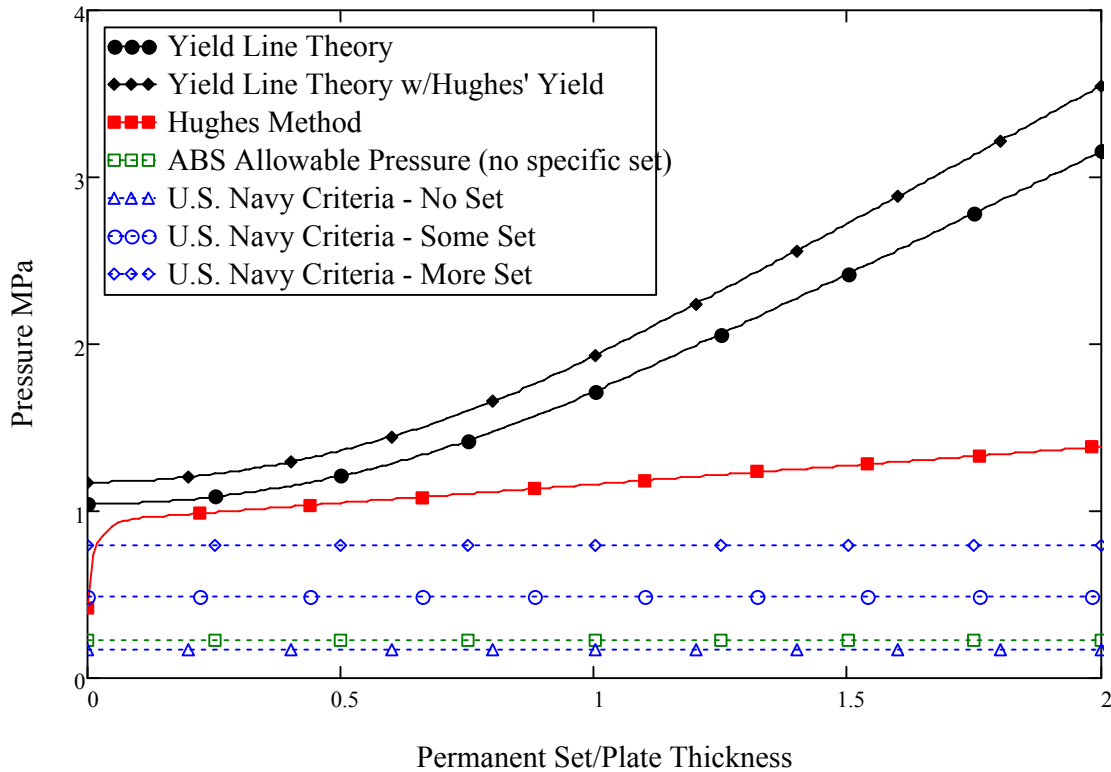
Figure 30: Comparison of Lateral Pressure Approaches for Long Plate with b=300mm, t=8mm

For the combination of in-plane loads, it is typical to construct an interaction curve based on two quantities, R_L and R_T, which are the ratios of the applied load in the longitudinal (R_L) and transverse (R_T) direction to the calculated ultimate strength in longitudinal and transverse directions. The general formula for determining the R values is shown in Equation 18. The equation specifies the combination of R_L and R_T that is required to cause failure.

$$R_x = \frac{Applied\_Load}{Ultimate\_Load} \text{ (in direction x)}$$

Equation 18

A variety of interaction formulas have been proposed. In general, the exact shape of the interaction curve depends on the slenderness of the plate. Very stocky plates will have interaction curves approaching the material multi-axis yield, which would be the von Mises yield criteria for aluminum, while a straight linear interaction appears a reasonable lower bound for very slender plates [17]. These two approaches are shown, respectively, in the top and bottom lines of Equation 19.

$$R_T^2 - R_T R_L + R_L^2 = 1$$
$$R_T + R_L = 1$$

Equation 19

As a general lower bound for steel plates, Stonor et. al [22] proposed the following formula:

$$R_T^{1.5} + R_L^{1.5} = 1 \qquad\qquad\qquad \textbf{Equation 20}$$

Kristensen [12] investigated a series of plates with aspect ratios of 1, 2, 3 and 5, and then developed specific interaction equations for each aspect ratio that also accounted for the plate slenderness ratio, β. These equations were developed by fitting regression equations to non-linear finite element analysis of aluminum plates typical of ship structures. Kristensen used a general interaction formula for all aspect ratios and slenderness values of:

$$R_T^{\zeta} + R_L^{\gamma} = 1 \qquad\qquad\qquad \textbf{Equation 21}$$

Where ζ and γ are given as function of β and the plate aspect ratio in Kristensen's thesis [12]. Kristensen's and Stonor's approaches are compared for six hypothetical plates in Figure 31. The result shows that plate slenderness has a much large impact than aspect ratio, especially as the aspect ratio of most aluminum plates on high-speed craft ranges from three to five. The Stonor interaction equation is not a lower bound for the aluminum plates investigated by Kristensen, but does match the shape of the interaction curve that Kristensen found for slender plates very well, and is significantly simpler than Kristensen's approach. Similar to lateral loading, no experimental investigations of the strength of marine aluminum plates under combined loads could be found. For the time being, Kristensen's interaction formulas appear to be the most comprehensive formulas available, although the error incurred from using Stonor's simpler formula appears slight.

2.1.5 Summary of Plate Response

The performance of plate elements under a wide variety of loads and load combinations has been investigated. Simplified formulas for plate buckling, especially those of the Aluminum Association and the Eurocode 9, do a very good job of predicting the ultimate strength of plate elements in uniaxial compression. In general, methods based on regression fits to finite element simulations performed well, but the underlying data set of finite element simulations used to generate the expression must be respected – both in terms of material and in factors such as weld extents and initial out-of-plane deformations. Methods that did not differentiate between 5xxx-series alloys and 6xxx-series alloys often had larger errors for one material type than the other. Alloy type should be considered in aluminum strength methods. In general, the performance of the uniaxial compression method was strongest at the lower strength (expressed as a proportion of the plate material yield strength) and weakest in the inelastic buckling region, where the plate achieved more than 70% of the base material yield strength. Unfortunately, most strength decks on aluminum vessels will seek to have plate elements in this high-strength region, a fact that should be considered when selecting which method to use.
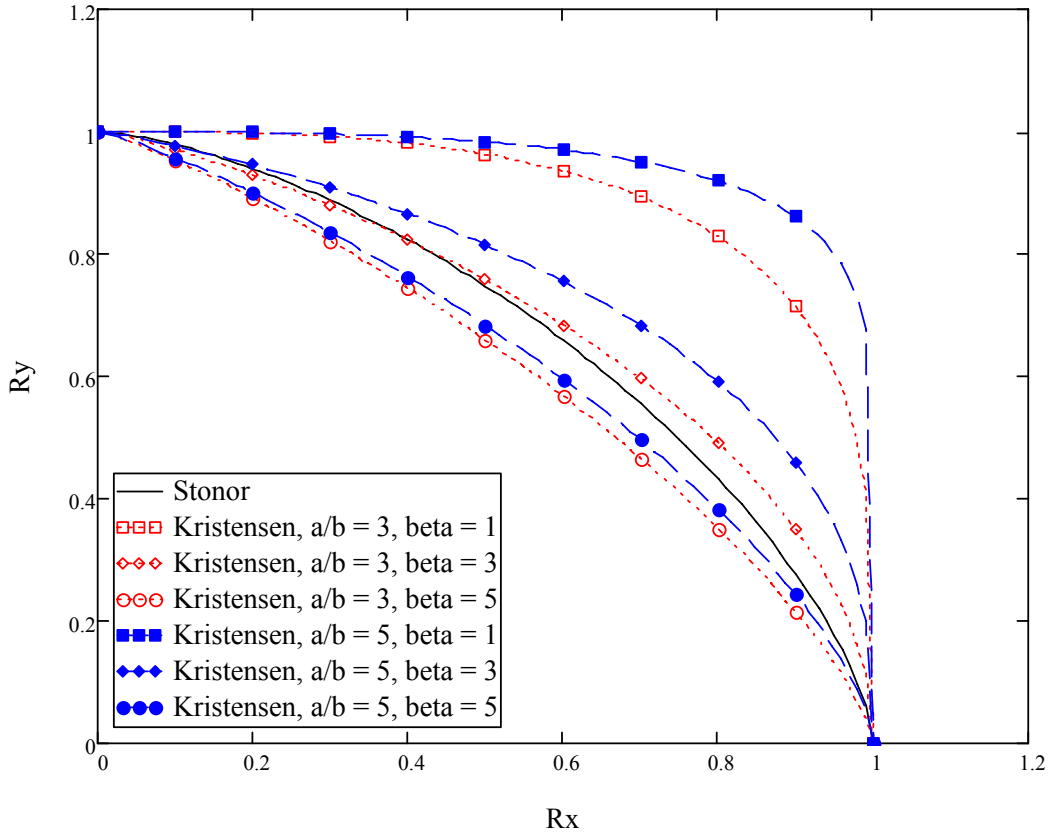
Figure 31: Comparison of Load Interaction Equations for Aluminum Plates

An initial exploration of variable thickness plates with non-linear finite element analysis showed increased post-buckling strength for plates with more material at the plate edges than in the mid-region of the plate. Unfortunately, as the plate strength increases so that the initial buckling of the plate is inelastic, the increase in strength reduces. At a plate slenderness value of 2, the increase was found to be negligible. However, in certain applications variable thickness plates may offer advantages when designing extrusions. Lateral loading and load interaction formulas were investigated, but no experimental results were available to benchmark these approaches. The lateral loading approaches showed a wide difference in the allowable lateral pressure, depending on whether permanent set was allowed or not. Additionally, all methods investigated were originally steel methods and, as such, could not handle welds in aluminum plates short of assuming the entire plate consisted of weld material. Some numerical simulation results were found for in-plane load interaction formulas, which appeared to agree well qualitatively with existing steel formulations.

2.2 Stiffened Panels

In high-speed vessel applications, individual plate elements are typically formed into stiffened panels that span the vessel's frames, carrying both in-plane loads and lateral pressures. In these panels, the individual plate elements act together to resist the applied loading, usually through a combination of beam and column action. In typical vessel structures, the stiffened panel is oriented with the stiffeners running fore and aft, thus carrying the primary longitudinal hull

girder bending in the long direction of the plate elements. However, on smaller vessels a transverse orientation may be used, especially if avoiding deep transverse frames is advantageous for maximizing usable space within the structure. The primary focus of the stiffened panels in this study will be on longitudinally-arranged stiffened panels, which are typical of large high-speed vessels.

In such panels, each plate element will typically be loaded differently. For example, in a conventionally-stiffened panel consisting of shell plating and stiffeners, the shell plate will carry the in-plane shear loads and transverse compressive loads, as well as the longitudinal and lateral loads, while the stiffener will typically only carry the longitudinal and lateral loads. The ability of extrusions, such as the sandwich extrusion shown in Figure 1, to present with different geometries – where additional elements can resist shear and transverse compression – may represent a potential weight savings. In this section, the response of stiffened panels will be examine. The response of the panels to uniaxial compression will be investigated first. Buckling or other failure modes in uniaxial compression is often one of the limiting strengths for stiffened panels, and several simple methods that aim to predict this behavior will be compared to recently-published experimental results. Second, more complex methods that can handle combined lateral loading and in-plane loading will be examined. As with plate elements, experimental data is not available for aluminum stiffened panels under such combined loads, but comparison with the uniaxial compression data set will be made. Many of these methods cannot handle all the different types of extrusions shown in Figure 1. In practice, a naval architect may need to use different approaches for different extrusion types.

2.2.1 Uniaxial Compression

For larger vessels, where hull girder bending is one of the dominant loads on the structure, the compressive response of the vessel's stiffened panel to in-plane loading is often one the governing structural design parameters. Paik and Thayamballi [23] list six principle failure modes of stiffened panels:
- Mode I: Overall collapse of plating and stiffeners as a unit
- Mode II: Biaxial compressive collapse
- Mode III: Beam-column type collapse
- Mode IV: Local buckling of stiffener web
- Mode V: Tripping of stiffeners
- Mode VI: Gross Yielding

In principle, all six failure modes should be checked for each candidate stiffened panel. Even such a check may not be sufficient, as several failure modes may interact; however, such interaction is usually too complex to be captured in any tool short of non-linear finite element analysis. For most structures, where the stiffener and plating have failure stresses that are close to each other, beam-column type collapses may be governing. However, the freedom that extrusion technology offers, to choose the thickness and span of each element individually, means that local failure modes such as Mode IV and V must be carefully investigated.

In this section, simple formulae that attempt to predict the strength of such panels under uniaxial compression will be reviewed. Similar to the plate slenderness parameter β, an equivalent

slenderness parameter, λ, will be introduced that measures the stiffened panel's column behavior, defined as:

$$\lambda = \frac{l}{\pi r}\sqrt{\frac{\sigma_{02}}{E}}$$

$$r = \sqrt{\frac{I}{A}}$$

<div align="right">**Equation 22**</div>

Where I is the panel's moment of inertia calculated from one stiffener and the attached plating, or, in the case of a more complex shape, one extrusion; A is the corresponding cross-sectional area; E is the elastic modulus; l is the panel length; and σ_{02} is the proof stress of the panel material. As these formulas may not specifically address all six failure modes but may focus on the more common failure modes, it is important to use care when using any such method in conjunction with an optimizer. For failure modes that the method may not address, such as local buckling of the stiffener web, it may be necessary to introduce constraints on the optimizer so that such failure modes are "constrained out" of the panel.

2.2.1.1 Experimental Data

Until recently, the amount of aluminum panel test data available in the literature has been quite limited, making rigorous comparison of methods difficult [1]. However, the Ship Structure Committee has recently commission a large series of panel tests under uniaxial compression, lead by Professor Paik of National Pusan University in Korea [11]. These tests covered 78 panels, constructed from 5083, 5383, and 6082 alloys in various combinations, constructed by conventional MIG welding. Stiffeners consisted of extruded Tee-shapes, flat bars, and some constructed Tee-shapes. Extensive measurements of initial imperfection were made. Distributions were fitted to these measurements, and residual stress measurements were made as well. These are all documented in the Ship Structure Committee report [11]. The majority of the panels were of single-bay construction, with four stiffeners with 300mm spacing on a 1,000mm panel width, with unloaded edges left free. Panel lengths ranged from roughly 1,000mm to 1,200mm. A limited number of three-bay panels were tested. These consisted of three 1,000mm long bays, again with four stiffeners on 300mm spacing. Plate thickness ranged from 5mm to 8mm, and stiffener heights of 60mm to 140mm were explored. Sample single-bay and three-bay panels are shown below in Figure 32.

<table>
<tr><td>Single Bay Construction</td><td>Three Bay Construction</td></tr>
</table>

Figure 32: Sample Single and Three-Bay Panels (After [11])

The distribution of the tested panels by their non-dimensional slenderness ratios, β and λ, is shown in Figure 33. As can be seen, three distinct plate slenderness ratios were targeted by the experimental plan. These are fairly slender plates but should be typical of the plating on large high-speed aluminum vessels, especially for deck plates, which tend to be thinner than the shell plating subjected to slamming loads. A wide range of column slenderness ratios was also achieved, which should cover a wide range of failure modes. Indeed, in the report, the failure modes of each panel were recorded along with the failure load, following the six failure mode breakdowns given in Section 2.2.1. A wide mix of failure modes three, four, and five were reported. One potential shortcoming of the test program is that compressive properties were not measured for the 5xxx-series alloys. Such tests are more difficult than typical tension tests but, as discussed in the introduction, the strain-hardening used to strengthen the 5083 and 5383 alloys often results in stronger tensile proof stresses than compressive proof stresses. Compared to 6xxx-extrusions, the residual stress and initial deformations present in the panels tested by SSC-451 are generally expected to be higher than those present in extruded structures where the stiffener-to-plate fillet weld is eliminated.
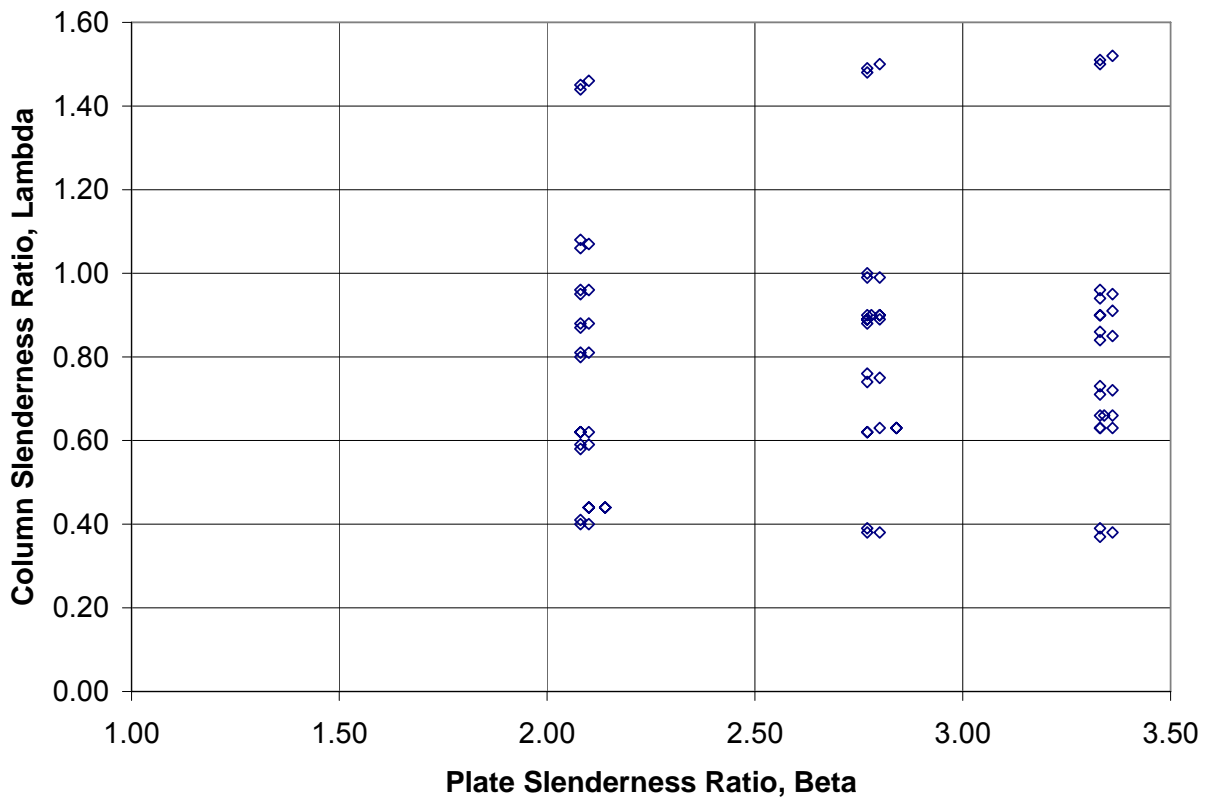
Figure 33: Distribution of Tested Panel in terms of Non-Dimensional Slenderness

2.2.1.2 Paik and Duran Formulation

Paik and Duran [10] addressed stiffened panels as well as plate elements with their finite element studies. All panels were conventional stiffened panels, where stiffeners were welded to plates,

not extrusions. Fifty panels were studied, covering a range of plate slenderness ratio, β, of 1.44 to 3.41 and a λ ratio of 0.23 to 2.24. Initial imperfections were introduced into the plating and the stiffeners. The plating initial imperfection was set to 0.009 times the plate width, as in the plate study, and the initial bow of the overall panel and the sideways twist of the stiffener was assumed to be 0.0025 times the panel length. Reduced-strength regions at the welds were included. All such HAZ regions were assumed to be 25mm wide. No residual stresses were included in the model. Paik and Duran extended the regression formulas they developed for plate elements, which were presented in Equation 7 and Equation 8, for stiffened panels by proposing the following equation:

$$\sigma_U = \frac{\sigma_{Yseq'}}{\sqrt{1.038 + 1.099(\lambda')^2 + 0.093(\beta')^2 - 0.047(\lambda'\beta')^2 + 1.648(\lambda')^4}}$$

$$\sigma_U \le \frac{\sigma_{Yseq'}}{(\lambda')^2}$$

Equation 23

Where the equivalent yield stress includes the influence of the HAZ, and leads to an equivalent λ' value, defined as:

$$\lambda' = \frac{l}{\pi r}\sqrt{\frac{\sigma_{Yseq'}}{E}}$$

Equation 24

Where $\sigma_{Yseq'}$ is the area-averaged proof stress of the panel cross-section, including the HAZ regions and any difference in proof stress between the plate and stiffener. Similar to Paik and Duran's formulation for plates, only 5xxx-series material panels were investigated, so the validity of Equation 23 for 6xxx-series extruded panels is not known.   Additionally, this approach can only be applied to conventional stiffened-panel type extrusions; extension to the hat or sandwich panel type extruded panels is not possible. The formulation was applied to the panels tested by SSC-451. The results are shown below in Figure 34, with a mean bias of 1.10 and a COV of 21.4%. The slightly higher bias and COV may be related to the number of stiffeners that failed by stiffener tripping – especially the flat bar stiffeners. There were no such stiffeners in the finite element data set that was used to generate Equation 23 and, as such, these failure modes are most likely not included in that equation. As part of the SSC-451 project, Paik updated the regression formula with new coefficients that reflect the new test data. This formula has better accuracy and consistency; however, as these coefficients were derived using the current test data, we can not validate the revised equation in this work.
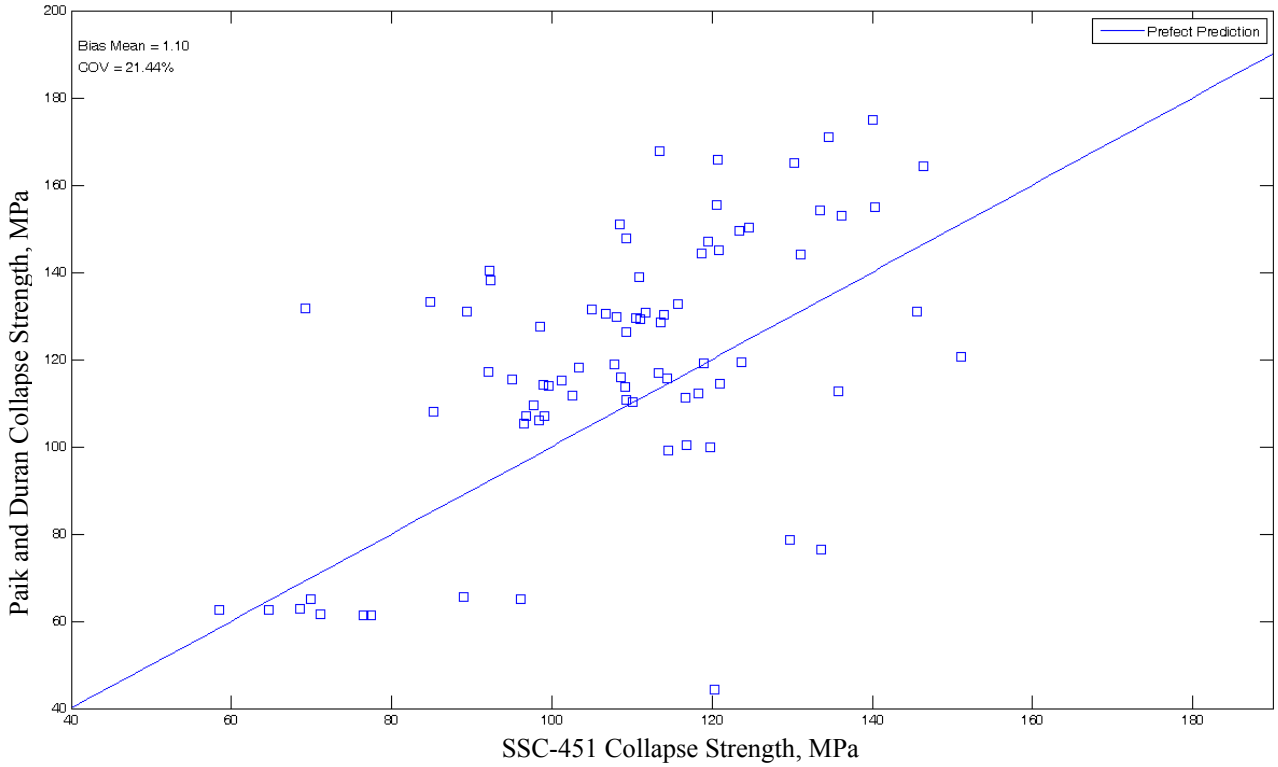
Figure 34: Results for the Paik and Duran Method

2.2.1.3 Wang et al. Formulation

Wang et al. [8] also presented an extension of their plate ultimate strength to column-type failures, using an adaption of the Johnston-Ostenfeld column buckling relation. In this approach, the critical buckling stress, σ_{CR}, can be found as:

$$\sigma_{CR} = \sigma_E \text{ if } \sigma_E \leq 0.5\sigma_{02}$$
$$\sigma_{CR} = \sigma_{02}\left(1 - \frac{\sigma_{02}}{4\sigma_E}\right) \text{if } \sigma_E \leq 0.5\sigma_{02}$$

Equation 25

Where the elastic buckling stress is calculated considering the effective width of the plate elements, using the ultimate strength formula presented in Equation 6:

$$\sigma_E = \frac{EI_E}{CA_El^2}$$

Equation 26

Where C is a unit-conversion constant, l is the panel length, E is the panel elastic modulus, and I_E and A_E are the effective moment of inertia and cross-sectional area, respectively, calculated with the actual plate width, b, replaced by an effective plate width, b_E, which is determined as:

$$b_E = bC$$
$$C = 1 \text{ if } \bar{\beta} \le 1$$
$$C = \frac{2}{\bar{\beta}} - \frac{1}{\bar{\beta}^2} \text{ if } \bar{\beta} > 1$$

Equation 27

The critical buckling stress from Equation 25 should not be directly compared to the ultimate strengths determined in the experimental tests in SSC-451. To extend the method presented in Wang et al. [8] to consider ultimate strength, it is necessary to reference the ABS *Guide for Buckling and Ultimate Strength Assessment for Offshore Structures* [9]. The conversion from column critical buckling stress to stiffened panel ultimate strength is given in Section 3/5.1 of this guide, provided the axial compressive load is applied to the effective cross-sectional area only. It simplifies for cases without lateral loads to:

$$\sigma_U = \frac{A_E}{A} \sigma_{CR}$$

Equation 28

Where A_E is the effective cross-sectional area, as defined for Equation 26, and A is the original cross-section area of the stiffener and attached plating. Wang et al. [8] compared the results of Equation 28 to the results of 56 FEA simulations, carried out on conventionally-welded stiffened aluminum panels. The details of the FEA panels were not presented in the paper, but explored strengths between 60% and 100% of the base material's proof stress. HAZ regions were included, and initial imperfections were included in the primary column failure mode, with an amplitude of 0.15% of the panel's length. Wang et al. reported a mean bias for the method with respect to the FEA data of 0.89, with a COV of roughly 5%, which indicates the method is conservative in general.

To apply this approach to general panel data, it is essential to perform several further checks that can be found in the ABS *Guide for Buckling and Ultimate Strength Assessment for Offshore Structures* [9]. If these additional formulations are not included, over-predictions of strength are a possibility.

1. The stiffener must satisfy the minimum required moment of inertia given in Section 3/9.1 of the ABS *Guide for Buckling and Ultimate Strength Assessment for Offshore Structures:*

$$I_R = \frac{bt^3}{12(1-v^2)} \gamma_0$$
$$\gamma_0 = (2.6 + 4.0\delta)\alpha^2 + 12.4\alpha - 13.2\sqrt{\alpha}$$
$$\delta = \frac{A_S}{bt}$$
$$\alpha = \frac{a}{b}$$

Equation 29

Where I_R is the required stiffener moment of inertia, a is the panel length, A_S is the cross-sectional area of the stiffener without attached plating, v is Poisson's ratio of the material,

and other variables are as previously defined. If the stiffener does not meet this criterion, then the current method can not be applied to the panel.

2. The stiffener must satisfy the following local proportion check on webs and flanges:

$$\frac{b}{t} \leq 0.5\sqrt{\frac{E}{\sigma_{02}}}, \text{For flat bars and outstanding flanges}$$

Equation 30

$$\frac{b}{t} \leq 1.5\sqrt{\frac{E}{\sigma_{02}}}, \text{For internal webs}$$

If the stiffener does not meet these local buckling requirements, it is still possible to apply the method to the panel in question; however, the critical buckling stress may need to be further reduced as discussed in Section 3/5.5 of the ABS *Guide for Buckling and Ultimate Strength Assessment for Offshore Structures.* Note that these formulas were originally developed for steel and do not account for any HAZ that may be present in the stiffener.

3. The ultimate stress must be below the stiffener tripping stress as calculated in Section 3/5.3 of the ABS *Guide for Buckling and Ultimate Strength Assessment for Offshore Structures.* Also note that the formula to evaluate the tripping stress was originally developed for steel, and HAZ effect was not taken into account.

Applying this method to the panel test results from SSC-451 indicated that 12 panels failed the minimum stiffener moment of inertia requirement given in Equation 29. These panels were removed from the experimental results used for comparison. The results for the remaining 66 panels are given in Figure 35. Of these remaining panels, a further 21 – primarily the flat-bar stiffened panels – failed stiffener web proportion checks and were further evaluated based on local web buckling criteria. As can be seen, the method performs quite well with a mean bias of 1.07 and COV of 15%.

2.2.1.4 Summary of Uniaxial Methods

Two simplified uniaxial methods were compared to the SSC-451 panel data test. Both methods were developed and verified based on finite element analysis of stiffened panel and plate data, but neither FEA set included all types of panels tested during the SSC-451 project. The Paik and Duran method performed reasonably but had a fairly large COV. By extending the published Wang et al. method to include the additional buckling formulations from the ABS *Guide for Buckling and Ultimate Strength Assessment for Offshore Structures,* a more consistent prediction was achieved. However, this indicates a potential problem in selecting which method to apply as part of an optimization routine – the methods need to address all potential failure modes of the panel types considered, or the optimizer will need to be constrained to produce panels similar to the panels used to develop and verify the method. As the goal in extrusion design is to explore novel panel arrangements, such constraints are likely to interfere with the primary objective of saving weight. Therefore, it appears that simplified panel collapse methods alone are probably not best suited for use with structural design optimizers. These methods remain valuable for preliminary design work and for strength checks on proposed designs to confirm that the results of more advanced approaches are reasonable.
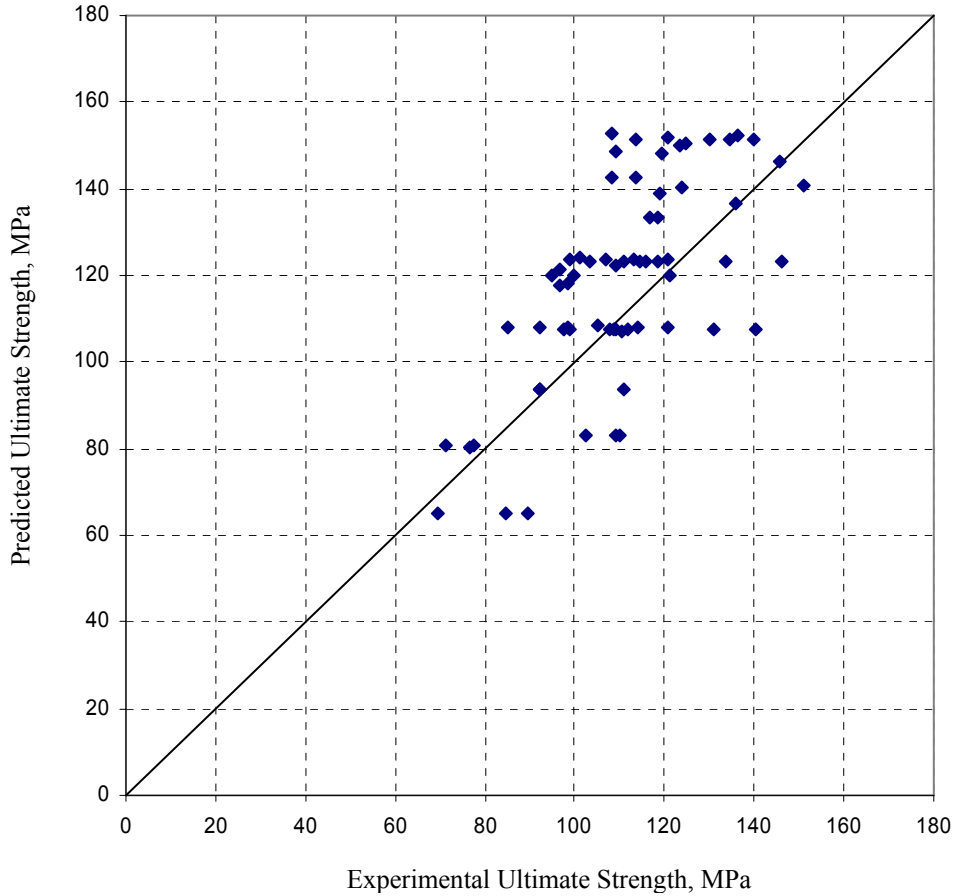
Figure 35: Results for the Wang et al. Method

2.2.2 In-Plane and Lateral Loads

Several authors have proposed methods for investigating stiffened panels under combined in-plane and lateral loads. Most of these methods idealize a single "unit" of a stiffened panel, consisting of a single stiffener and attached plating, acting as an independent beam-column spanning the distance between transverse frames. For non-conventional extruded panels, the basic repeating shape of the extrusion can be idealized as the beam-column "unit". In this section, two different approaches to this beam-column formulation will be reviewed: first, a method developed by Hughes [17] for conventional steel panels; and, second, an adaptation of the U.S. Aluminum Association design code for beam-columns for conventional panels and extrusions. These methods will be compared to the test data from SSC-451 for uniaxial compression. Unfortunately, no test data was found for panels loaded by in-plane loads and lateral loads simultaneously.

2.2.2.1 Hughes Method

Hughes [17] developed a collapse methodology for conventional steel stiffened panels using the beam-column approach. In this approach, three explicit failure modes are checked, and the lowest failure mode is taken as limiting. The three failure modes were defined as:

- Mode I: Failure induced by yielding in the stiffener flange, which occurs when the panel lateral load places the stiffener flange in compression, which is further increased by the in-plane loading.
- Mode II: Failure induced by compressive collapse in the plate, which can occur when the plate is placed in compression by the applied lateral load or, in cases of weak plates, from the in-plane loading alone regardless of the direction of the applied lateral loading.
- Mode III: A combined failure of the plating in compression and the stiffener flange in tension. This occurs when large tensile stresses are caused in the stiffener flange from the applied lateral loading.

For all three failure modes, Hughes adapts the basic elastic beam-column formula as a starting point:

$$\sigma = \sigma_a + \frac{M_0 y}{I} + \frac{\sigma_a A (\delta_0 + \Delta) y}{I} \phi \qquad \textbf{Equation 31}$$

Failure is assumed to occur when the resulting stress, σ, reaches a pre-defined value, typically the yield or proof stress of the material. σ_a is the applied in-plane compressive loading, y is the distance from the neutral axis to the location of interest, M_0 is the applied bending moment, A and I are the cross-sectional area and moment of inertia of the beam-column, δ_0 is the deflection from the lateral loading, Δ is the initial column-type imperfection, and ϕ is magnification factor on the deflection from the applied lateral loads. For Mode I, the case of tensile failure in the stiffener flange, this formula can be applied as-is, as the amount of inelastic response before failure is small. However, for Modes II and III, the buckling of the plate requires a more advanced approach, and Hughes proposes an effective width approach based on empirical relations for steel plates. Details of the approach to Mode II and III can be found in *Ship Structural Design*[17].

The Hughes method was applied to panels in SSC-451. As no lateral loading was present in these panels, only Modes I and II were calculated. However, the Hughes effective width treatment of the plate is based on empirical relationships developed for steel, which was seen as a potential weakness in applying the method to aluminum. Two variants of the method were carried out, where:

- The Hughes plate strength equation was replaced by the Aluminum Association plate strength formula reviewed in Section 2.1.2.6.
- The Hughes plate strength equation was replaced by the Aluminum Association plate strength formula and, furthermore, the effective width formula for the plate was replaced by Faulkner's [7] effective width formula.

The results are shown in Figure 36. Overall, the method performed fairly well, with mean bias less than 10% and a lower COV than the simplified methods. Replacing the plate strength formulas and effective breadth relations had negligible effects on the performance of the method, as the bias was only slightly reduced, at a cost of a slightly higher COV. Unlike the plate

methods, which seem to have more variable prediction accuracy for the stockier plates, the prediction variability for the Hughes method appears to be fairly constant over a wide range of strengths. The concerns over proof stresses supplied for 5xxx-series alloys in the SSC-451 test program remains, and this may have had an impact on the predicted panel strengths. Moreover, the lack of an explicit stiffener tripping check may have contributed to the slight non-conservative bias shown in the method as well. This method is not easily extendable to more complex extrusions, as it was developed assuming that only one plate element in the panel would undergo buckling before the ultimate strength of the panel was reached. However, it is a useful option for conventional panels and extrusions that feature stiffener profiles.
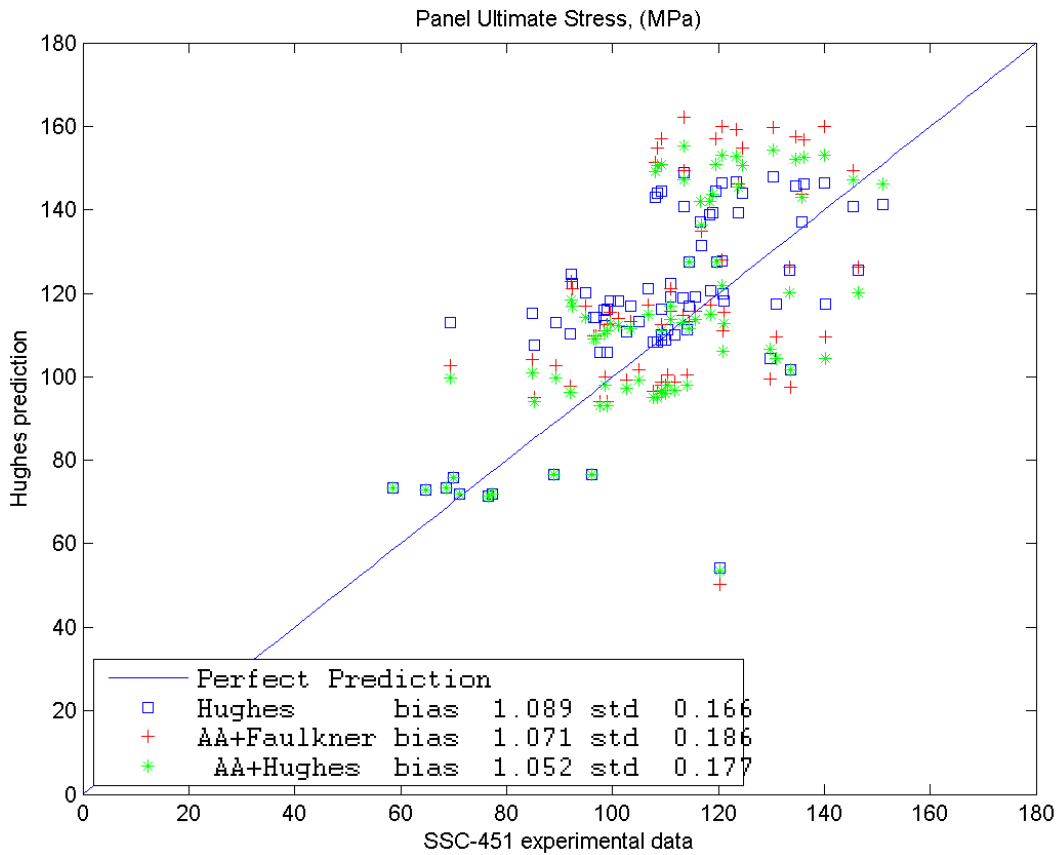
Figure 36: Comparison Hughes' Method to Panel Collapse Test Data

2.2.2.2 Aluminum Association Method

The U.S. Aluminum Association has published formulas for beam and column action in its *Specification for Aluminum Structures* as part of the *Aluminum Design Manual* [13] (the *Specification*). While this section does not explicitly address the modeling of stiffened panels as beam-columns, the individual strength formulations within the specification can be assembled into a formulation capable of addressing the principle failure modes of such panels. This has the advantage that such formulations can be extended to extruded shapes as well as conventional plate-and-stiffener panels.

The approach developed considers beam and column action separately, and uses an interaction equation to combine the two sources of loading. For column behavior, the governing strength was taken as the least of the following three strengths:

- The strength of the overall combination as a column. This was calculated following the formulas in Section 3.4.7 of the *Specification*, which use the column slenderness parameter, λ, as a way of dividing up the column failures into regions. In these regions, the column can reach the full material proof stress where inelastic buckling occurs, and also where elastic buckling occurs, following a similar arrangement to that used for plates, as shown in Equation 13. For cases where the panel consists of both 5xxx and 6xxx series alloys, volume-averaged material properties were used in these calculations.
- The area-averaged local plate buckling strength of all plate elements in the column cross-section, with each plate strength calculated in accordance with Equation 13. This is defined in Section 4.7.2 of the *Specification*.
- Local-overall buckling interaction as defined in Section 4.7.4 of the *Specification*. This was assumed to occur only when the elastic buckling strength of a plate element in the column is less than the elastic buckling strength over the overall column. In these cases, the strength of the column was calculated in accordance with Equation 32, where the partial safety factors included in the design code have been removed for clarity. σ_{EC} is the elastic buckling stress of the column, and σ_{RC} is the lowest elastic buckling stress of any sub-component of the column.

$$\sigma_U = \sigma_{EC}^{1/3} \sigma_{RC}^{2/3}$$
Equation 32

In a similar fashion, the bending strength of the panel as a beam was calculated using the beam strength formulations in the *Specification*. Simply-supported end conditions were assumed. The beam limitations consisted of:

- Calculating the applied moment that would result in tensile yielding of the extrusion, in accordance with Section 3.4.2 of the *Specification*.
- Calculating the applied moment that would cause compressive collapse of each flat plate element in the cross-section, in accordance with Section 3.4.15/16 of the *Specification*.
- Calculating the applied moment that would cause compressive collapse of the vertical plate elements (webs) in the cross section that are bending in their own plane, in accordance with Section 3.4.18 of the *Specification*.
- Calculating the lowest shear buckling capability of the vertical plate elements (webs). This was taken as the limiting shear stress, calculated in accordance with Section 3.4.20 of the *Specification*. A corresponding applied moment was calculated assuming the shear force was uniformly distributed over the web elements of the extrusion. This is a simplification, but fairly accurate, given that details of the end connections of the panel were not included in this study.

Limiting stresses were reduced to include the impact of welds when the weld cross-sectional area was more that 15% of the panel gross area for column buckling, or more than 15% of the flange area for bending, where the flange is defined as the material falling more than two-thirds of the distance from the neutral axis to the extreme fiber away from the neutral axis. This was done by

using the weighted-average stress approach presented in Section 7.2 of the *Specification*, and is shown in Equation 33.

$$\sigma_{U\_W} = \sigma_{NW} - \frac{A_W}{A}(\sigma_{NW} - \sigma_{AW})$$

Equation 33

Where σ_{U_W} is the final strength of the component considering the weld, σ_{NW} is the strength of the component as if it had no welds, σ_{AW} is the strength of the component as if it were entirely composed of welded material, A_W is the weld cross-sectional area, and A is the cross sectional area either of the entire panel (for columns), or of the relevant flange (for beam action).

For the cases where lateral pressure and in-plane loads co-exist, interaction equations were used to determine the limiting loads. First, two interaction equations from Section 4.1.1 of the *Specification* were checked, which deal with overall combined bending and in-plane loads. These equations were simplified, as there is only bending in one direction:

$$\frac{f_a}{F_A} + \frac{Cf_b}{F_B\left(1 - \frac{f_a}{F_E}\right)} \leq 1.0$$

$$\frac{f_a}{F_{AVG}} + \frac{f_b}{F_B} \leq 1.0$$

Equation 34

Where f_a is the applied in-plane compressive stress, F_A is the limiting in-plane compressive stress with no other loads acting, f_b is the applied bending compressive stress and F_B is the limiting compressive bending stress. F_E is the elastic buckling stress of the beam-column unit as a column, C, is an interaction coefficient, and F_{AVG} is the limiting column stress calculated from the area-average compressive strength of each element of the column only. In addition to the combined bending and compression, the webs of the beam-column unit were checked for combined shear and compression, using the formula given in Section 4.4 of the *Specification*.

$$\frac{f_a}{F_A} + \left(\frac{f_s}{F_S}\right)^2 \leq 1.0$$

Equation 35

Where f_s is the applied shear stress, F_S is the limiting shear stress with no other loads acting, and all other variables are as above.

The methodology developed by the Aluminum Association was applied to the panels from SSC-451, which were loaded in axial compression only. Thus, the limiting strength was calculated as the lowest strength from Sections 3.4.7, 4.7.2, and 4.7.4 of the *Specification*. In implementing this approach, all partial safety factors were set as equal to 1.0. The results are shown in Figure 37, where a perfect prediction is again shown as a heavy line. The method has a mean bias of 1.20, and a COV of 0.16. The results are slightly more optimistic than the Hughes' method, explored in the previous section, and the over-prediction appears to grow as the failure stress approaches the proof strength of the material. Some of the over-prediction may be a result of the lack of a true tripping failure mode check in the portions of the Aluminum Association code implemented in the current study – such lateral instability of the entire stiffener about its point of attachment would be expected to lower the failure stresses. Another potential shortcoming is the

reliance on tensile strength measurements of the proof strength, as discussed when reviewing the experimental data. For 5xxx-series alloys with significant strain hardening, the compressive proof stress may be 15%-20% below the tensile yield, as indicated in material properties suggested in the Aluminum Association *Specification*. As an experiment, the compressive proof stress of the 5083 and 5383 materials were reduced by 15%, and the calculation was re-run. This resulted in a slightly lower mean bias of 1.12 and a COV of 15%. The results from this run are shown Figure 38, which also shows that the increasing over-prediction at higher stresses has now been reduced. It still appears that the method is generally slightly non-conservative, which may be a result of missing failure modes, as several of the SSC-451 panels failed via stiffener tripping. In actual applications, the partial safety factor specified by the code would further reduce the predicted strength, so the over-prediction shown here may not be present in actual code predictions for structures.
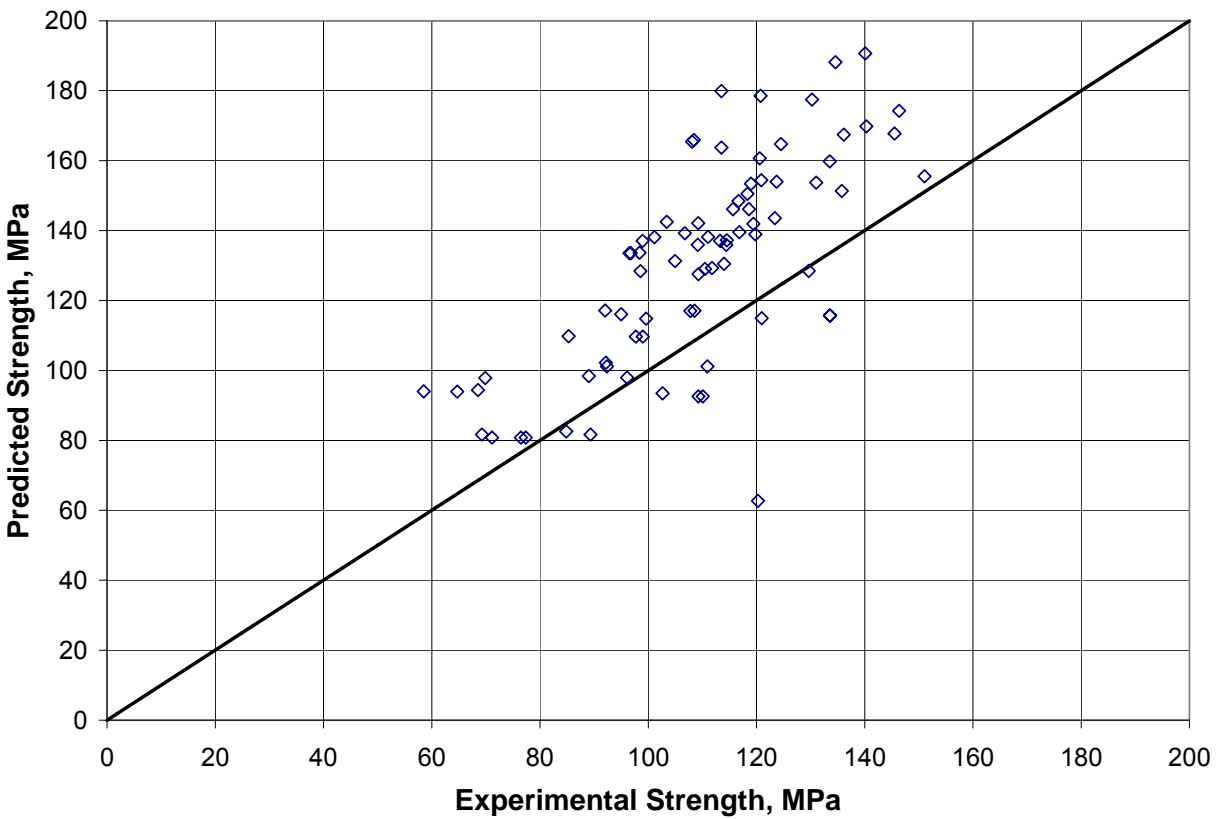
Figure 37: Comparison of Aluminum Association Code and SSC-451 Data
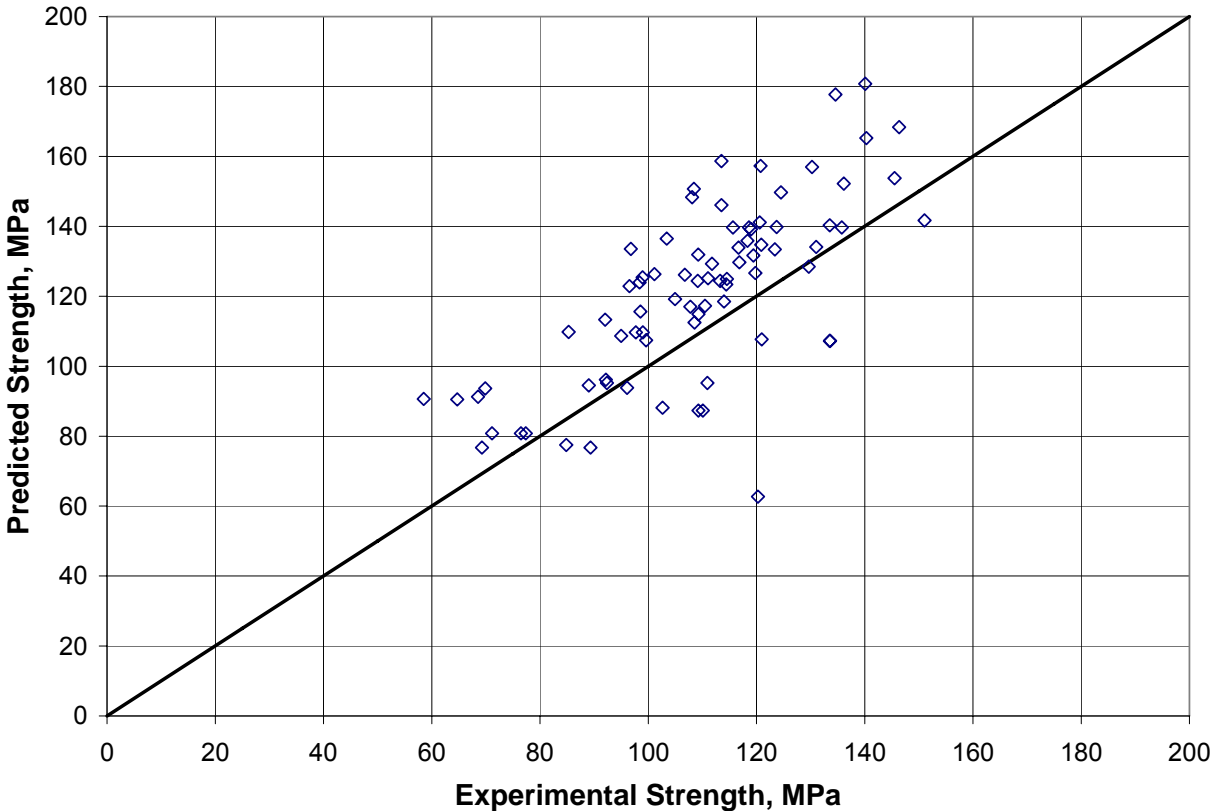
Figure 38: Comparison of Aluminum Association Code and SSC-451 Data, 5xxx-Series Alloys Proof Stress Reduced 15%

2.2.2.3 Summary for Methods Capable of In-Plane and Lateral Loads

The two beam-column approaches reviewed in this section had fairly good performance when compared to the experimental data in SSC-451, being notably more consistent than the simplified uniaxial compressive collapse only method. However, both methods were slightly non-conservative with respect to the SSC-451 panel data. Neither the Hughes method, as implemented here, nor the Aluminum Association method includes stiffener tripping, though Hughes [17] shows how the method can be extended to include such failure modes. As a number of the experimental panels failed via stiffener tripping, this lack of a tripping method may have been part of the reason for the over-prediction. An additional source of the over-prediction may be the reliance on tensile coupons to determine the proof stress of the aluminum material in the SSC-451 study. As 5xxx-series alloys often have lower proof stresses in compression, some of the stockier panels may be been given too much credit for their material strength, leading to high strength predictions.

Unfortunately, there are still no experimental tests on aluminum panels with lateral loads, and the tests on complex extrusions that were found were very limited and often tested with inconsistent boundary conditions that made validation efforts difficult. Of the two methods reviewed, either one is capable of handling lateral loads, but only the Aluminum Association approach has the necessary tools to handle complex extrusions such as hat and sandwich type panels. Given this situation, it is likely that any practical design efforts for custom aluminum extrusions would need

to embark on limited experimental testing or assign a sufficient safety factor to remove the non-conservative bias. Further refining the two methods reviewed to include stiffener tripping may also remove their non-conservative bias enough that either method could be used in a design setting.

2.3 Aluminum Extrusion Production Limitations

In addition to predicting the strength of aluminum extrusions, making sure the proposed extrusion is practical to produce is an important element of the overall extrusion design. While aluminum in general, and the 6xxx-series alloys in particular, are generally easy to extrude, there are some important factors that impact the cost of producing aluminum extrusions. Several excellent resources are available on aluminum extrusion, including a large section describing the process in the Ship Structure Committee report SSC-452 [20]. Further information on aluminum extruding is available from the Aluminum Extruders Council, including the *Aluminum Extrusion Manual* [24] that gives a very good overview of the extrusion process along with more detailed engineering information. Free resources are also available from Hydro Aluminum [25] and a number of other sources on the web [26, 27].

While there are many factors that influence the cost of manufacturing aluminum extrusions, perhaps three of the most significant for marine design are:

1. **Selection of extrusion alloy:** While it is possible to extrude 5xxx-series alloys such as 5083 and 5383, they are much more difficult to extrude and are difficult or impossible to form into complex hollow shapes such as the sandwich-type panel. Additionally, wall thickness typically must be significantly higher for 5xxx-series alloys. For this reason, the work in this study will focus on 6xxx-series alloys.
2. **Minimum circumscribing circle diameter (CCD)**: The minimum CCD is the smallest circle that can be drawn around the extrusion cross-section. This diameter determines the size of the die and press that will be required to form the extrusion. There are a large number of presses with CCD of roughly 12" or less, making smaller shapes easier and less expensive to produce than larger shapes.
3. **Hollow vs. solid shapes:** Shapes that are hollow or feature enclosed voids, such as the hat-shaped stiffener and the sandwich panel of Figure 1, are more expensive to produce than solid shapes, such as an extruded stiffener and attached plates. The hollow shapes are normally produced with a multi-part die that has a series of ports to allow the hollow voids to be produced.

In general, there is a relationship between the minimum CCD and the minimum wall thickness that can be produced in an extrusion. This relationship varies with alloy, and also with presses, as some presses are set up to extruded thin, rectangular shapes more efficiently than the shape's minimum CCD would indicate. In general, hollow extrusions require larger wall thickness than solid extrusions. Several different "rule of thumb" relationships between CCD and minimum wall thickness were discovered in the literature [25,26,27]. These have been plotted on a common set of axes in Figure 39. For most sections of roughly 12", or 300mm, CCD, the minimum wall thickness appears to be between 2mm and 3mm for solid shapes, and between 4mm and 5mm for hollow shapes.
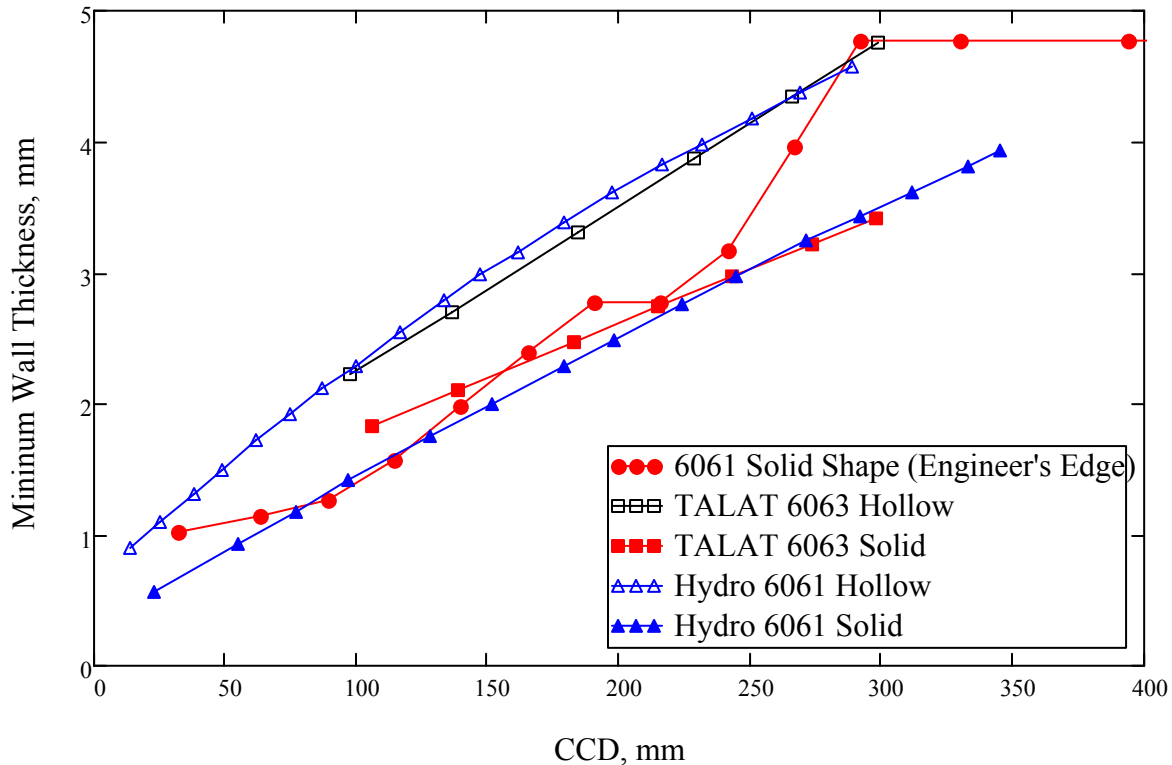
Figure 39: Comparison of Generic Wall Thickness to CCD Relationships

These wall thickness values seem conservative based on the extrusions in use today. In a recent paper [28], marine-specific extrusions were proposed with wall thicknesses less than 3mm for hollow sandwich-type extrusions over 600mm wide. In SSC-452 [20], similar thicknesses are noted for hollow extrusions. These are probably the result of specific presses and processes optimized for such shapes, and as such the designer of a hollow-type extrusion would be advised to work closely with the operators at the targeted extrusions presses to be sure that specific wall-thickness limitations for the project are established. Based on these observations, it seems reasonable to establish a lower limit for wall thickness in the 2mm-3mm range for this project. Reviewing the presses available in the U.S., it seems that 16"/406mm is a reasonable upper-bound on the extrusion circle, and hence the maximum stiffener spacing for the optimization to follow in Section 4. Further restricting the CCD to 12"/300mm would allow a wider range of presses to be used, and may be more practical for compact shapes such as the extruded stiffener and attached plate.

In addition to the three major production factors reviewed above, there are additional refinements that can be made to the extrusion shape to ensure ease of production. In general, it is desirable to keep a balanced material flow through all areas of the die. This is fairly easy to achieve in marine profiles, as the sections generally have at least one axis of symmetry. However, a further optimization constraint that is recommended is keeping the ratio of the wall thickness of adjacent members of the cross section to less than or equal to 2:1. While close cooperation with the extrusion producer of choice is recommended for real-world design problems, the limitations discussed in this section should sufficiently constrain the optimization process such that realistic extrusion cross-sections will result from the optimization process.

3 Optimization Techniques

3.1 Multi-Objective Optimization

3.1.1 Background

In the real world it is rare for any problem to have only a single objective. Optimization problems often have to consider many objectives, and we thus have multi-objective (MO) optimization. A trade-off between the objectives exists, and we rarely have a situation in which all the objectives can be satisfied simultaneously. MO optimization provides the information about the different possible alternative solutions that can be achieved for a given set of objectives. By analyzing the spectrum of solutions, the most appropriate solution can be selected. In this study, we use a genetic algorithm-based approach to find a set of alternative solutions, and present the range of possible solutions to the reader.

The MO problem (also called multi-criteria optimization or vector optimization), can be defined as the problem of determining a vector of decision variables that satisfies a set of constraints and optimizes a vector function whose elements represent "M" objective functions. These functions form a mathematical description of performance criteria that are usually in conflict with each other. Hence, MO means searching for a set of solutions that would give the most acceptable results for all of the objective functions. Mathematically, MO can be formulated as in Equation 36.

$$\min \boldsymbol{F}(\mathbf{x}) = \{f_m(\mathbf{x})\}, \qquad m = 1,2,\cdots,M$$
$$\text{s.t. } g_j(\mathbf{x}) \le 0, \qquad j = 1,2,\cdots,J$$
$$h_k(\mathbf{x}) = 0, \qquad k = 1,2,\cdots,K$$
$$x_i^L \le x_i \le x_i^U \qquad i = 1,2,\cdots,n$$
$$\mathbf{x} = (x_1, x_2, \cdots, x_n)^T$$

Equation 36

Decision variables x_i, $i=1,...,n$ form an n-dimension design space in which values are chosen in an optimization problem. In order to know how good a certain solution is, we need to have some criteria for evaluation. These criteria are expressed as computable functions $f_1(\mathbf{x}),...f_m(\mathbf{x})$ of the decision variables, which are called objective functions. These form a vector $\boldsymbol{F}(\mathbf{x})$. In general, some of these will be in conflict with others, and some will have to be minimized while others are maximized. The MO problem can be now defined as finding the vector $\mathbf{x}=(x_1, x_2,..., x_n)^T$, i.e. finding a solution that optimizes the vector function $\boldsymbol{F}$.

The constraints define the feasible region $\mathbf{x}$, and any point $\mathbf{x}$ defines a feasible solution. Generally, constraints can be categorized into two groups: inequality constraints and equality constraints. The vector function $\boldsymbol{F}(\mathbf{x})$ is a function that maps the set $\mathbf{x}$ into the set $\boldsymbol{F}$ that represents all possible values of the objective function. Normally, we would never have a situation in which all the $f_m(\mathbf{x})$ values have an optimum in $\mathbf{x}$ at a common point $\mathbf{x}$. We therefore

have to establish certain criteria to determine what would be considered an optimal solution. One interpretation of the term optimum in multi-objective optimization is the Pareto optimum.

3.1.2 Pareto Optimality

Before explaining Pareto optimality, let's define the concept of **domination**: Solution x_1 dominates solution x_2 if: (1) x_1 is no worse than x_2 in all objectives; and (2) x_1 is strictly better than x_2 in at least one objective.

By this definition, one says that **x*** is Pareto optimal if there does not exist another feasible solution in the entire design space that would decrease some objectives without causing a simultaneous increase in at least one other objective. Unfortunately, this concept almost always gives not a single solution but, rather, a set of solutions called the Pareto optimal set. The solutions included in the Pareto optimal set are called non-dominated. The plot of the objective functions whose non-dominated vectors are in the Pareto optimal set is called the Pareto front. Figure 40 shows the Pareto front in a 2-objective problem that minimizes both objectives. Solutions A and B are non-dominated, but C is dominated by both A and B.
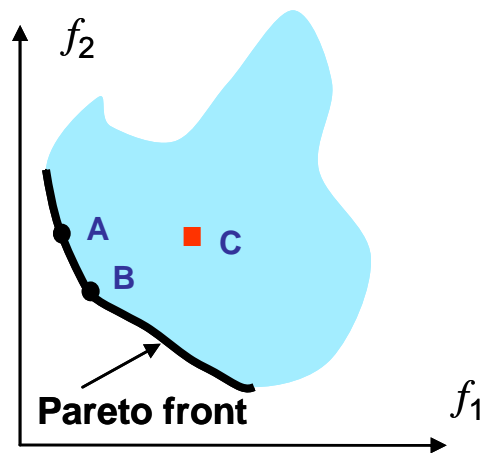
Figure 40: Pareto Front and Domination

3.1.3 Approach

There are many classic methods for solving multi-objective optimization problems, but the primary method is by converting a multi-objective optimization program into a single objective one. Some of popular methods include Weighted Sum, ε-Constraint, and Goal Programming, among others. One of the major problems with these methods is that, if successful, a single run would produce only one solution. In other words, to find a set of Pareto optimal solutions, a series of runs – manipulating a set of additional parameters, such as the weights used by Weight Sum method and ε values by ε-Constraint method – is necessary. Another major drawback for some of the classic methods (e.g., Weighted Sum) is that they will fail to find all the Pareto optimal solutions of non-convex problems.

In the last 10 to 15 years, evolution-based algorithms have become more and more mature and popular for both single and multi-objective optimization. Evolution-based algorithms use a different search strategy; instead of point-by-point search, they conduct searches in multiple points simultaneously, using operators inspired by evolution, such as crossover and mutation to

produce offspring, and by applying selection pressure to evolve multiple search points for optimal solutions.

3.2   Multi-Objective Genetic Algorithm

There exist many different evolution-based algorithms that have proved capable of tackling a wide variety of real world problems. In this study, we use a version of multi-objective genetic algorithm (MOGA) that implements elitism strategy and non-dominated sorting (the so-called NSGA-II approach[29]). There are two main advantages with MOGA. First of all, MOGA deals simultaneously with a set of possible solutions (the so-called population) that generally results in discovering multiple members of the Pareto optimal set in a single optimizer run. Secondly, MOGA can easily handle discontinuous and/or non-convex Pareto fronts.

To implement MOGA, a coding strategy must be selected to encode the design variables in a certain structure (e.g., vector or matrix) that forms what is called a chromosome or individual. Two coding strategies are widely used; one is the classical binary coding, the other is real-value-based coding. The binary or real elements in a chromosome are usually called genes. In most cases, a predefined number of individuals is randomly generated to constitute the population, and the population number is kept constant throughout the entire search process. The duration of the search process is defined by the number of generations of the population that the method creates. Three types of genetic operators are usually used to generate new search points and form new generations: crossover, mutation and selection. Crossover is used to produce two offspring individuals from two randomly selected parents. Mutation is used to alter one or more randomly selected genes of a chromosome. A selection operator is used to pick individuals in a population with higher fitness values (e.g., objective values) to create the next generation.

To briefly illustrate how MOGA works, a flow chart is provided in Figure 41 using the binary coding strategy. As can be seen, design variables are coded as a binary vector chromosome. A certain number of chromosomes is predetermined and initially randomly generated to form the current population. For each chromosome, a fitness evaluation is performed to assign a fitness value as a base to carry out ranking among individuals. Fitness evaluation in MOGA involves computing every objective value given an individual. Crossover and mutation then operate on the current population to produce offspring. The elitist non-dominated sorting algorithm in Deb [29] is used as the selection procedure to create the next population. The key issues with MOGA are to make sure that the selection pressure from the fitness and elitist sorting methods causes the solution to approach the true Pareto front while, at the same time, maintaining sufficient diversity in the population so the approach does not become trapped in local optima or converge to a few sparsely scattered solutions. The elitist non-dominated sorting algorithm has proven quite robust (refer to Deb [29] for details).
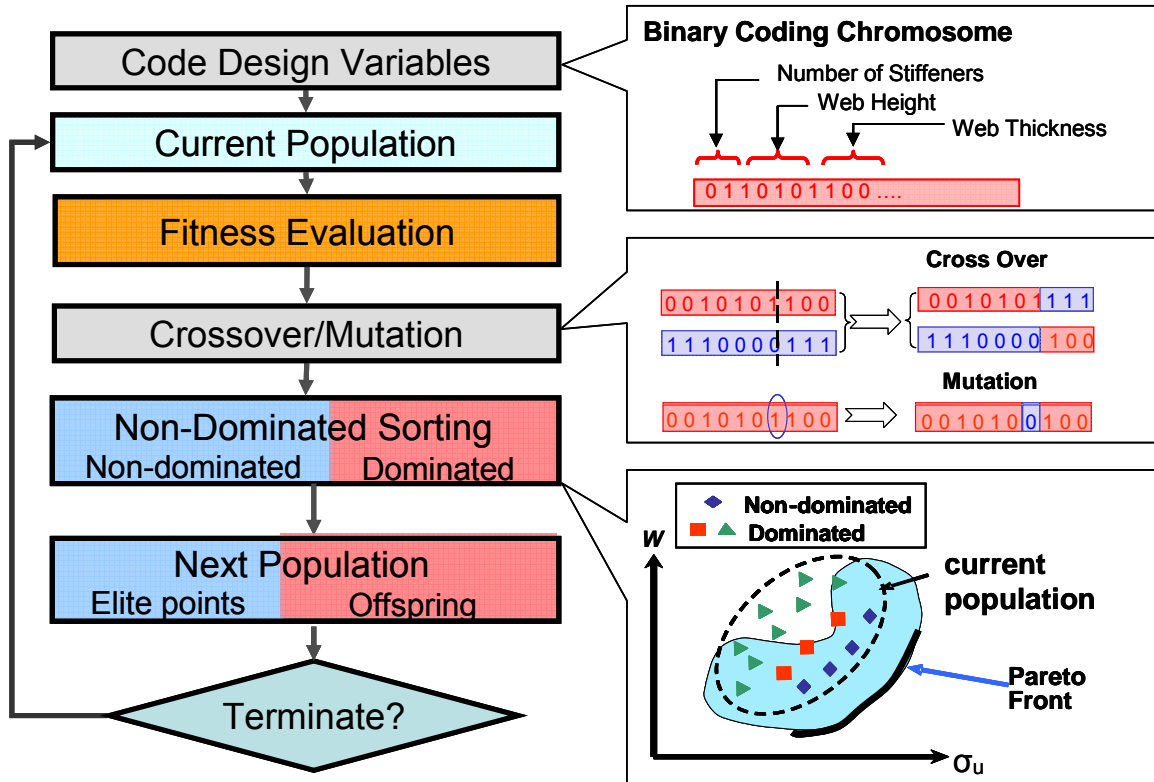
Figure 41: Multi-Objective Genetic Algorithm

A real-coded MOGA was implemented in C++ for this study using the elitist non-dominated sorting algorithm described in Deb [29]. We chose the real value coding strategy since most engineering problems involve continuous variables. The use of real coded genes allows us to achieve arbitrary precision in the design space and also to avoid the Hamming cliffs effects associated with binary-coded genetic algorithms. Hamming cliffs arise due to significant change in real value by altering just a single bit (such as 10000 to 00000 by flipping the left-most bit from 1 to 0) in a binary coded chromosome, which hinders a smooth search in continuous variable space.

Two specific genetic operators were developed for the real valued chromosome: arithmetic crossover and delta mutation (Li [30]).

Suppose the chromosome has the form of

$$C = (x_1, \cdots, x_i, \cdots, x_n).$$

Given two parent chromosomes C_u and C_v, the arithmetic crossover is defined as:

$$C_u' = \lambda C_u + (1-\lambda)C_v, \quad C_v' = (1-\lambda)C_u + \lambda C_v \qquad \textbf{Equation 37}$$

Where:

$$\lambda = r + (1-r)^{\sqrt{t/T}}$$

<div align="right">**Equation 38**</div>

$r \in [0,1]$ is a random value drawn from a uniform distribution, t is the current generation and T is the maximum number of generations.

The delta mutation is defined as follows: suppose the i-th gene is selected for mutation; the resulting gene will be:

$$x_i' = \begin{cases} x_i + \Delta, & \text{if a random number is } 0 \\ x_i - \Delta, & \text{if a random number is } 1 \end{cases}$$

<div align="right">**Equation 39**</div>

Where:

$$\Delta = \begin{cases} (x_i^u - x_i) \cdot (1 - r^{(1-t/T)^2}), & \text{if a random value is } 0 \\ (x_i - x_i^l) \cdot (1 - r^{(1-t/T)^2}), & \text{if a random value is } 1 \end{cases}$$

<div align="right">**Equation 40**</div>

$r \in [0,1]$ is a random value drawn from a uniform distribution, t is the current generation and T is the maximum number of generations.

It is clear from Equation 38 and Equation 40 that λ and Δ are functions of t/T, which implies that, as the search approaches the maximum number of generations, the changes made to the selected solutions through these genetic operators get smaller and smaller. It is generally true that in later generations the non-dominated set of solutions is getting closer to the true Pareto front and we do not want to introduce significant alternations to the population that could slow down convergence. Results have shown these two operators are very effective.

The selection procedure follows the Crowded Tournament Selection operation described in Deb [29] except that the constraint violations of individuals are taken into accord when performing selection. First, non-dominated sorting is conducted for a pair of individuals to determine their domination status. Then, each individual is assigned a rank. The ones within the best non-dominated set are ranked 0, the ones within the next-best set are ranked 1, and so on. In so doing, the individuals with the same ranks are grouped into the same fronts, which divide the population into non-overlapping sets. Second, a randomly picked pair of individuals takes part in the tournament selection to decide who will win the tournament and survive into the next generation. In this step, when the two individuals are in the same front, the crowding distance metric is used to break the tie, so that individuals in the less crowded regions are given a better chance to enter the next round of search. This has proven to be critical in obtaining more widely scattered solutions in the end.

The steps in generating an offspring population, Q, from a given parent population, P, in the NSGA-II algorithm are listed below. This assumes that the population size, N, is greater than 0. These steps are:

1. Given P_t, generate Q_t using the crowded tournament selection, arithmetic crossover, and delta mutation.
2. Combine P_t and Q_t and perform non-dominated sorting to group individuals into different fronts based on their ranks.
3. Generate P_{t+1} by combining the first *r* fronts identified in (2) until encountering the *r*+1-th front where adding all the individual in this front will cause the overall population in P_{t+1} to exceed N.
4. Compute crowding distances for individuals within front *r*+1 and perform the crowding distance tournament to fill the rest in P_{t+1} while not exceeding N.
5. If termination criteria not met, repeat (1).

4 Example Application

4.1 Description of the Problem

The multi-objective optimization scheme described in Section 3 was applied to the optimization of two different stiffened panels on a nominal high-speed car ferry, a typical use of aluminum extrusions. A nominal high-speed vessel was selected, based on previous Ship Structure Committee work in SSC-438, *Structural Optimization for Conversion of Aluminum Car Ferry to Support Military Vehicle Payload* [31]. SSC-438 studied the conversion of a 122m LOA catamaran commercial car/truck ferry to handle military cargoes. This vessel was constructed out of aluminum alloy. The midship section of the vessel is shown below in Figure 42. The frame spacing is 1,200mm. It was decided to use the centerline stiffened panels on the strength deck and main vehicle deck as the target of optimization. These panels extend 3,375mm off centerline, ending on the first longitudinal girder. In addition to the vessel's frame spacing of 1,200mm it was decided to include an additional panel with a hypothetical length of twice the actual frame spacing, or 2,400mm. Thus, overall dimensions of both the main deck and strength deck panels are identical, and are given in Table 5:

Table 5: Overall Panel Dimensions

Length	1200mm & 2400mm
Breadth	3375mm
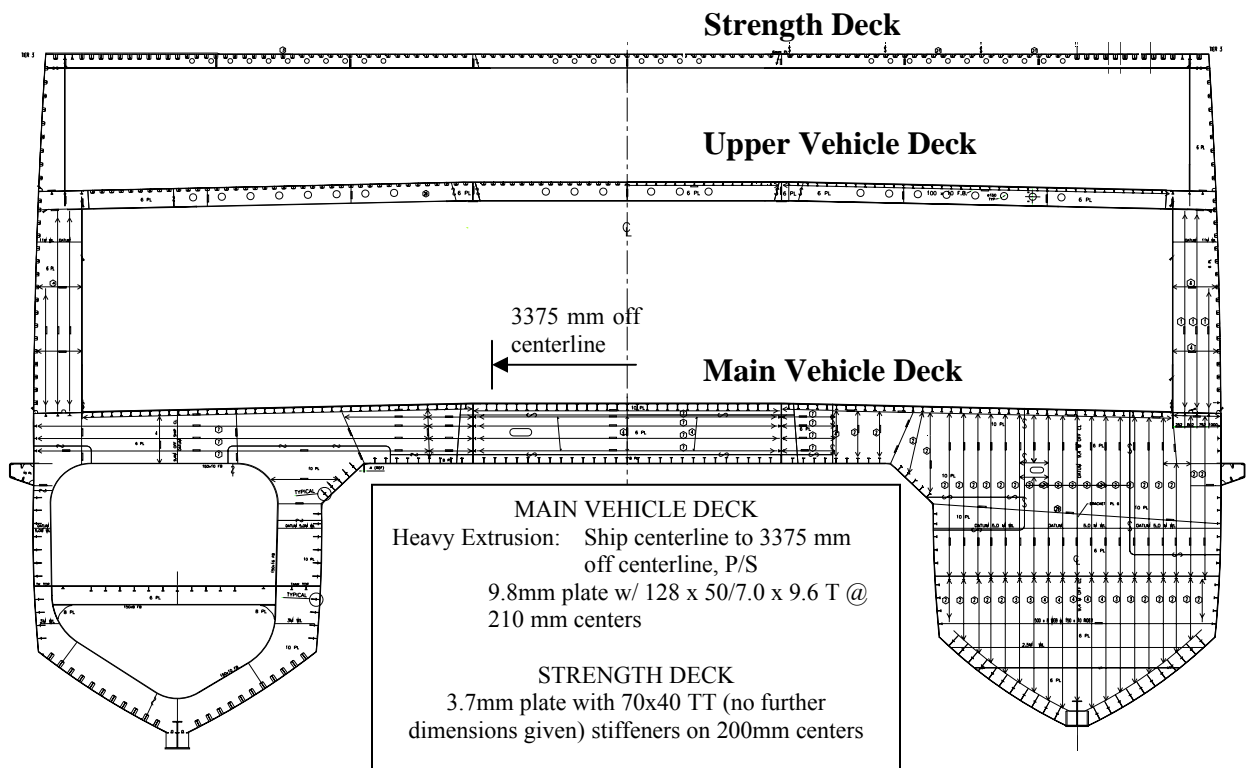
Figure 42: Midship Section of SSC-438 Vessel, after [31]

The material selected for each panel was 6082-T6, which is a practical alloy with good extrudability for flat decks above the waterline. Most of the material properties were taken from the ABS HSNC Guide [21], while the Ramberg-Osgood exponents were estimated based upon past experimental results, and are shown in Table 6.

Table 6: 6082-T6 Material Properties for Optimization

Property	Value
Proof Stress	262 MPa
Welded Proof Stress	138 MPa (Taken from 6061-T6 as 6082-T6 not included in ABS weld tables)
Elastic Modulus	70000 MPa
Poisson's Ratio	0.3
Ramberg-Osgood Exponent	30
Ramberg-Osgood Exponent welded	15

The two different locations will give different dominant loading modes. Each panel will be optimized for a dominant mode of loading, with the optimizer producing a Pareto front between panel weight and strength for the loading mode. The optimization problem was set up as follows for each location:

1. **Main Vehicle Deck Location**: Panels located on the main vehicle deck will be optimized for the greatest out-of-plane strength. The out-of-plane load is considered a uniform pressure load. In-plane loading is assumed to be small in this location, as it is close to the vessel's neutral axis in both horizontal and vertical bending. Constant in-plane loading in the longitudinal and transverse directions will be assumed. This in-plane loading will be equal in each direction, and is assumed to be 26 MPa.

2. **Strength Deck Location**: Panels located on the strength deck will be optimized for the greatest in-plane compressive strength to assist in carrying global sagging bending moments. A small constant out-of-plane load equal to 0.71 psi / 4900 MPa is assumed to act on this panel; this is the lateral pressure for an enclosed accommodation deck according to the ABS HSNC Guide[21]. A constant transverse compression equal to 26 MPa is also assumed to act on this panel.

For each deck type, the optimizer was run for each of the three types of stiffeners shown in Figure 43. Thus a total of twelve Pareto fronts were generated, three panel types, two panel lengths, and two panel locations.

(a) Extruded stiffener construction **(b) Sandwich-type extrusion** **(c) Hat-type extrusion**
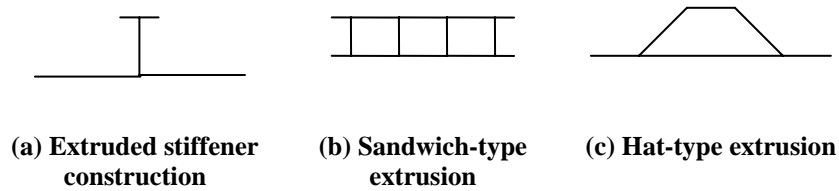
Figure 43: Examined Stiffener Types

4.2 Variables and Constraints for Each Optimization Problem

4.2.1 Extruded Stiffener Construction

The extruded stiffener panel was assumed to consist of a tee-shaped stiffener and attached plating. The optimization problem was broken down to select the width and thickness of four plate elements, as shown in Figure 44. In reality, plate 1 in Figure 44 would be split, with half being extruded on either side of the stiffener, and the assemblies joined by a butt-weld running in the middle of the plate between stiffeners. However, the depiction in Figure 44 is more useful for structural strength analysis. The dimensions given refer to the centerline of the plate elements.

Figure 44: Optimization Variables for Extruded Stiffener Construction

The design variables for the optimization problem for these plates and their bounds are listed in Table 7. Plates 3 and 4 were restricted to be mirror-images of each other. Once the number of stiffeners was known, the plate width was selected by the requirement that the panel span the 3,375mm from centerline to the first longitudinal girder. The lower bounds in Table 7 were selected to ensure that the cross-section would be extrudable in 6082-T6 material. The web height was selected to be a reasonable upper bound based on the frame spacing and midship section presented in SSC-438.

Table 7: Design Variables for the Extruded Stiffener Panel

Design Variable	Lower Bound	Upper Bound
Plate thickness (plate 1)	2mm	14mm
Web thickness (plate 2)	2mm	14mm
Web height (plate 2)	20mm	150mm
Flange thickness (plate 3&4)	2mm	14mm
Flange width (plate 3&4)	10mm	100mm
Number of stiffeners	1	22

The following constraint is enforced to ensure that the section is practical to extrude:

- The ratio of maximum thickness in the section to minimum thickness shall be kept at less than 2:1.

Table 8 lists the assumed welds for the construction, where the HAZ width is given in term of the corresponding plate thickness. In cases where the total width of the extrusion was less than 150mm, it was assumed that the two plate/stiffener combinations could be extruded together in a single die, and the amount of welding was proportionally reduced. This corresponds to a limiting CCD of the extrusion of 300mm, which is reasonable for most mills. For the strength algorithm, the support column determines whether the plate was assumed to be supported on all four edges (true) or on three edges (false).

Table 8: Welding & Support for the Extruded Stiffener Panel

Plate	HAZ 1	HAZ 2	Support
1	3t	3t	True
2	0	0	True
3	0	0	False
4	0	0	False

4.2.2 Sandwich Panel Construction

The sandwich panel extrusion was assumed to consist of two face sheets joined together by vertical webs, such as that shown in Figure 43. An alternative arrangement with webs angled to provide greater in plane shear strength may be required in some locations; however, the current optimization system does not consider such loads. The sandwich panel structure can be broken down into the repeating structure shown in Figure 45. The dimensions given refer to the centerline of the plate elements.
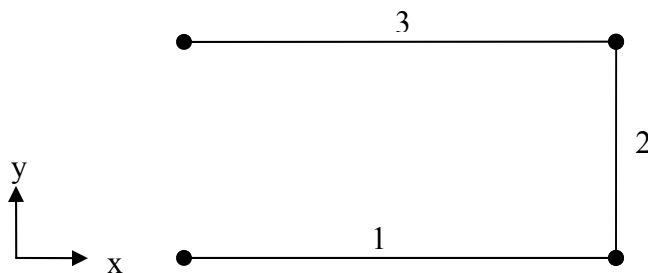
Figure 45: Optimization Variables for Sandwich Panel Construction

The design variables and their bounds for the optimization problem are listed in Table 9. As with the extruded stiffener panel above, the number of webs was selected first. Then the width of plate elements 1 and 3 was selected so that the panel would span the required 3,375mm. The top and bottom face sheets were allowed to vary independently. The lower and upper limits were selected to give good extrudability, and to be compatible in terms of depth with the plate-and-stiffener combination presented in the previous section.

Table 9: Design Variables for Sandwich Type Extrusion Panel

Design Variable	Lower Bound	Upper Bound
Plate thickness top & bottom (plate 1 and 3)	2mm	14mm
Web thickness (plate 2)	2mm	14mm
Web height (plate 2)	15mm	150mm
Number of webs	1	70

The following constraint is enforced to ensure that the section is practical to extrude:

- The ratio of maximum thickness in the section to minimum thickness shall be kept at less than 2:1.

Table 10 lists the assumed welds for the construction, where the HAZ width is given in term of the corresponding plate thickness. In cases where the total width of the extrusion was less than 150mm, it was assumed that the two extrusion combinations could be extruded together in a single die, and the amount of welding was proportionally reduced. This corresponds to a limiting CCD of the extrusion of 300mm, which is reasonable for most mills. The support column determines whether the plate was assumed to be supported on all four edges (true) or on three edges (false).

Table 10 Welding & Support for Sandwich Type Extrusion Panel

Plate	HAZ 1	HAZ 2	Support
1	3t	3t	True
2	0	0	True
3	3t	3t	True

4.2.3 Hat-Type Extrusion

The hat-type extrusion was assumed to consist of five plates, with a trapezoidal closed-form stiffener attached to the plate, as shown in Figure 46. For practical extrusion, plate 1 would be split, with half the total width extruded on each side of plate 2; however, the configuration depicted in Figure 46 make the structural analysis more straightforward. Plates 3 and 4 were restricted to be mirror images of each other, but the thickness of plates 1 and 2 were allowed to vary independently. The dimensions given refer to the centerline of the plate elements.
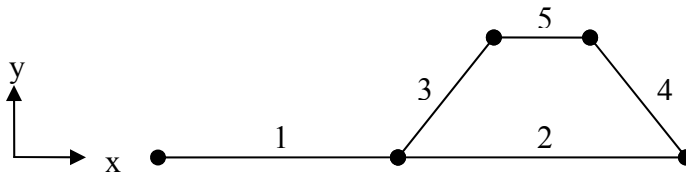
Figure 46: Optimization Variables for Hat Panel Construction

The design variables and their bounds for the optimization problem are listed in Table 11. Again, the minimum and maximum thickness and spans were established to ensure good

extrudability and compatibility with the more conventional plate-and-stiffener extrusion. The number of stiffeners and the hat "bottom" width were selected first. Then the extent of plate 1 was established so that the panel would span the required 3,375mm and the minimum width of plate 1 was preserved.

Table 11: Design Variables for Hat Type Extrusion Panel

Design Variable	Lower Bound	Upper Bound
Plate thickness- between hats (plate 1)	2mm	14mm
Plate thickness- bottom of hat (plate 2)	2mm	14mm
Hat "side" thickness (plate 3 and 4)	2mm	14mm
Hat "top" thickness (plate 5)	2mm	14mm
Hat height	20mm	150mm
Hat "top" width as % of bottom width (plate 5)	50%	100%
Hat "bottom" width (plate 2)	30mm	350mm
Plate width between hats (plate 1)	20mm	None
Number of stiffeners	1	22

The following constraint is enforced to ensure that the section is practical to extrude:
- The ratio of maximum thickness in the section to minimum thickness shall be kept at less than 2:1.

Table 12 lists the assumed welds for the construction, where the HAZ width is given in term of the corresponding plate thickness. In cases where the total width of the extrusion was less than 150mm in width, it was assumed that the two extrusion combinations could be extruded together in a single die, and the amount of welding was proportionally reduced. This corresponds to a limiting CCD of the extrusion of 300mm, which is reasonable for most mills. The support column determines if the plate was assumed to be supported on all four edges (true) or on three edges (false).

Table 12 Welding & Support for Hat Type Extrusion Panel

Plate	HAZ 1	HAZ 2	Support
1	3t	3t	True
2	0	0	True
3	0	0	True
4	0	0	True
5	0	0	True

4.3   Strength and Weight Algorithm

The optimizer developed in Section 3 requires an objective function that can compute the weight and strength of the panel. No single method explored in Section 2 could address all the different types of load cases and extrusions proposed in the previous sections, so a hybrid methodology was developed, shown in Figure 47. This methodology is based primarily on the Aluminum Association *Specification* approach that was described in detail in Section 2.1.2.6. In this approach, the panel's in-plane and out-of-plane strengths were calculated separately, then

combined via the interaction equations discussed in Section 2.1.2.6. Limit states considered include ultimate strength in compression, shear buckling or yielding failures, and yielding in tension (defined as exceeding the material's proof stress) . Figure 47 shows how these calculations are made, and which sections of the *Specification* were used in each step of the overall process.

Figure 47: Strength Calculation for Optimizer

Again, partial safety factors in the *Specification* were set to be equal to 1.0 for this research work. The basic Aluminum Association method was extended, with the following modifications:

1. Bi-axial compression was assumed to act in the continuous in-plane plates. The bi-axial interaction equation proposed by Stonor (Equation 20) was used, and the regression equation developed by Kristensen [12] for transverse compression was used for calculating the transverse plate strength. This plate strength reduction was applied before any further column or beam limit states were carried out. The reduction occurs in Figure 47, where the phrase "including interaction" occurs. Bi-axial loading was assumed to apply to the following plate elements:
    a. Plate 1 for the stiffener extrusion
    b. Plates 1 and 3 for the sandwich panel extrusion

      c.   Plates 1 and 2 for the hat-type stiffener extrusion

2. The lateral load capability of the individual plate elements were checked via the ABS HSNC Guide [21] formula (Equation 17). The limiting lateral load was then determined by the lowest lateral load that could be carried by beam action, or the lowest lateral pressure allowed by the ABS HSNC Guide on any of the plate elements subject to lateral load. This is an allowable stress approach which should result in little or no permanent set in the plating under the design load.

No constraints were placed on the b/t ratio of the different plate elements in this approach beyond those limits listed in the previous section. Weight was calculated by a simple volume calculation of the panel, assuming the density of the aluminum was 2,700 kg/m^3. One potential shortcoming of the current strength method is that stiffener tripping for conventional extruded stiffeners cannot be explicitly checked for. An additional failure check for this failure mode would be a valuable addition to the methodology.

In principle, this approach can also be extended to conventional panels that are formed by welding stiffeners to large sections of plate. In these structures, the stiffener and plate may be of different alloy types, such as 5xxx-series plate and 6xxx-series stiffeners. For such panels, it is recommended that the individual plate element limit states be evaluated using the alloy and temper specific properties and formulation for the plate element alloy. Overall limit states, such as column buckling – in Section 3.4.7 of the Aluminum Association *Specification* – could be evaluated by using averaged properties based on material volume in the panel, as discussed in Section 2.2.2.2, although further exploration of this topic is recommended.

4.4   Results of the Optimization

The optimizer developed in Section 3 was applied to the optimization problems described in this section, using the hybrid strength methodology as an objective function. Several different combinations of parameters were tried with the optimizer. In general it was found that a stable Pareto frontier was generated after processing 300 generations of 40 individuals for the sandwich and hat stiffener, and 200 generations of 40 individuals for the extruded stiffener panels. Pareto frontiers showing strength vs. weight for the strength deck panel are shown in Figure 48 andFigure 49, for the two panel lengths assumed. In each figure, all three types of extrusions are plotted together to allow the relative efficiency of each extrusion to be judged. Weight is plotted on the y-axis, and allowable in-plane load is plotted on the x-axis, including the reduction for the transverse compression and lateral load present on these panels. Both Pareto fronts show a fairly sharp corner, where weight increases rapidly as the panel strength approaches the proof strength of the material – the upper strength bound for the strength method used. Below roughly 200 MPa of strength, the relationship between strength and weight is roughly linear for all types of extrusions. For the 1,200mm long panel shown in Figure 48, all three types of extrusions perform roughly equally well, with the sandwich panel being perhaps slightly less weight-efficient than the other two types of panels. This trend is extended for the 2,400mm long panel that is shown in Figure 49, where the sandwich panel is noticeably heavier than the other two panels. Interestingly, the hat-type stiffener panel appears to be roughly as weight-efficient as the conventional stiffener extrusion. This was unexpected, as the hat-type appears to use more

material than a conventional stiffener. While the hat-type panel does have the advantage that stiffener tripping is likely to be precluded by stiffener shape, stiffener tripping was not included as an explicit failure mode in the current strength routine, so this benefit should not be apparent in the current results. The genetic optimization approach does not allow an explicit range of panel weights and strengths to be specified ahead of time. It was seen in the 2,400mm long panel of Figure 49 that the optimizer focused on lower weight and lower strength panels, as compared to the 1,200mm long panel of Figure 48. The complete listing of all panels on the Pareto front is given in Appendix A.
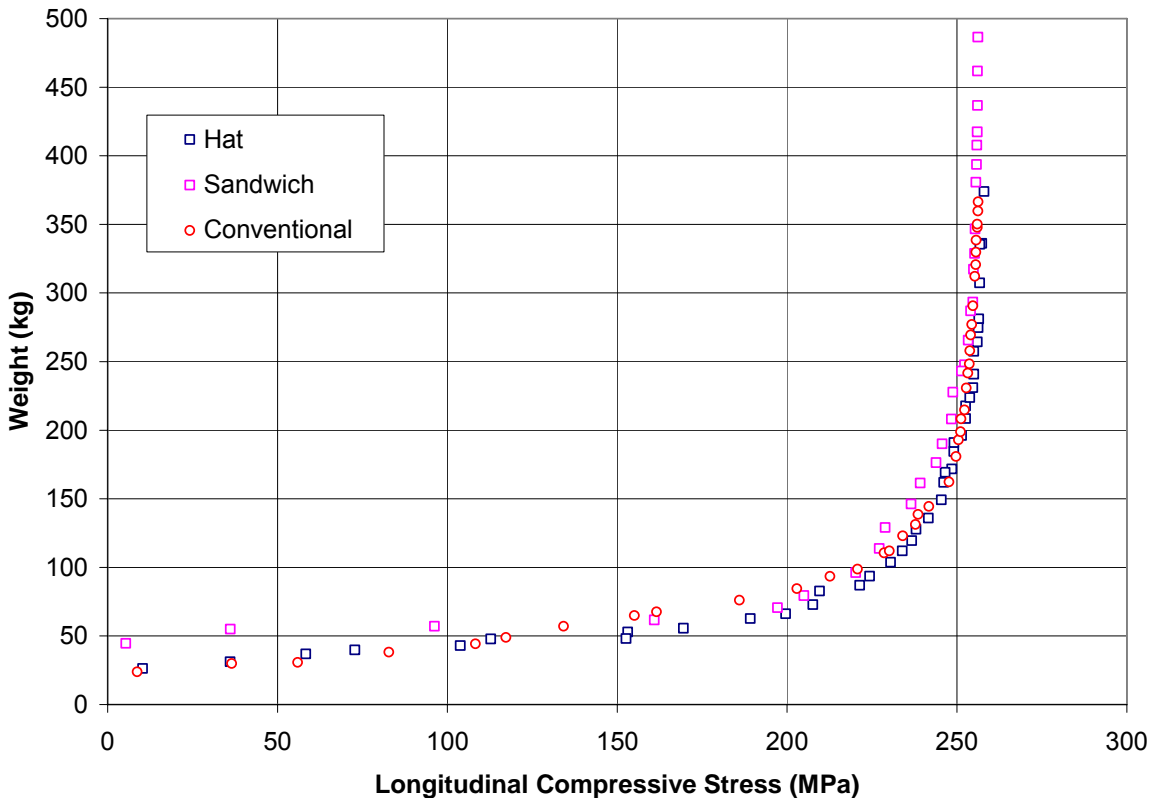
Figure 48: Pareto Fronts – Tier 3 Strength Deck, Panel Length = 1,200mm

The parameters for selected points on the 1200mm strength deck Pareto front are listed in Table 13 through Table 15. As would be expected in an extruded structure, the optimizer tended to favor numerous, small stiffeners. As stiffeners do not need to be individually attached and welded, as with steel construction, this is often an effective way to save weight in aluminum construction without driving up the build cost significantly. The optimizer results are interesting – in some cases it may seem possible to further improve the structure through the addition of more material in "logical" places, such as where web thickness is greater than flange thickness for conventional stiffeners. However, what is normally found is that in making such changes, the weight will also change enough that a different point on the Pareto front is now slightly better than the modified panel – typically a point using entirely different parameters to solve the problem. It is also worth noting that many of the sandwich panels come very close to the 2mm limiting wall thickness. Slight changes to this wall thickness restriction may significantly shift

72

the Pareto front for these panels. Clearly, working with the extrusion producer to establish realistic extrusion limitations is a key step before undertaking such an optimization.
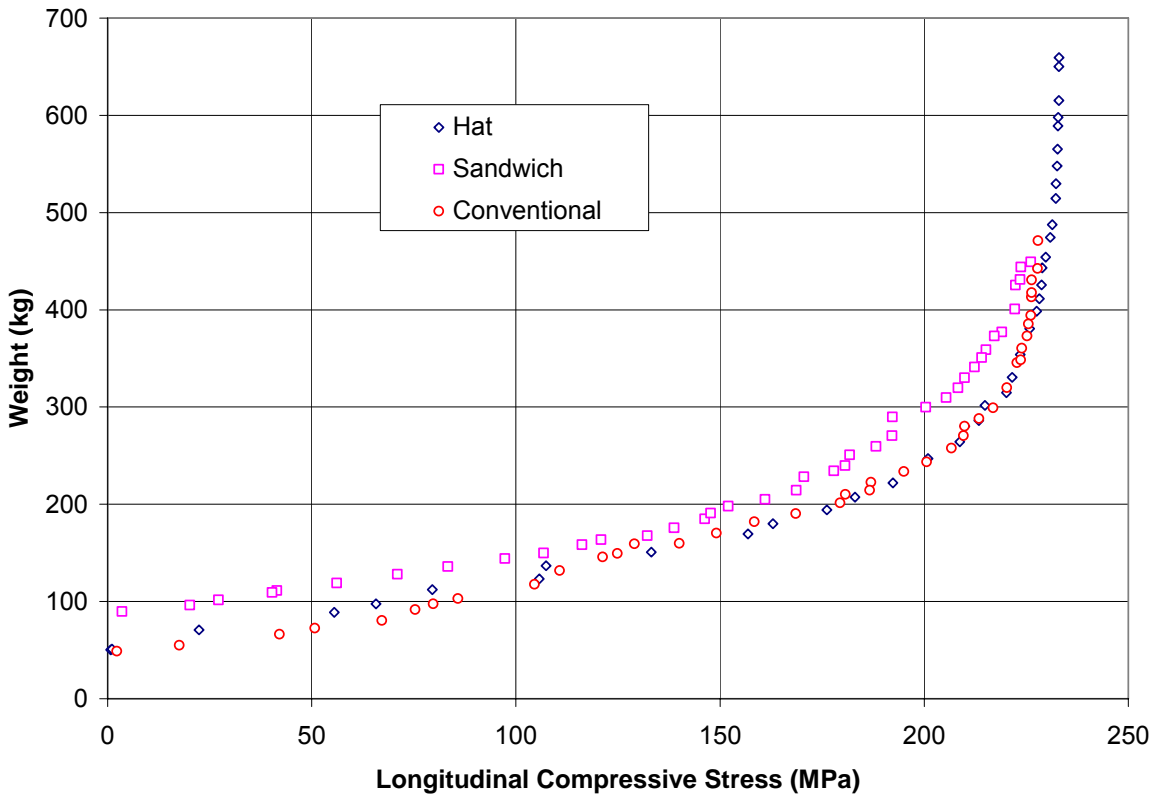
Figure 49: Pareto Fronts – Tier 3 Strength Deck, Panel Length = 2,400mm

Table 13: Sample Pareto Front Members for Strength Deck, 1200mm Panel Spacing, Extruded Stiffeners

Strength, MPa	108	162	213
Weight, kg	44.2	67.4	93.4
Stiffener spacing, mm	153	153	148
Plate thickness, mm	2	4.2	5.1
Web height, mm	95.7	70	93.3
Web thickness, mm	2.8	3.3	4.5
Flange width, mm	19.2	31.5	17
Flange thickness, mm	2.8	2.8	6.4

Table 14: Sample Pareto Front Members for Strength Deck, 1200mm Panel Spacing, Sandwich Panels

Strength, MPa	96.3	160.93	205
Weight, kg	57	61.7	79.43
Web spacing, mm	56.3	56.3	52.7
Top plate thickness, mm	2	2	2.7
Bottom plate thickness, mm	2	2	2.1
Web plate thickness, mm	2	2	2.1
Web height, mm	33.8	47	64.8

Table 15: Sample Pareto Front Members for Strength Deck, 1200mm Panel Spacing, Hat-Stiffener Panels – See Figure 46 for Plate Element Number Definitions

Strength, MPa	103.9	153.2	207.6
Weight, kg	43	52.8	72.9
Plate 1 thickness, mm	2.1	3.2	2.9
Plate 1 width, mm	114	114	89
Plate 2 thickness, mm	2.2	2.0	4.1
Plate 2 width, mm	34	34	59.5
Plate 3 & 4 thickness, mm	2.3	2.0	2.7
Hat height, mm	52.7	63.2	78
Plate 5 thickness, mm	2.2	2.3	2.5
Plate 5 width, mm	18.5	17.7	33.8

The Pareto front results for the main vehicle deck are shown in Figure 50 andFigure 51, and the complete listing of all panels on the Pareto front is given in Appendix A. As with the strength deck panels, the panel weight is plotted on the y-axis, and the allowable uniform lateral load is plotted on the x-axis, including the reductions required to support the small amount of in-plane loading assumed for these panels. For the 1,200mm long panel, the performance of the actual extrusion used in SSC-438, shown in Figure 42, is also given for comparison. As can be seen in Figure 50, the optimization bounds were too high for the 1,200mm long panel. By increasing all the allowable plate thicknesses towards their maximum values, the optimizer was able to support pressures far higher than those that would be required in service. In this high-load region, the hat panel proved the most weight-efficient; however, the results are probably only of passing interest as the lateral pressures are beyond what would be experienced in service. Toward the left side of Figure 50, it can be seen that all three types of panels are roughly equal in performance, with a slight disadvantage for the sandwich stiffener panel. The actual extrusion used in SSC-438 falls above the Pareto front, indicating that, for the bounds and load cases of the current optimization problem, the as-constructed panel is less weight-efficient than the panels generated by the optimizer.

For the longer panel, Figure 51 reinforces this conclusion. At higher loads, the hat-type panel is again the most weight-efficient for the 2,400mm panel. Within the variable ranges adopted for this problem, the sandwich-type panel can carry the highest lateral load but, again, these loads

are probably too high to be of interest for practical ship design. For strength deck panels, the strength could not exceed the proof stress of the extrusion material. This limitation caused the Pareto front to rise sharply as the material proof stress was approached, indicating that a significant weight investment is required for diminishing strength returns. The laterally-loaded panels did not have such a limitation; their Pareto fronts continued to rise smoothly until the maximum plate thickness and panel depths permitted in the optimization were reached.

Given the difficulties in evaluating the different panel types at relatively low lateral pressures, the optimization problem was re-run with lower bounds set on the maximum plate element thicknesses, in place of the 14mm thicknesses permitted in the initial optimization limits. A maximum plate element thickness of 6mm was permitted for both the extruded stiffener and hat-shaped stiffener panels, and a maximum plate element thickness of 5mm was permitted for the sandwich panels. These limits produced more designs with lower allowable lateral pressures, as shown in Figure 52. Figure 52 confirms that, for lateral pressures less than about 0.08 MPa, the sandwich panel became less weight-efficient, while the extruded stiffener and hat-stiffener panels were roughly equal in performance. The higher weight of the sandwich panel is likely a result of the 2mm minimum thickness requirement, as the sandwich panel must have both a top and bottom surface – the panel cannot go below an "average" material thickness of 4mm. In practical design problems, local concentrated loads or class society minimum thicknesses may force the use of thicker plate elements than the 2mm allowed here, but such requirements are likely to shift all three Pareto fronts upward by the same amount in the lower lateral pressure region.
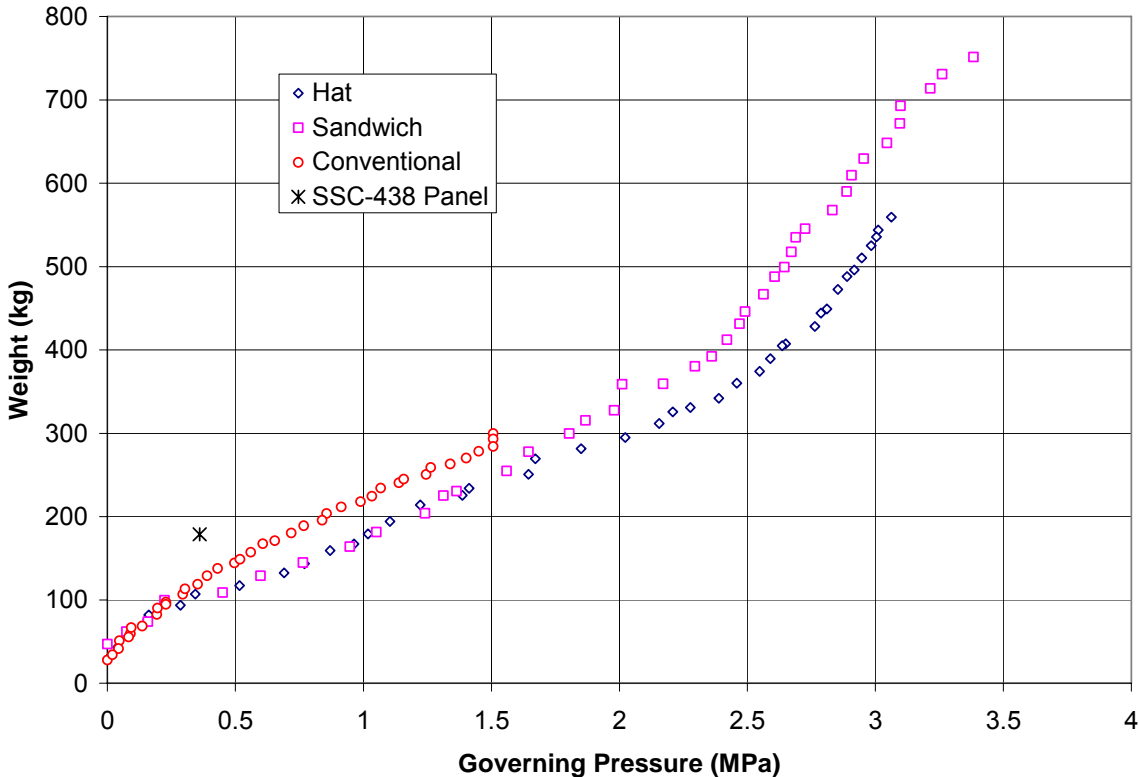
Figure 50: Pareto Fronts – Main Vehicle Deck, Panel Length = 1,200mm

Overall, applying the optimization procedure was fairly straightforward. Coupling the optimizer to a series of closed-form strength equations, such as those adopted in Section 4.3, lead to a very rapid system, with complete Pareto fronts able to be generated in a few minutes on a typical desktop PC. Interestingly, the performance of the three extrusions types was largely the same for each application, with the sandwich panel slightly lagging the other two panel types in terms of weight efficiency for the lower strength ranges. This indicates that, for highly-loaded panels, the selection of panel type could be made in conjunction with other criteria, such as fatigue life or ease of construction, and that an optimized panel of any type would be fairly weight-efficient for its primary structural purpose.
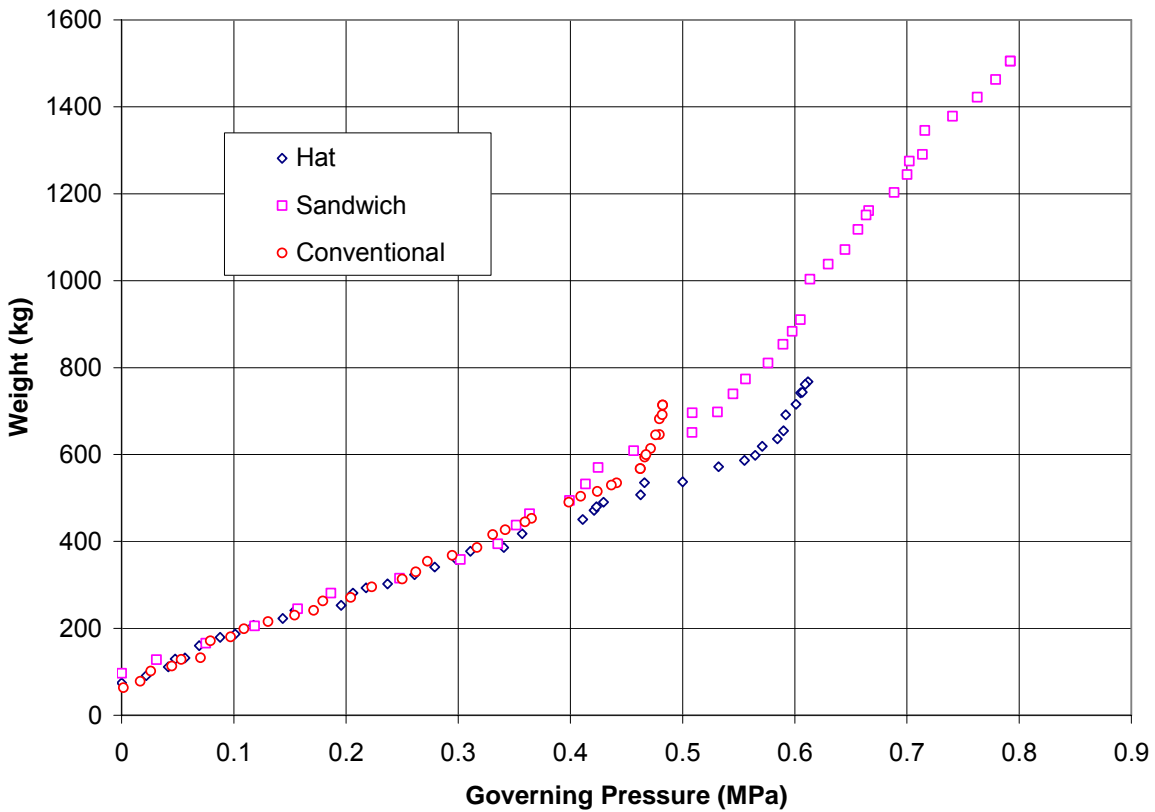
Figure 51: Pareto Fronts – Main Vehicle Deck, Panel Length = 2,400mm
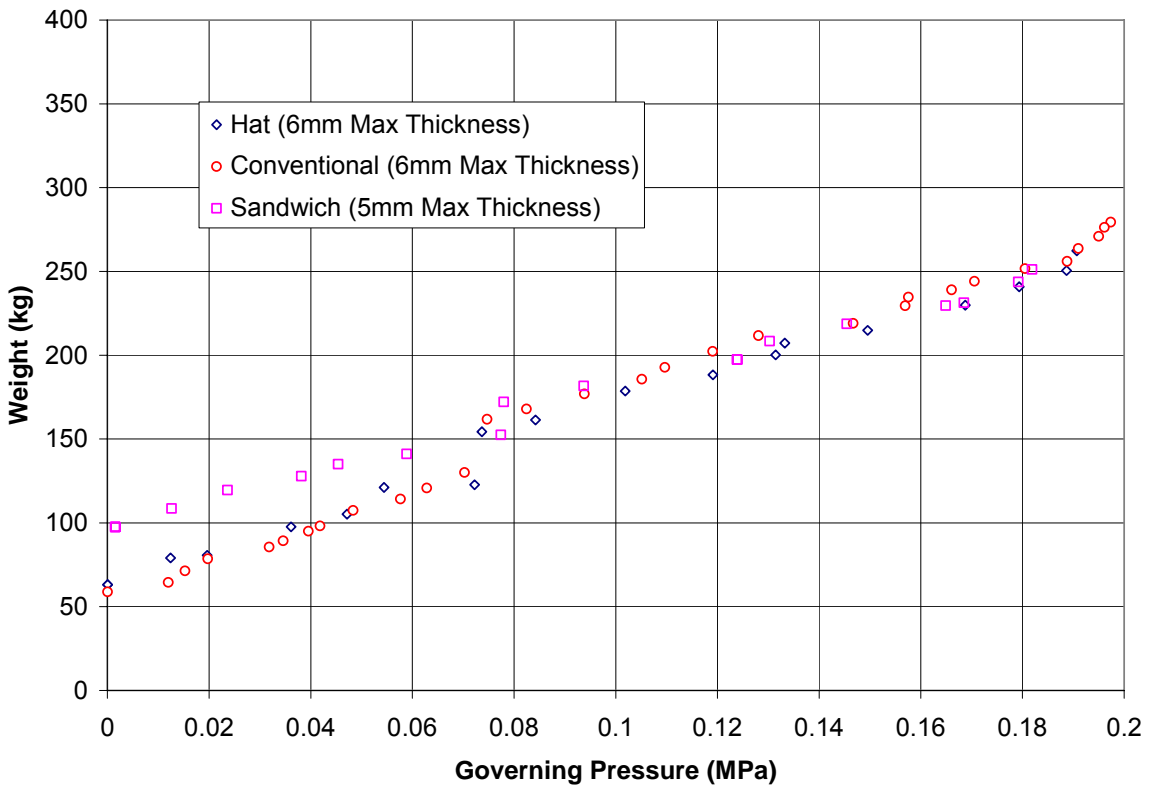
Figure 52: Pareto Fronts – Main Vehicle Deck, Panel Length = 2,400mm, Maximum Thickness reduced

5 Conclusions and Recommendations for Future Work

5.1 Conclusions

The ability to extrude aluminum easily into custom profiles is one of aluminum's advantages as a structural material for high-speed vessels. To maximize this advantage, efficient methods are needed to design and optimize such extrusions. A number of potential strength-analysis methods have been investigated in this work, and a hybrid system for calculating the strength of aluminum extrusions was developed. Several different plate and panel strength methods were reviewed. For plate strength under uniaxial compression, most methods proved fairly accurate when compared to experimental data sets, although care must be taken when applying regression equations to be sure that the alloy type, welding and HAZ parameters, and initial imperfections in the candidate structure match those used to develop the regression equation. In this respect, strength methods from civil engineering design codes proved especially adapt at covering a wide range of potential alloys and welding configurations. For plates under lateral loads, experimental data was lacking, and a large difference was noted between allowable stress methods and methods based on allowable permanent set. At the present time, allowable stress methods appear to be the most practical, especially as the impact of welding on allowable permanent set methods has not yet been quantified. Combined loading on plate elements is another area where experimental data is currently lacking; several different methods were compared to each other in this work. Currently, only a conservative approach can be taken for such load combinations. Two categories of panel strength methods were compared to the recent SSC-451 panel tests: simplified methods aiming at predicting uniaxial compressive collapse; and methods that can handle both lateral loads and uniaxial compression. In general, the simpler compressive-only models were highly varied in their performance, with better performance seen for the more complex methods. Most methods appeared to have a higher mean bias than expected, which may be a reflection of the lack of an explicit stiffener tripping limit state in many of the methods implemented in this study.

A multi-objective genetic algorithm optimizer was developed to investigate trade-offs between strength and panel weight. The approach used an implementation of the NSGA-II algorithm to progressively determine a Pareto frontier for a given multi-objective function. Using the large high-speed vehicle ferry investigated in SSC-438, two hypothetical optimization problems were developed, one for a strength deck panel primarily loaded in-plane, and one for a vehicle deck panel primarily loaded out-of-plane. Out-of-plane loading was assumed to be a uniform lateral pressure. A hybrid strength method was developed to handle a wide range of potential extrusions, and the optimizer was run on candidate extruded conventional stiffener panels, sandwich panels, and hat-shape stiffener panels. In general, the optimization approach proved robust, and Pareto frontiers could be determined in a matter of minutes on a standard desktop PC. The performance of the three extrusions types was very similar for each application, without any clear favorites for improved strength-to-weight ratio, though the sandwich panel did slightly lag the other two for low-load applications. This finding suggests that, for these applications, it may be possible to select the panel type based on considerations other than primary strength – such as fatigue or ease of construction, and that a weight-efficient panel can then be optimized from any of the three types of extrusions investigated. Overall, the combination of the robust multi-

objective genetic algorithm optimizer and the closed-form strength equations proved a powerful tool for optimizing the design of aluminum extrusions.

5.2 Recommendations for Future Work

While the optimization approach developed in this work was very successful in optimizing aluminum extrusion, several areas for future research were identified during the course of this project. These areas are listed below:

1. Improved lateral-load capacity equations for aluminum plates, including the impact of HAZ. Ideally, allowable permanent set equations would be developed for aluminum plates, including the effects of welds at the plate boundaries, or at the boundaries and the plate center-plane (as is typical when joining extrusions). Both uniform lateral loads and wheel patch loads should be considered. The optimization presented in this report could then be repeated, using allowable permanent set criteria in place of the ABS HSNC Guide formulation for plate strength. Studying any difference in the Pareto fronts between uniform lateral loads and wheel-pressure patches would also be interesting.

2. Further analysis of the distortion difference between conventional panels, extruded panels, and extruded panels with friction-stir welds. It may be possible to increase the allowable in-plane strength for extrusions if it can be shown that the initial distortions are generally less than those typical of welded conventional construction.

3. Further analysis of combined loads, for both plates and panels. No experimental data was found for aluminum plates and panels under bi-axial compression, compression and shear, or compression and lateral loads. In lieu of experimental results, an initial survey could be made with finite element analysis, but particular care must be given to modeling alloy-specific material properties, initial imperfections, and welds.

4. The current hybrid strength method used for optimization could be extended to include tripping failure modes and the influence of in-plane shear loads, and the optimization repeated for several panel lengths.

5. Further strength investigation of variable-thickness plates under lateral loads and transverse compression, and the inclusion of variable-thickness plates in the optimization for each extrusions type. Local increases in thickness to offset the impact of welding would also be an interesting study, as would the development of equivalent thickness expressions for variable-thickness plates to allow such panels to be investigated by existing simplified methods.

6. Design guidelines for extrusions could be developed from further investigations of the optimizer strength output. Such guidelines could provide recommendations on minimum extrusion slenderness ratios to avoid specific local and global collapse modes, allowing efficient extrusions to be designed easily, without using an optimizer for each design.

7. Extension of the optimization approach to consider cost as an additional objective, including both build cost and through-life costs associated with additional weight on the structure.

8. Extension of the optimization approach to consider multiple load cases (combinations of shear, in-plane loading, and lateral loading) in the strength analysis.

9. Extension of the optimization approach to include transverse frames so that an entire grillage could be optimized, instead of just the longitudinal continuous members. Fatigue life and potential cost could also be added to such an optimization.

10. Extension of the optimization approach to include a non-linear finite-element code to evaluate the strength of the candidate panels, in place of the closed-form expressions used in this study.

Several of these extensions would require a significant undertaking to adequately cover the proposed scope; however, other items – such as an extension of the developed method to tripping and shear failures – could be attempted with less effort, perhaps as part of a Master's thesis or undergraduate honors thesis.

6 References

1. Collette, M. *Strength and Reliability of Aluminium Stiffened Panels,* PhD Thesis, School of Marine Science and Technology, University of Newcastle, 2005.
2. Collette, M. *Impact of Fusion Welds on the Ultimate Strength of Aluminum Structures*, 10th International Symposium on Practical Design of Ships and Other Floating Structures (PRADS 2007), Houston, Texas, 30 September-5 October 2007.
3. Romanoff, J. and Klanac, A., *Design Optimization of Steel Sandwich Hoistable Car-Decks Applying Homogenized Plate Theory*, 10th International Symposium on Practical Design of Ships and Other Floating Structures (PRADS 2007), Houston, Texas, 30 September-5 October 2007.
4. Anderson, R.A., and Anderson, M.S., *Correlation of Crippling Strength of Plate Structures with Material Properties*, NACA Technical Note 3600, January 1956.
5. Mofflin, D.S. *Plate Buckling in Steel and Aluminum*, PhD Thesis, Trinity College, University of Cambridge, 1983.
6. Naval Sea Systems Command, *Design Data Sheet 100-4 – Strength of Structural Members*, Revised 15 November 1982.
7. Faulker, D. *A. Review of Effective Plating for Use in the Analysis of Stiffened Plating in Bending and Compression*, Journal of Ship Research, 19 (1), March 1975, pp 1-17.
8. Wang, X., Sun, H., Akiyama, A., and Du, A., *Buckling and Ultimate Strength of Aluminum Plates and Stiffened Panels in Marine Structures*, 5th International Forum on Aluminum Ships, Tokyo, Japan, 11-13 October 2005.
9. American Bureau of Shipping, *Guide for Buckling and Ultimate Strength Assessment for Offshore Structures*, Houston, TX: American Bureau of Shipping, April 2004, including revisions through June 2007.
10. Paik, J.K., and Duran, A., *Ultimate Strength of Aluminum Plates and Stiffened Panels for Marine Applications*, Marine Technology, Vol. 41, No. 3, July 2004, pp. 108-121.
11. Paik, J.K., Thayamballi, A.K., Ryu. J.Y., Jang, J.H., Seo, J.K., Park, S.W., Soe, S.K., Renaud, C., and Kim, N.I., *Mechanical Collapse Testing on Aluminum Stiffened Panels for Marine Applications*, Ship Committee Report SSC-451, Washington, DC:, Ship Structure Committee, March 2007.
12. Kristensen, O. H. H. *Ultimate Capacity of Aluminium Plates Under Multiple Loads, Considering HAZ Properties*, PhD thesis, Norwegian University of Science and Technology, 2001.
13. The Aluminum Association, *Aluminum Design Manual: Specification for Aluminum Structures - Load and Resistance Factor Design Specification*, 8th ed., Washington, D.C. Aluminum Association, 2005.
14. European Committee for Standardization (CEN), *Eurocode 9: Design of Aluminium Structures*, 1998, Brussels: European Committee for Standardization (CEN). ENV 1999-1-1: 1998 E.
15. Dhondt, G. *The Finite Element Method for Three-Dimensional Thermomechanical Applications*, Wiley, 2004.
16. Matsuoka, K., Tanaka, Y., Kitamura, S., and Sakuma, M., *Buckling Strength of a Lightened Aluminium Hull Structure*, Welding International, Vol. 11, No. 10, pp 765-773, 1997.
17. Hughes, O. *Ship Structural Design*, Society of Naval Architects and Marine Engineers, New York, 1988.

18. Kmiecik, M. *Usefulness of Yield Line Theory in Design of Ship Plating*, Marine Structures Vol. 8, 1995, pp 67-79.

19. Hughes, O.F. *Design of Laterally Loaded Plating – Uniform Pressure Loads*, Journal of Ship Research, Vol. 25 No. 2, June 1981, pp 77-89.

20. Sielski, R. *Aluminum Marine Structure Design and Fabrication Guide*, Ship Structure Committee Report SSC-452, Washington, DC: Ship Structure Committee, February 2008.

21. American Bureau of Shipping, *Guide for Building and Classing High-Speed Naval Craft*, Houston, TX: American Bureau of Shipping,, 2008.

22. Stonor, R et al., *Test on Plates under Biaxial Compression*, Report CUED/D-Struct/TR98, Cambridge: Cambridge University, Engineering Department, 1983.

23. Paik, J.K. and Thayamballi, A.K., *Ultimate Limit State Design of Steel-Plated Structures*, John Wiley and Sons, Chichester, UK.

24. AEC, *Aluminum Extrusion Manual*, Aluminum Extruders Council, Wauconda, Illinois, 2002.

25. Hydro Aluminum, *Hydro Extrusion Design Manual*, 2006 Edition, Hydro Aluminum. Available by request to Hydro Aluminum online at: http://www.hydro.com/en/.

26. Woodward, Roy, *Aluminum Extrusion: Alloys, Shapes and Properties*, TALAT Lecture 1302, Training in Aluminum Application Technologies, European Aluminum Association (EAA) Version 2.0 1999, Available online at: http://www.eaa.net/eaa/education/TALAT/index.htm, Accessed August 14, 2008.

27. Engineers Edge, *Extrusion Design Data and Information (Aluminum)*, Available at: http://www.engineersedge.com/extrusion.htm, Accessed December 12, 2007.

28. Siegrist, M, *Aluminium Extrusions for Shipbuilding*, Alumitech '97: 2nd International Aluminum Conference and Trade Exposition, The Aluminum Association, pp 365-386, 1997.

29. Deb, K., *Multi-Objective Optimization using Evolutionary Algorithms*, John Wiley & Sons, Ltd., 2001.

30. Li. J., *Oil Tanker Market Model, Analysis and Forecasting using Neural Network, Fuzzy Logic and Genetic Algorithms*, Ph.D., Thesis, University of Michigan, Ann Arbor, 1997.

31. Kramer, R.K., McKesson, C., McConnell, J., Cowardin, W, and Samuelsen, B., *Structural Optimization for Conversion of Aluminum Car Ferry to Support Military Vehicle Payload,* Ship Structure Committee Report SSC-438, Washington, DC: Ship Structure Committee, February, 2005.

Appendix A: Complete Optimization Pareto Fronts

Strength Deck Optimization: 1.2m Long Extruded Stiffener Panels

Bottom Plate Thickness	Web Plate Thickness	Web Plate Height	Flange Thickness	Flange Width	Number of Stiffeners	Limiting Compressive Stress	Panel Weight
meters	meters	meters	meters	meters	--	Mpa	kg
0.002007	0.002069	0.020002	0.002032	0.010042	9	8.7	23.7
0.002041	0.002095	0.112658	0.002025	0.010139	9	36.5	29.8
0.002005	0.002401	0.043344	0.002092	0.011506	21	56.0	30.6
0.002005	0.002401	0.089692	0.002092	0.011506	21	82.8	38.2
0.002014	0.002837	0.095769	0.002829	0.019238	21	108.3	44.2
0.002016	0.00299	0.100178	0.002431	0.03886	21	117.3	48.9
0.002177	0.003179	0.101403	0.003239	0.044322	22	134.2	57.0
0.004182	0.003304	0.069825	0.00228	0.022251	21	155.0	64.9
0.004182	0.003304	0.069825	0.002829	0.03145	21	161.6	67.5
0.004805	0.003933	0.079773	0.002737	0.011604	21	185.9	76.0
0.00501	0.003564	0.064957	0.005999	0.030806	22	202.9	84.5
0.00509	0.004516	0.093297	0.006347	0.017038	22	212.7	93.4
0.005602	0.004738	0.092504	0.005191	0.016534	22	220.7	98.6
0.005948	0.004934	0.104378	0.004951	0.02477	22	228.6	110.5
0.005996	0.005136	0.098803	0.007595	0.018974	22	230.1	112.0
0.006315	0.005471	0.119805	0.004541	0.022407	22	234.1	123.0
0.006411	0.004371	0.091405	0.008069	0.056768	22	237.8	131.2
0.006276	0.00686	0.105616	0.007205	0.035596	22	238.6	138.5
0.006683	0.007512	0.126232	0.004985	0.010289	22	241.8	144.3
0.007182	0.007931	0.135395	0.008846	0.011324	22	247.7	162.2
0.00754	0.007518	0.13992	0.009738	0.033645	22	249.7	180.8
0.007447	0.008175	0.143631	0.011847	0.032878	22	250.4	192.9
0.0079	0.008073	0.145171	0.010238	0.039656	22	251.1	198.9
0.007524	0.009304	0.132351	0.009543	0.056044	22	251.2	208.2
0.008575	0.007013	0.143409	0.010926	0.063451	22	252.2	214.9
0.008571	0.007011	0.14415	0.012202	0.074747	22	252.8	230.8
0.008438	0.01045	0.144241	0.01139	0.051534	22	253.2	241.6
0.008942	0.007614	0.148557	0.012846	0.076279	22	253.6	248.2
0.008806	0.011649	0.139769	0.010853	0.058853	22	253.8	257.9
0.008405	0.013382	0.149736	0.009688	0.050222	22	254.1	269.4
0.008806	0.01258	0.139769	0.013224	0.058853	22	254.3	277.1
0.008638	0.011947	0.145542	0.012413	0.081574	22	254.7	290.6
0.009585	0.013329	0.136612	0.011966	0.091057	22	255.3	312.3
0.010195	0.010321	0.149728	0.01399	0.09933	22	255.5	320.7
0.008785	0.01373	0.148555	0.012871	0.096352	22	255.6	329.8
0.010673	0.013662	0.127455	0.01392	0.098489	22	255.7	338.5
0.010247	0.01371	0.14744	0.013161	0.097686	22	256.0	347.8
0.009277	0.013999	0.149725	0.01398	0.099719	22	256.0	350.2
0.010673	0.013662	0.149339	0.01392	0.098489	22	256.2	359.9
0.010769	0.013997	0.149725	0.01398	0.099719	22	256.3	366.5

Strength Deck Optimization: 2.4m Long Extruded Stiffener Panels

Bottom Plate Thickness	Web Plate Thickness	Web Plate Height	Flange Thickness	Flange Width	Number of Stiffeners	Limiting Compressive Stress	Panel Weight
meters	meters	meters	meters	meters	--	Mpa	kg
0.002004	0.002	0.020176	0.00207	0.010003	13	2.2	49.0
0.002002	0.002	0.056678	0.00202	0.010003	13	17.6	55.0
0.002008	0.002	0.085125	0.002024	0.010001	18	42.1	66.1
0.002008	0.002	0.112336	0.002024	0.010001	18	50.7	72.5
0.002058	0.002122	0.099621	0.002146	0.017076	22	67.2	80.4
0.002058	0.002538	0.115747	0.00291	0.017076	21	75.3	91.7
0.002405	0.002037	0.097847	0.002736	0.042559	22	79.7	97.6
0.002477	0.00229	0.097815	0.002746	0.043025	22	85.8	102.9
0.002632	0.002233	0.091165	0.004135	0.052649	22	104.6	117.6
0.002712	0.003865	0.127833	0.003468	0.019002	20	110.7	131.9
0.004198	0.002218	0.105253	0.00303	0.047825	22	121.2	145.7
0.004161	0.002349	0.104199	0.003316	0.04953	22	124.9	149.3
0.002743	0.003212	0.128858	0.005301	0.059604	21	129.0	159.3
0.004462	0.002777	0.112073	0.003316	0.037826	22	140.0	159.8
0.004428	0.003204	0.111713	0.004221	0.037374	22	149.1	170.4
0.00457	0.004017	0.127207	0.002483	0.026099	22	158.4	182.0
0.005173	0.003294	0.12366	0.005623	0.028641	21	168.5	190.5
0.005173	0.003699	0.12366	0.005381	0.029969	22	179.4	201.3
0.005573	0.004172	0.134835	0.006859	0.01732	20	180.7	210.2
0.005173	0.003699	0.12366	0.005381	0.04711	22	186.6	214.5
0.00483	0.004726	0.141223	0.003689	0.041584	22	187.0	222.6
0.005426	0.004636	0.146579	0.004769	0.026558	22	195.0	233.6
0.005544	0.004877	0.146749	0.003574	0.039719	22	200.6	243.5
0.006132	0.00458	0.14257	0.006275	0.040677	21	206.7	257.7
0.005667	0.005126	0.146925	0.005381	0.05122	22	209.6	270.6
0.006558	0.004763	0.149474	0.007714	0.051706	19	209.9	280.2
0.006095	0.004778	0.140459	0.008268	0.056375	21	213.4	288.0
0.006558	0.005217	0.149474	0.008151	0.051706	20	216.9	299.1
0.006646	0.005274	0.149944	0.008999	0.061717	20	220.3	319.8
0.006589	0.00523	0.149431	0.008731	0.088488	20	222.7	345.5
0.007268	0.005525	0.149979	0.01049	0.075875	18	223.6	348.5
0.007929	0.005998	0.149656	0.009667	0.093751	16	223.9	360.4
0.007929	0.005998	0.149656	0.010965	0.093751	16	225.2	373.1
0.007929	0.005998	0.149656	0.010965	0.093751	17	225.5	385.5
0.007929	0.005998	0.149656	0.011429	0.096851	17	226.1	394.2
0.007948	0.006288	0.149859	0.011937	0.093009	18	226.3	413.2
0.007989	0.006906	0.149944	0.013397	0.087356	17	226.3	417.7
0.007962	0.006498	0.149925	0.012305	0.090228	19	226.3	430.8
0.009099	0.006457	0.149755	0.012759	0.097461	17	227.8	442.5
0.009099	0.006457	0.149755	0.012759	0.097461	19	227.9	471.1

Strength Deck Optimization: 1.2m Long Sandwich Panels

Top Plate Thickness	Bottom Plate Thickness	Web Plate Thickness	Web Plate Height	Number of Webs	Limiting Compressive Stress	Panel Weight
meters	meters	meters	meters	--	MPa	kg
0.002	0.002	0.002	0.015248	9	5.3	44.6
0.002148	0.002063	0.002035	0.064794	21	36.1	55.0
0.002007	0.002018	0.002018	0.033833	59	96.2	57.1
0.002	0.002	0.002	0.04699	59	160.9	61.7
0.002	0.002078	0.002002	0.060862	66	197.2	70.6
0.002676	0.002063	0.002089	0.064794	63	204.9	79.4
0.002357	0.002519	0.002714	0.077413	63	220.2	96.2
0.00307	0.002667	0.003603	0.085725	51	227.2	113.8
0.004992	0.00268	0.003164	0.086417	51	228.9	129.1
0.002796	0.003229	0.004725	0.100713	52	236.5	146.1
0.004587	0.003556	0.005479	0.099473	41	239.2	161.4
0.003211	0.003622	0.005145	0.117214	52	243.9	176.3
0.005074	0.004204	0.006298	0.117391	37	245.7	190.1
0.004641	0.003312	0.006458	0.128723	45	248.4	208.2
0.004603	0.003674	0.007314	0.128616	45	248.8	227.7
0.006406	0.005539	0.006824	0.130364	39	251.3	243.0
0.00376	0.004888	0.007358	0.142703	45	252.3	247.7
0.004012	0.006052	0.007246	0.140967	47	253.3	265.6
0.004303	0.004353	0.0073+C2258	0.14938	54	254.0	287.0
0.004224	0.005247	0.007812	0.149928	50	254.7	293.3
0.006421	0.005247	0.007812	0.149928	50	254.9	317.3
0.004093	0.007215	0.007677	0.149926	55	255.2	328.8
0.005317	0.00643	0.008238	0.1487	55	255.3	346.7
0.007209	0.006498	0.009503	0.149984	50	255.6	380.8
0.007209	0.006498	0.009293	0.149919	54	255.8	393.6
0.007209	0.006498	0.01062	0.149979	50	255.9	407.9
0.006081	0.008243	0.008658	0.149962	62	256.0	417.4
0.008055	0.006808	0.010078	0.149986	56	256.0	436.8
0.008423	0.007062	0.009712	0.149968	62	256.1	461.9
0.009022	0.007317	0.0096	0.149976	66	256.2	486.6
0.008121	0.008924	0.010233	0.149965	65	256.2	509.6
0.007849	0.009786	0.010233	0.149972	68	256.3	531.0
0.010345	0.008625	0.011422	0.149879	65	256.3	568.0
0.010383	0.009279	0.013605	0.14947	57	256.3	590.6
0.012087	0.00916	0.012469	0.149834	68	256.4	644.0
0.010263	0.011058	0.013432	0.149976	65	256.4	657.4
0.010345	0.011568	0.013825	0.14992	65	256.5	676.1
0.011871	0.01091	0.013545	0.149911	68	256.5	696.5
0.012023	0.011008	0.013544	0.149876	70	256.5	712.3
0.012406	0.010833	0.01378	0.149904	70	256.6	722.6

Strength Deck Optimization: 2.4m Long Sandwich Panels

Top Plate Thickness	Bottom Plate Thickness	Web Plate Thickness	Web Plate Height	Number of Webs	Limiting Compressive Stress	Panel Weight
meters	meters	meters	meters	--	MPa	kg
0.002	0.002012	0.002001	0.015754	9	3.5	89.6
0.002001	0.002003	0.002001	0.039617	17	20.1	96.3
0.002002	0.002005	0.002	0.067886	16	27.2	101.7
0.002	0.002003	0.002	0.052532	32	40.3	109.3
0.002	0.002002	0.002	0.065689	28	41.4	111.4
0.002016	0.002057	0.00309	0.059925	25	56.1	119.1
0.002013	0.002012	0.003197	0.074286	26	71.0	128.1
0.002023	0.002214	0.002014	0.073598	45	83.3	135.9
0.002001	0.002001	0.002001	0.090962	48	97.3	144.1
0.002025	0.002001	0.002	0.083733	57	106.8	149.9
0.002044	0.00215	0.002085	0.086656	57	116.2	158.4
0.002453	0.002354	0.002286	0.085834	46	120.9	163.6
0.002025	0.003182	0.002179	0.086484	44	132.2	167.6
0.002069	0.003146	0.002234	0.088895	48	138.7	175.8
0.002076	0.003554	0.002257	0.096106	44	146.2	185.0
0.002092	0.003399	0.002423	0.107351	42	147.7	190.9
0.002106	0.003543	0.002402	0.10892	44	152.0	198.1
0.002056	0.003476	0.002774	0.103922	45	161.0	205.0
0.002328	0.003607	0.002755	0.107674	44	168.7	214.4
0.002369	0.002752	0.003077	0.112138	52	170.5	228.3
0.003165	0.003618	0.002752	0.117557	41	177.9	234.3
0.002485	0.003501	0.003318	0.114896	44	180.6	239.6
0.00282	0.003271	0.003454	0.122131	43	181.8	250.8
0.00307	0.003501	0.003318	0.122432	44	188.2	259.5
0.003199	0.003482	0.003416	0.124989	45	192.1	270.6
0.003001	0.004518	0.003641	0.136146	39	192.2	289.7
0.002643	0.005095	0.004318	0.129728	36	200.4	299.9
0.004834	0.004315	0.00387	0.132669	33	205.4	309.9
0.004514	0.004518	0.003641	0.132863	39	208.3	319.8
0.004947	0.004534	0.004652	0.135694	30	209.9	330.0
0.004054	0.005607	0.004116	0.139114	35	212.3	341.1
0.004961	0.005372	0.003999	0.137547	35	214.1	350.7
0.005493	0.00648	0.003329	0.13239	34	215.1	358.9
0.005561	0.006972	0.004702	0.135245	24	217.2	373.0
0.004676	0.005824	0.004599	0.149996	33	219.0	377.1
0.006832	0.006012	0.004446	0.148655	28	222.2	400.8
0.006001	0.008081	0.004832	0.144072	26	222.3	425.3
0.00677	0.007293	0.004167	0.147617	31	223.5	431.1
0.007001	0.006718	0.005729	0.149287	26	223.7	444.1
0.007038	0.007964	0.004795	0.149983	26	226.1	449.3

Strength Deck Optimization: 1.2m Long Hat Stiffener Panels

Note: For plate element dimensions, please refer to Figure 46 in the main body of the report.

Plate Element 1 Thickness	Plate Element 2 Thickness	Plate Elements 3 & 4 Thickness	Plate Element 5 Thickness	Hat Height	Ratio of Plate Element 5 to Element 2 Width	Plate Element 2 Width	Number of Stiffeners	Longitudinal Compressive Stress	Panel Weight
meters	meters	meters	meters	meters	--	meters	--	MPa	kg
0.002004	0.002369	0.002004	0.002003	0.02092	0.523739	0.030697	10	10.3	26.2
0.002017	0.002206	0.002042	0.002007	0.039341	0.502796	0.030829	14	36.1	31.2
0.002037	0.002303	0.002214	0.002011	0.033588	0.582646	0.03652	22	58.3	36.9
0.002003	0.002153	0.002001	0.002002	0.08303	0.504241	0.030525	15	72.8	39.8
0.002075	0.002165	0.002255	0.002217	0.052691	0.541675	0.034129	22	103.9	43.0
0.002018	0.002412	0.002068	0.002049	0.088639	0.500971	0.034129	19	112.8	47.7
0.002166	0.002107	0.002228	0.002111	0.055535	0.644624	0.068097	22	152.6	48.1
0.003153	0.002003	0.002018	0.00225	0.063197	0.51645	0.034299	22	153.2	52.8
0.003177	0.0022	0.002387	0.002113	0.060599	0.572183	0.052247	21	169.6	55.6
0.003342	0.002284	0.002527	0.002795	0.063145	0.665814	0.054926	22	189.2	62.7
0.003342	0.002427	0.00254	0.002795	0.075306	0.653358	0.054926	21	199.6	66.2
0.002852	0.00414	0.00267	0.00252	0.078087	0.568381	0.05952	22	207.6	72.9
0.0028	0.004982	0.003352	0.003614	0.073169	0.573869	0.080626	19	209.6	82.8
0.003065	0.005144	0.002764	0.003168	0.080124	0.786829	0.074345	21	221.4	86.9
0.003085	0.003495	0.003588	0.00385	0.093802	0.672049	0.067444	21	224.3	93.6
0.003758	0.002427	0.004208	0.004458	0.096387	0.720386	0.056283	21	230.5	103.7
0.005548	0.004474	0.003165	0.005734	0.098442	0.745533	0.078996	18	233.9	111.9
0.004109	0.003142	0.004251	0.00485	0.098474	0.981012	0.068177	21	236.7	119.5
0.006965	0.005187	0.003961	0.005109	0.108884	0.834254	0.109489	14	238.0	127.8
0.003318	0.004732	0.005159	0.00446	0.115241	0.590057	0.082853	20	241.6	135.9
0.005024	0.006081	0.004902	0.004236	0.117571	0.904305	0.077426	19	245.4	149.2
0.005937	0.006863	0.004474	0.006889	0.109328	0.82036	0.090299	19	246.1	161.9
0.005706	0.009784	0.006594	0.00615	0.131702	0.547296	0.160798	11	246.6	169.3
0.007644	0.007654	0.006594	0.006341	0.131392	0.69165	0.160798	11	248.5	171.6
0.003918	0.006465	0.006385	0.006117	0.130349	0.706545	0.074883	20	249.1	184.4
0.00615	0.007011	0.005713	0.009191	0.126205	0.781795	0.046746	21	249.2	191.0
0.008382	0.008515	0.006276	0.012365	0.131108	0.631928	0.102831	13	251.4	196.1
0.007658	0.008699	0.00744	0.008083	0.148763	0.654444	0.082986	14	252.5	208.4
0.007656	0.008681	0.007508	0.010784	0.147984	0.510562	0.05385	16	252.6	217.6
0.008239	0.006046	0.0078	0.010194	0.149418	0.513642	0.122715	15	253.8	223.8
0.006459	0.007469	0.007272	0.012607	0.14793	0.548314	0.056134	19	254.7	230.9
0.005924	0.006081	0.007508	0.009777	0.145874	0.695045	0.074651	20	255.0	240.8
0.009853	0.009625	0.007167	0.0077	0.147229	0.73934	0.082285	18	255.0	257.4
0.005914	0.009209	0.007871	0.010293	0.146853	0.889089	0.074671	19	256.0	264.2
0.007795	0.008965	0.007639	0.007819	0.149728	0.995807	0.07102	20	256.3	274.7
0.007401	0.009197	0.007639	0.009462	0.149934	0.997418	0.07102	20	256.4	281.1
0.008479	0.009368	0.007722	0.013814	0.149917	0.99492	0.080076	19	256.7	307.4
0.008251	0.00995	0.011026	0.013865	0.149606	0.524603	0.121939	17	256.8	335.6
0.007183	0.009704	0.008039	0.012418	0.149374	0.999195	0.08119	22	257.3	336.1
0.007017	0.008162	0.010811	0.013984	0.149541	0.989382	0.09042	20	258.0	374.0

Strength Deck Optimization: 2.4m Long Hat Stiffener Panels

Note: For plate element dimensions, please refer to Figure 46 in the main body of the report.

Plate Element 1 Thickness	Plate Element 2 Thickness	Plate Elements 3 & 4 Thickness	Plate Element 5 Thickness	Hat Height	Ratio of Plate Element 5 to Element 2 Width	Plate Element 2 Width	Number of Stiffeners	Longitudinal Compressive Stress	Panel Weight
meters	meters	meters	meters	meters	--	meters	--	MPa	kg
0.002021	0.002	0.002	0.002	0.02004	0.515754	0.030073	8	0.8	50.2
0.002021	0.002	0.002	0.002	0.02004	0.790353	0.030073	8	1.1	50.8
0.002021	0.002	0.002	0.003911	0.11241	0.50859	0.030073	8	22.4	70.6
0.002576	0.00256	0.002105	0.002363	0.07082	0.585533	0.1643	9	55.5	88.7
0.002361	0.002199	0.002225	0.002048	0.11899	0.797273	0.077548	11	65.7	97.6
0.002344	0.002199	0.002225	0.002095	0.13619	0.797273	0.075551	13	79.5	112.1
0.002746	0.00336	0.002489	0.002039	0.10269	0.607962	0.095827	14	105.7	123.3
0.00273	0.003099	0.002476	0.002829	0.10102	0.762048	0.095227	16	107.4	136.8
0.002888	0.003555	0.002376	0.003031	0.10855	0.808578	0.104409	16	133.2	150.6
0.003635	0.004413	0.002957	0.003223	0.10737	0.646734	0.120476	14	156.8	169.5
0.00357	0.003664	0.003119	0.002265	0.11708	0.787846	0.101781	17	162.9	179.9
0.004525	0.004892	0.002814	0.004488	0.11601	0.907406	0.107527	13	176.2	194.2
0.004722	0.005128	0.003078	0.004703	0.12058	0.939904	0.101795	13	183.0	207.2
0.004888	0.005259	0.003217	0.005013	0.12295	0.986197	0.108146	13	192.3	222.0
0.005317	0.005598	0.003574	0.005814	0.13317	0.95542	0.124536	12	200.9	246.8
0.005613	0.005783	0.003823	0.00637	0.13187	0.908646	0.135815	12	208.7	264.2
0.005551	0.006583	0.003916	0.006701	0.13202	0.797789	0.15684	12	209.9	280.2
0.006464	0.006284	0.004539	0.007973	0.13891	0.736697	0.168275	10	213.4	286.2
0.007056	0.008373	0.004824	0.005902	0.14448	0.789845	0.187182	9	214.9	301.6
0.006898	0.008094	0.00471	0.008624	0.14585	0.780118	0.1798	9	220.1	314.8
0.007145	0.008396	0.004837	0.008898	0.14606	0.791329	0.188227	9	221.6	330.4
0.007683	0.009657	0.005222	0.00922	0.1495	0.755312	0.21174	8	223.3	348.3
0.007683	0.010052	0.005222	0.00922	0.1495	0.755312	0.214374	8	223.5	353.9
0.008459	0.010835	0.00574	0.010916	0.14966	0.866816	0.218334	7	225.9	380.5
0.008431	0.010788	0.00572	0.010868	0.14941	0.86605	0.254779	7	227.5	398.4
0.007816	0.010479	0.005503	0.01021	0.14958	0.995157	0.23346	8	228.2	411.5
0.008107	0.011605	0.006086	0.011609	0.14974	0.866747	0.268269	7	228.8	425.6
0.007964	0.011397	0.005817	0.011314	0.14967	0.876313	0.257668	8	228.9	443.2
0.007699	0.012497	0.006487	0.012414	0.14984	0.866668	0.279202	7	229.8	454.3
0.007706	0.013717	0.007031	0.013785	0.14998	0.917615	0.308167	6	230.9	474.4
0.007707	0.013903	0.007113	0.013994	0.15	0.944715	0.312576	6	231.4	487.6
0.008928	0.013695	0.007113	0.01399	0.14996	0.984103	0.327957	6	232.2	514.6
0.010219	0.013795	0.007127	0.013991	0.14998	0.986264	0.330297	6	232.3	529.7
0.010846	0.013992	0.007166	0.013997	0.15	0.993327	0.342666	6	232.5	547.9
0.012272	0.014	0.007202	0.013998	0.15	0.999113	0.348272	6	232.6	565.2
0.009657	0.013983	0.007177	0.013996	0.14999	0.99849	0.337706	7	232.8	589.2
0.010628	0.013879	0.007173	0.014	0.14998	0.993571	0.344069	7	232.8	597.9
0.012763	0.013998	0.007174	0.013996	0.15	0.999992	0.345365	7	233.0	615.4
0.011118	0.0139	0.007175	0.013989	0.14998	0.997799	0.340524	8	233.0	650.2
0.011738	0.014	0.007212	0.013999	0.15	0.999755	0.344903	8	233.1	659.6

Main Vehicle Deck Optimization: 1.2m Extruded Stiffener Panels

Bottom Plate Thickness	Web Plate Thickness	Web Plate Height	Flange Thickness	Flange Width	Number of Stiffeners	Allowable Lateral Pressure	Panel Weight
meters	meters	meters	meters	meters	--	Mpa	kg
0.002013	0.002001	0.109816	0.002	0.017133	7	0.000	27.8
0.002447	0.002059	0.062701	0.002012	0.017846	14	0.020	34.2
0.002612	0.002352	0.057573	0.003106	0.021175	20	0.044	41.6
0.003421	0.002466	0.051465	0.003135	0.020739	22	0.047	51.1
0.003279	0.002216	0.101093	0.002319	0.021588	22	0.083	55.4
0.003422	0.002067	0.102546	0.003734	0.026005	22	0.090	59.5
0.004014	0.002701	0.109892	0.003126	0.023371	19	0.094	66.7
0.004208	0.002119	0.127038	0.002276	0.020739	22	0.136	68.6
0.005046	0.002684	0.106508	0.003086	0.031779	22	0.193	82.5
0.005046	0.003913	0.103785	0.002607	0.031779	22	0.196	90.0
0.005457	0.003046	0.109538	0.003846	0.040593	22	0.229	94.6
0.005705	0.003186	0.109116	0.003106	0.053126	21	0.229	97.3
0.006185	0.003347	0.106507	0.003267	0.058317	22	0.294	106.6
0.006281	0.003774	0.115631	0.003267	0.058317	22	0.303	113.4
0.006924	0.00363	0.112866	0.004309	0.045194	22	0.353	118.8
0.007119	0.004175	0.144008	0.003763	0.030761	22	0.390	129.0
0.007825	0.004034	0.137751	0.004722	0.044913	21	0.431	137.8
0.008038	0.004108	0.138776	0.004821	0.045932	22	0.497	144.3
0.008208	0.004207	0.141798	0.004934	0.046562	22	0.518	148.7
0.008849	0.00444	0.123586	0.006192	0.048243	22	0.560	157.2
0.009303	0.004857	0.128019	0.005907	0.050525	22	0.607	167.3
0.009225	0.005018	0.146313	0.005904	0.042579	22	0.655	171.1
0.009668	0.005244	0.146862	0.006268	0.044156	22	0.719	180.3
0.009989	0.005519	0.149132	0.006523	0.045017	22	0.767	188.8
0.010448	0.005278	0.140812	0.006425	0.061714	22	0.840	195.5
0.01085	0.005745	0.141869	0.006685	0.056351	22	0.856	203.6
0.010901	0.005782	0.128856	0.007771	0.070969	22	0.914	211.6
0.01135	0.005922	0.133275	0.007052	0.074504	22	0.989	217.8
0.011592	0.005922	0.133275	0.007778	0.074504	22	1.033	224.3
0.012393	0.006198	0.145662	0.006962	0.068931	22	1.068	234.1
0.012169	0.006221	0.130786	0.00731	0.094686	22	1.139	240.4
0.012304	0.007029	0.138652	0.008249	0.069579	22	1.158	244.9
0.012842	0.006513	0.145097	0.007116	0.08395	22	1.245	250.4
0.012816	0.006654	0.139414	0.007553	0.097574	22	1.263	258.8
0.013195	0.006899	0.149444	0.007289	0.086968	22	1.339	263.0
0.013657	0.007003	0.149958	0.007357	0.087825	22	1.402	270.2
0.013736	0.007037	0.148373	0.008333	0.090566	22	1.451	278.4
0.013998	0.007195	0.136821	0.00892	0.095739	22	1.507	284.1
0.013998	0.007195	0.136821	0.010215	0.095739	22	1.507	293.0
0.014	0.009085	0.136117	0.01039	0.078812	22	1.507	299.6

Main Vehicle Deck Optimization: 2.4m Extruded Stiffener Panels

Bottom Plate Thickness	Web Plate Thickness	Web Plate Height	Flange Thickness	Flange Width	Number of Stiffeners	Allowable Lateral Pressure	Panel Weight
meters	meters	meters	meters	meters	--	MPa	kg
0.002107	0.002	0.149951	0.002066	0.015742	8	0.002	63.3
0.002107	0.002	0.149951	0.002006	0.015742	15	0.017	78.3
0.003025	0.002226	0.14588	0.002251	0.042466	13	0.026	101.6
0.002412	0.002226	0.088907	0.002539	0.088982	22	0.045	113.2
0.003025	0.002226	0.14588	0.002251	0.080389	19	0.053	128.4
0.003025	0.00208	0.145811	0.002377	0.068735	22	0.070	132.7
0.004743	0.00254	0.149515	0.002884	0.040062	21	0.079	171.1
0.004655	0.002523	0.148007	0.00272	0.065322	22	0.097	180.4
0.004743	0.00254	0.14794	0.003032	0.096132	22	0.109	198.9
0.005232	0.00323	0.14813	0.003416	0.067454	22	0.130	215.5
0.005841	0.003101	0.149548	0.005174	0.071519	19	0.154	230.4
0.005841	0.003101	0.149548	0.005174	0.071519	21	0.171	241.2
0.006352	0.003508	0.139254	0.005613	0.075179	21	0.179	262.8
0.006444	0.003355	0.148881	0.005675	0.080521	21	0.204	271.1
0.006743	0.00382	0.149741	0.005948	0.077981	22	0.223	295.1
0.007264	0.003749	0.149335	0.007022	0.081862	21	0.250	313.3
0.007497	0.004396	0.14979	0.008592	0.072711	20	0.262	330.3
0.007478	0.004837	0.149821	0.008713	0.077535	21	0.273	354.1
0.008405	0.00475	0.149709	0.008337	0.085268	20	0.295	368.1
0.008989	0.004943	0.149917	0.00921	0.096016	18	0.317	386.2
0.009866	0.005599	0.14942	0.009513	0.092448	18	0.331	415.9
0.009866	0.005599	0.14942	0.009513	0.092448	19	0.342	427.1
0.010238	0.005928	0.149824	0.010598	0.095096	18	0.359	445.0
0.010313	0.006507	0.149922	0.010908	0.099723	17	0.365	452.8
0.011412	0.006493	0.14963	0.012327	0.098493	17	0.399	490.3
0.011731	0.006646	0.149905	0.012692	0.098535	17	0.409	504.1
0.01214	0.006953	0.149745	0.013684	0.09964	16	0.424	514.8
0.012621	0.007067	0.149932	0.013867	0.099894	16	0.437	529.5
0.012848	0.007067	0.149932	0.013867	0.099931	16	0.441	534.5
0.013829	0.007725	0.149984	0.013999	0.099967	16	0.462	567.7
0.013829	0.007725	0.149997	0.014	0.099967	16	0.462	567.7
0.013829	0.009414	0.149984	0.014	0.09997	16	0.466	593.9
0.013842	0.009756	0.15	0.014	0.099972	16	0.467	599.5
0.013942	0.011877	0.149994	0.014	0.099924	15	0.472	614.0
0.01393	0.012546	0.149997	0.014	0.099997	16	0.476	644.9
0.014	0.014	0.15	0.014	0.099901	15	0.479	646.2
0.01393	0.013498	0.149993	0.014	0.099985	17	0.479	681.9
0.013999	0.014	0.15	0.014	0.09988	17	0.482	691.5
0.014	0.013967	0.15	0.014	0.099901	18	0.482	713.7
0.014	0.013967	0.15	0.014	0.099993	18	0.482	713.8

Main Vehicle Deck Optimization: 1.2m Sandwich Panels

Top Plate Thickness	Bottom Plate Thickness	Web Plate Thickness	Web Plate Height	Number of Webs	Allowable Lateral Pressure	Panel Weight
meters	meters	meters	meters	--	MPa	kg
0.002001	0.002	0.002003	0.015001	35	0.000	47.2
0.002025	0.002191	0.002013	0.037966	64	0.074	62.0
0.002004	0.002022	0.002009	0.077779	59	0.158	73.9
0.002082	0.002341	0.002057	0.14782	52	0.224	99.6
0.002198	0.004039	0.002415	0.101598	51	0.450	108.7
0.002427	0.003133	0.002309	0.133912	68	0.598	128.9
0.003245	0.00382	0.002375	0.148792	59	0.764	144.8
0.00426	0.004615	0.002424	0.14716	58	0.947	164.1
0.003828	0.00679	0.003631	0.138792	40	1.050	181.4
0.004102	0.006424	0.004049	0.147108	46	1.241	203.9
0.004102	0.006424	0.004049	0.147229	57	1.312	225.2
0.005971	0.006424	0.003462	0.148705	57	1.364	230.6
0.006861	0.007547	0.004246	0.147002	48	1.559	254.6
0.00595	0.009012	0.005007	0.149679	47	1.645	277.7
0.007395	0.011014	0.005861	0.143771	36	1.804	299.6
0.007167	0.012561	0.006953	0.147645	30	1.868	315.5
0.010717	0.011101	0.005575	0.149085	33	1.979	327.4
0.010879	0.010268	0.005841	0.149673	45	2.011	358.7
0.008913	0.013993	0.008285	0.149999	27	2.171	359.2
0.009197	0.013825	0.008021	0.14999	33	2.295	380.4
0.011351	0.01389	0.007241	0.149999	33	2.361	392.1
0.012121	0.013971	0.007905	0.149996	33	2.420	412.1
0.012642	0.013986	0.008736	0.149998	33	2.470	431.3
0.011616	0.013995	0.010344	0.149998	33	2.491	445.9
0.013934	0.013996	0.00754	0.149994	44	2.563	466.6
0.011527	0.013986	0.013022	0.149998	33	2.607	487.8
0.012107	0.013979	0.013355	0.149998	33	2.644	499.4
0.013994	0.013659	0.013416	0.149999	33	2.672	517.5
0.013806	0.013984	0.009916	0.15	48	2.689	535.2
0.011351	0.013996	0.012539	0.149999	44	2.726	545.3
0.01398	0.013963	0.012253	0.149999	44	2.832	567.6
0.01398	0.013996	0.013287	0.149999	44	2.888	590.1
0.013993	0.013997	0.013287	0.149999	47	2.907	609.6
0.014	0.013957	0.00965	0.149998	69	2.955	629.3
0.013948	0.010477	0.01376	0.149982	57	3.045	648.2
0.013998	0.010362	0.012453	0.15	67	3.096	671.9
0.013989	0.014	0.013484	0.149999	59	3.098	692.7
0.013266	0.010662	0.01368	0.149972	68	3.215	713.7
0.013983	0.010501	0.013818	0.149965	69	3.261	731.0
0.013999	0.011237	0.013977	0.15	70	3.383	751.4

Main Vehicle Deck Optimization: 2.4m Sandwich Panels

Top Plate Thickness	Bottom Plate Thickness	Web Plate Thickness	Web Plate Height	Number of Webs	Allowable Lateral Pressure	Panel Weight
meters	meters	meters	meters	--	MPa	kg
0.002	0.002	0.002	0.028805	25	0.000	96.8
0.002	0.002001	0.002	0.125662	25	0.031	128.2
0.003506	0.002182	0.002371	0.084619	32	0.075	166.0
0.002628	0.004126	0.002167	0.147128	28	0.119	205.5
0.002628	0.004126	0.002278	0.137387	48	0.157	245.0
0.004213	0.005363	0.003216	0.14327	24	0.187	281.1
0.004183	0.005737	0.003175	0.145444	33	0.248	315.7
0.00525	0.006963	0.003916	0.149949	24	0.302	358.4
0.005711	0.007595	0.004643	0.149919	23	0.335	394.7
0.00597	0.008697	0.005448	0.149921	22	0.352	437.2
0.006365	0.008867	0.006112	0.149803	22	0.364	463.6
0.007011	0.009855	0.005882	0.149942	22	0.399	494.6
0.007312	0.010109	0.006759	0.149827	23	0.413	531.9
0.007773	0.010522	0.006721	0.149936	26	0.425	569.9
0.009099	0.010835	0.008082	0.14994	22	0.456	608.7
0.007426	0.013958	0.008193	0.149992	23	0.508	650.8
0.011185	0.012213	0.00861	0.149962	22	0.509	695.8
0.009103	0.013817	0.009188	0.149976	22	0.531	697.7
0.010377	0.01371	0.009944	0.149965	22	0.545	739.4
0.013043	0.01344	0.009081	0.149977	22	0.556	773.3
0.01365	0.013944	0.009679	0.149968	22	0.576	810.4
0.013972	0.013991	0.011321	0.149999	22	0.589	853.6
0.013972	0.013991	0.012721	0.149999	22	0.598	883.6
0.013947	0.013988	0.013999	0.149999	22	0.605	910.3
0.013925	0.013425	0.007077	0.149753	59	0.613	1003.3
0.013955	0.013297	0.013779	0.14999	33	0.630	1038.0
0.012263	0.01396	0.011642	0.149986	44	0.645	1071.4
0.012263	0.01396	0.012727	0.149986	44	0.656	1117.7
0.013916	0.013451	0.01236	0.149978	46	0.664	1151.1
0.013916	0.013898	0.01236	0.149978	46	0.666	1160.8
0.013832	0.010535	0.01209	0.14999	57	0.689	1202.7
0.013951	0.010491	0.013039	0.149984	56	0.700	1244.2
0.013947	0.01023	0.013244	0.149937	58	0.702	1275.1
0.013832	0.010535	0.013674	0.14999	57	0.714	1290.5
0.013847	0.0137	0.013183	0.149979	58	0.716	1345.6
0.013772	0.010665	0.012767	0.14999	68	0.741	1378.2
0.013985	0.01102	0.013055	0.14996	69	0.763	1422.2
0.013832	0.011295	0.013829	0.149899	68	0.779	1462.9
0.014	0.011279	0.013999	0.15	70	0.792	1505.3
0.014	0.011279	0.013999	0.15	70	0.792	1505.3

Main Vehicle Deck Optimization: 1.2m Hat Stiffener Panels

Note: For plate element dimensions, please refer to Figure 46 in the main body of the report.

Plate Element 1 Thickness	Plate Element 2 Thickness	Plate Elements 3 & 4 Thickness	Plate Element 5 Thickness	Hat Height	Ratio of Plate Element 5 to Element 2 Width	Plate Element 2 Width	Number of Stiffeners	Allowable Lateral Load	Panel Weight
meters	meters	meters	meters	meters	--	meters	--	MPa	kg
0.002	0.002004	0.002002	0.002733	0.021344	0.510866	0.052057	13	0.001	29.1
0.002618	0.002947	0.002355	0.003428	0.038297	0.563032	0.060068	14	0.040	43.4
0.003384	0.003356	0.003145	0.005156	0.054349	0.625035	0.072919	21	0.158	76.8
0.003384	0.004402	0.003145	0.005156	0.054349	0.625035	0.072919	21	0.162	82.0
0.003707	0.003759	0.003064	0.005188	0.075938	0.754334	0.078401	21	0.285	93.6
0.00444	0.004118	0.003216	0.005571	0.100446	0.781613	0.074956	19	0.343	107.1
0.005216	0.003651	0.002923	0.004023	0.136895	0.837193	0.070655	20	0.516	117.2
0.005504	0.003681	0.003037	0.004352	0.148496	0.890127	0.078093	21	0.690	132.5
0.00555	0.003972	0.003149	0.005391	0.148095	0.945589	0.080271	21	0.770	143.4
0.005764	0.005314	0.003666	0.006898	0.146243	0.721394	0.09033	20	0.870	159.3
0.005756	0.005453	0.003715	0.006427	0.148117	0.931591	0.089514	20	0.964	167.2
0.006021	0.007225	0.003678	0.005986	0.149697	0.873663	0.100482	20	1.018	179.2
0.005983	0.007041	0.004436	0.006409	0.149689	0.870246	0.09948	20	1.104	194.3
0.00628	0.007931	0.005019	0.008882	0.143193	0.732546	0.112353	19	1.222	214.1
0.006192	0.00858	0.004909	0.008612	0.148163	0.902043	0.109025	19	1.387	225.5
0.006302	0.008574	0.004458	0.007572	0.149758	0.898811	0.107837	22	1.413	233.9
0.006419	0.009316	0.005214	0.009194	0.14751	0.951093	0.119733	19	1.645	250.7
0.006857	0.01147	0.005739	0.010656	0.146819	0.84228	0.121076	18	1.672	269.4
0.007206	0.011109	0.006176	0.011731	0.149014	0.908711	0.126357	17	1.851	281.6
0.007325	0.011461	0.006362	0.011987	0.149072	0.952832	0.128842	17	2.023	295.0
0.007397	0.01265	0.006456	0.012176	0.149999	0.955894	0.133375	17	2.155	311.7
0.006772	0.012327	0.006572	0.012435	0.14999	0.957714	0.134096	18	2.208	325.6
0.007414	0.012731	0.006572	0.012435	0.14999	0.957714	0.134096	18	2.277	330.8
0.007646	0.013796	0.006982	0.01356	0.149883	0.926431	0.138639	17	2.389	341.8
0.008043	0.013576	0.007482	0.013527	0.149424	0.980259	0.143785	17	2.458	359.9
0.007923	0.013992	0.00744	0.013338	0.149525	0.97262	0.142019	18	2.547	374.1
0.007621	0.013727	0.007333	0.012863	0.14978	0.95338	0.13757	20	2.590	389.5
0.007538	0.013803	0.007788	0.012541	0.1495	0.919018	0.135586	21	2.636	405.1
0.007564	0.013841	0.007915	0.012605	0.149539	0.892873	0.136963	21	2.650	407.3
0.007431	0.013999	0.007595	0.013952	0.149999	0.999958	0.13742	21	2.764	428.1
0.007442	0.013852	0.008414	0.013879	0.149773	0.994173	0.139082	21	2.787	444.1
0.007444	0.01393	0.008543	0.01398	0.149757	0.996734	0.139432	21	2.811	449.2
0.007585	0.013992	0.009854	0.013928	0.149478	0.992189	0.137407	21	2.854	472.5
0.007585	0.013992	0.010607	0.013928	0.149478	0.994648	0.137407	21	2.889	488.1
0.007431	0.013999	0.010915	0.013969	0.15	0.999764	0.13742	21	2.918	496.1
0.007457	0.013975	0.011699	0.01392	0.149987	0.991086	0.137565	21	2.946	510.5
0.007431	0.013999	0.012333	0.013968	0.149999	0.999778	0.13742	21	2.983	525.0
0.007465	0.013968	0.012892	0.013919	0.149981	0.997985	0.137612	21	3.004	535.7
0.007435	0.013826	0.013294	0.013893	0.149728	0.999467	0.138923	21	3.011	543.8
0.007431	0.014	0.014	0.013986	0.15	0.999884	0.13742	21	3.062	559.2

Main Vehicle Deck Optimization: 2.4m Hat Stiffener Panels

Note: For plate element dimensions, please refer to Figure 46 in the main body of the report.

Plate Element 1 Thickness	Plate Element 2 Thickness	Plate Elements 3 & 4 Thickness	Plate Element 5 Thickness	Hat Height	Ratio of Plate Element 5 to Element 2 Width	Plate Element 2 Width	Number of Stiffeners	Allowable Lateral Load	Panel Weight
meters	meters	meters	meters	meters	--	meters	--	MPa	kg
0.002291	0.002722	0.002035	0.00375	0.061533	0.894423	0.043654	9	0.000	74.4
0.0023	0.002734	0.002043	0.00376	0.078784	0.875736	0.043915	13	0.022	91.2
0.002309	0.002746	0.00205	0.003769	0.095436	0.857699	0.044166	17	0.042	111.5
0.003222	0.003756	0.002451	0.00437	0.094949	0.664511	0.084065	12	0.048	129.5
0.002644	0.003215	0.00229	0.004188	0.098214	0.87885	0.053095	17	0.056	132.3
0.003197	0.004339	0.002536	0.002725	0.142632	0.94656	0.073417	14	0.069	160.4
0.003945	0.00359	0.002802	0.002616	0.148037	0.84805	0.104833	14	0.088	179.4
0.00402	0.003783	0.002865	0.002906	0.14892	0.835399	0.108488	14	0.101	187.0
0.00402	0.003783	0.002865	0.005138	0.14892	0.560228	0.108488	16	0.118	207.2
0.004605	0.005278	0.00288	0.004777	0.144195	0.954007	0.117831	13	0.144	222.6
0.005582	0.006373	0.003496	0.005933	0.136345	0.843618	0.186882	9	0.154	241.2
0.005141	0.005636	0.003011	0.005558	0.147914	0.948288	0.134731	13	0.196	252.9
0.005136	0.006656	0.003797	0.007239	0.149898	0.646502	0.163071	12	0.206	281.1
0.005652	0.006858	0.003898	0.006594	0.147042	0.816191	0.156271	12	0.218	293.2
0.005528	0.006561	0.003683	0.006342	0.146494	0.958248	0.151035	13	0.237	302.3
0.006192	0.007948	0.004507	0.007471	0.147042	0.98975	0.172129	10	0.261	323.4
0.006564	0.008181	0.004172	0.007648	0.146294	0.979031	0.170125	11	0.279	341.0
0.006062	0.007839	0.004611	0.007426	0.148849	0.988041	0.168196	12	0.298	358.5
0.006134	0.008173	0.004739	0.007822	0.149005	0.973285	0.177822	12	0.311	377.5
0.006256	0.009357	0.005178	0.009264	0.149645	0.959039	0.191291	10	0.341	385.8
0.008576	0.009572	0.005276	0.009481	0.149661	0.958038	0.195626	10	0.357	417.7
0.008364	0.010464	0.005907	0.011398	0.148714	0.970584	0.214894	9	0.411	450.4
0.007878	0.010786	0.006061	0.010616	0.148388	0.990187	0.210305	10	0.421	471.7
0.008505	0.01064	0.005644	0.010061	0.147447	0.940653	0.21149	11	0.423	479.6
0.007856	0.01139	0.006685	0.011435	0.147824	0.959175	0.240456	9	0.430	490.5
0.009329	0.011657	0.006343	0.011477	0.148861	0.995337	0.241199	9	0.463	507.6
0.008696	0.011549	0.0073	0.011392	0.148771	0.962786	0.227991	10	0.466	535.2
0.010231	0.012234	0.006493	0.01218	0.149861	0.963834	0.249404	9	0.500	537.2
0.010566	0.01293	0.007083	0.012929	0.149971	0.94802	0.254278	9	0.532	571.9
0.010928	0.01374	0.007841	0.013626	0.149986	0.988663	0.267614	8	0.555	586.8
0.011105	0.013856	0.007672	0.0138	0.149996	0.997679	0.27578	8	0.565	598.4
0.010174	0.01398	0.007492	0.013985	0.15	0.866071	0.284455	9	0.571	618.7
0.01131	0.01397	0.007286	0.013938	0.149992	0.937532	0.284455	9	0.584	635.9
0.011294	0.01398	0.007492	0.013985	0.15	0.998835	0.284455	9	0.590	654.4
0.011309	0.013984	0.011256	0.013871	0.149992	0.8753	0.284455	9	0.592	691.4
0.01129	0.013955	0.011133	0.013906	0.149997	0.995846	0.284288	9	0.601	715.5
0.011287	0.013944	0.012935	0.013881	0.149989	0.97441	0.284376	9	0.605	741.6
0.01131	0.013975	0.012966	0.013914	0.149992	0.974833	0.284455	9	0.607	743.5
0.011275	0.013913	0.013819	0.013903	0.15	0.997535	0.283683	9	0.609	761.5
0.011294	0.013939	0.013996	0.013979	0.15	0.998835	0.284455	9	0.612	767.4

Main Vehicle Deck Optimization: 2.4m Extruded Stiffener Panels, Maximum Thickness 6mm

Bottom Plate Thickness	Web Plate Thickness	Web Plate Height	Flange Thickness	Flange Width	Number of Stiffeners	Allowable Lateral Pressure	Panel Weight
meters	meters	meters	meters	meters	--	Mpa	kg
0.002026	0.002178	0.043327	0.002469	0.021989	15	0.000	58.8
0.002026	0.002098	0.082148	0.002469	0.013881	15	0.012	64.4
0.002026	0.002061	0.067865	0.002469	0.056034	15	0.015	71.3
0.00229	0.002405	0.088591	0.002804	0.022059	16	0.020	78.6
0.002127	0.002061	0.102604	0.002183	0.034549	21	0.032	85.5
0.002224	0.002057	0.102172	0.002523	0.034987	21	0.035	89.3
0.002268	0.00205	0.106538	0.002535	0.039589	22	0.040	95.0
0.002332	0.002102	0.107284	0.002594	0.040489	22	0.042	98.1
0.002587	0.002191	0.118065	0.002322	0.04224	22	0.048	107.4
0.002738	0.002025	0.133194	0.002713	0.040914	22	0.058	114.2
0.00296	0.002059	0.13651	0.002116	0.052859	22	0.063	120.7
0.003022	0.00236	0.140923	0.002082	0.055567	22	0.070	130.0
0.004412	0.002369	0.146867	0.002217	0.049645	22	0.075	161.8
0.004491	0.002371	0.147991	0.002686	0.051268	22	0.082	167.9
0.004606	0.002374	0.149602	0.003357	0.053595	22	0.094	177.0
0.004774	0.002534	0.148979	0.00296	0.065077	22	0.105	185.7
0.004906	0.002562	0.149407	0.003374	0.072596	21	0.110	192.7
0.004892	0.00258	0.149517	0.003171	0.089256	22	0.119	202.3
0.00534	0.002907	0.149825	0.004346	0.053016	22	0.128	211.7
0.005406	0.002782	0.149066	0.004091	0.07136	22	0.147	219.0
0.005622	0.00303	0.149611	0.00478	0.068831	21	0.157	229.4
0.005974	0.003037	0.149976	0.005926	0.058692	20	0.158	234.8
0.006	0.003076	0.149998	0.005938	0.069736	19	0.166	239.0
0.005748	0.003176	0.146171	0.005578	0.065735	22	0.171	244.2
0.005841	0.003325	0.149833	0.005424	0.068504	22	0.181	251.7
0.006	0.003076	0.149998	0.005938	0.069736	22	0.189	256.0
0.005993	0.003531	0.149989	0.005872	0.068276	22	0.191	263.7
0.006	0.003434	0.15	0.005898	0.07884	22	0.195	270.9
0.005999	0.003699	0.149998	0.005971	0.077494	22	0.196	276.3
0.005999	0.003706	0.149999	0.005982	0.080892	22	0.197	279.4
0.006	0.003588	0.15	0.006	0.09243	22	0.200	287.0
0.005992	0.003749	0.149999	0.005922	0.099169	22	0.202	294.9
0.005997	0.004523	0.149996	0.005997	0.087056	22	0.204	302.3
0.005985	0.00482	0.149987	0.005927	0.090373	22	0.205	310.3
0.005998	0.004981	0.149997	0.005998	0.091067	22	0.207	315.5
0.006	0.004956	0.15	0.005999	0.099644	22	0.210	322.4
0.006	0.005231	0.15	0.006	0.099999	22	0.211	328.6
0.005999	0.005698	0.15	0.005692	0.099976	22	0.212	334.2
0.005999	0.005698	0.15	0.005992	0.099917	22	0.214	338.4
0.006	0.005999	0.15	0.006	0.1	22	0.215	345.0

Main Vehicle Deck Optimization: 2.4m Sandwich Panels, Maximum Thickness 5mm

Top Plate Thickness	Bottom Plate Thickness	Web Plate Thickness	Web Plate Height	Number of Webs	Allowable Lateral Pressure	Panel Weight
meters	meters	meters	meters	--	MPa	kg
0.002	0.002	0.002	0.040464	19	0.002	97.4
0.002	0.002	0.002	0.040464	19	0.002	97.4
0.005	0.005	0.005	0.15	70	0.317	558.9
0.004894	0.00499	0.004699	0.149964	67	0.306	522.1
0.004791	0.005	0.004865	0.149999	69	0.311	540.4
0.002882	0.004902	0.002888	0.149631	38	0.210	276.6
0.004479	0.004985	0.004246	0.149963	52	0.273	421.5
0.003378	0.004955	0.002923	0.149831	39	0.220	292.9
0.002002	0.00367	0.002024	0.107633	34	0.078	172.0
0.004823	0.004993	0.004571	0.149978	62	0.296	490.1
0.002038	0.003897	0.002068	0.11378	34	0.094	181.6
0.004646	0.004989	0.002821	0.149953	44	0.236	331.3
0.002934	0.004902	0.002489	0.149631	38	0.200	263.1
0.004705	0.004976	0.003715	0.149914	52	0.266	399.4
0.002	0.002226	0.002225	0.048799	23	0.013	108.6
0.002384	0.004237	0.002295	0.13805	36	0.145	218.7
0.002233	0.004175	0.002282	0.128324	36	0.130	208.4
0.004915	0.005	0.004662	0.149991	47	0.277	429.8
0.002083	0.002407	0.002146	0.061658	25	0.024	119.6
0.00285	0.004569	0.002547	0.145662	37	0.182	251.2
0.002416	0.004588	0.002509	0.14649	38	0.179	243.7
0.002281	0.002085	0.002434	0.106289	34	0.077	152.5
0.004375	0.004975	0.004332	0.149965	43	0.260	385.5
0.004968	0.004994	0.004535	0.149982	65	0.301	504.4
0.004724	0.004998	0.004392	0.149998	54	0.282	443.2
0.003356	0.004974	0.003119	0.149917	41	0.228	306.4
0.004995	0.004998	0.004934	0.149995	70	0.316	554.3
0.002168	0.002159	0.002459	0.094224	31	0.059	141.2
0.003962	0.004971	0.003491	0.149902	45	0.246	348.0
0.004795	0.004995	0.00452	0.149984	59	0.291	473.3
0.003816	0.004962	0.003834	0.149913	45	0.249	359.6
0.0022	0.002083	0.002186	0.075234	32	0.038	127.8
0.004985	0.004998	0.004673	0.149978	53	0.287	459.0
0.003988	0.004952	0.003827	0.149974	46	0.252	366.6
0.002094	0.004016	0.002009	0.139687	35	0.124	197.3
0.002267	0.004379	0.00241	0.148781	37	0.168	231.3
0.002028	0.002147	0.002051	0.109396	30	0.045	134.9
0.004283	0.004997	0.004556	0.14998	61	0.289	473.1
0.002267	0.004379	0.00241	0.14574	37	0.165	229.6
0.002094	0.004016	0.002009	0.139687	35	0.124	197.3

Main Vehicle Deck Optimization: 2.4m Hat Stiffener Panels, Maximum Thickness 6mm

Note: For plate element dimensions, please refer to Figure 46 in the main body of the report.

Plate Element 1 Thickness	Plate Element 2 Thickness	Plate Elements 3 & 4 Thickness	Plate Element 5 Thickness	Hat Height	Ratio of Plate Element 5 to Element 2 Width	Plate Element 2 Width	Number of Stiffeners	Allowable Lateral Load	Panel Weight
meters	meters	meters	meters	meters	--	meters	--	MPa	kg
0.002001	0.002006	0.002	0.002003	0.049155	0.500146	0.030232	13	0.000	63.1
0.002001	0.002006	0.002	0.002003	0.049155	0.500146	0.030399	13	0.000	63.1
0.002001	0.002452	0.002	0.002003	0.049155	0.500146	0.188027	10	0.012	79.1
0.002102	0.002002	0.00201	0.003636	0.057567	0.506827	0.092917	13	0.020	80.6
0.002615	0.002009	0.002054	0.002635	0.103864	0.556763	0.096912	12	0.036	97.6
0.002772	0.002015	0.002075	0.002556	0.113527	0.552775	0.131776	12	0.047	105.2
0.002528	0.002162	0.002256	0.003706	0.11568	0.761983	0.130175	12	0.054	121.1
0.002882	0.002014	0.00226	0.003688	0.113527	0.748279	0.131776	12	0.072	122.7
0.003667	0.003566	0.002	0.002592	0.114841	0.894628	0.095962	17	0.074	154.3
0.003708	0.003643	0.002021	0.002652	0.124818	0.89403	0.097169	17	0.084	161.4
0.003774	0.003769	0.002054	0.00275	0.141218	0.893047	0.099154	18	0.102	178.6
0.004037	0.004269	0.002187	0.003139	0.146586	0.889169	0.106984	16	0.119	188.3
0.00404	0.004281	0.002199	0.003972	0.146684	0.959307	0.10711	16	0.131	200.2
0.00404	0.004281	0.002199	0.003972	0.146684	0.959307	0.10711	17	0.133	207.2
0.004118	0.004604	0.002355	0.004355	0.147481	0.955584	0.109444	16	0.150	214.8
0.004287	0.004858	0.002569	0.004621	0.148106	0.964675	0.109638	16	0.169	229.8
0.004302	0.005451	0.002744	0.005072	0.149616	0.943314	0.115917	15	0.179	240.8
0.004625	0.005412	0.002984	0.005165	0.148679	0.985295	0.110546	15	0.189	250.5
0.004674	0.005462	0.003182	0.004711	0.148783	0.982171	0.110154	16	0.191	262.2
0.004493	0.005107	0.003317	0.004921	0.148572	0.972381	0.11	17	0.201	272.3
0.004672	0.005902	0.003059	0.005227	0.1498	0.985466	0.11008	17	0.216	280.5
0.004744	0.005537	0.003387	0.005807	0.148926	0.986836	0.106347	17	0.228	291.3
0.004921	0.005874	0.003475	0.00565	0.149968	0.988894	0.107653	18	0.243	311.3
0.005055	0.005894	0.003408	0.005805	0.149962	0.989895	0.105666	19	0.252	322.1
0.00516	0.005991	0.003414	0.005996	0.149956	0.990537	0.103728	20	0.261	336.6
0.005135	0.005927	0.003893	0.005995	0.149863	0.996455	0.098999	20	0.263	350.3
0.005086	0.005905	0.003755	0.005874	0.149819	0.987888	0.109531	21	0.265	363.0
0.005152	0.005993	0.00385	0.005968	0.149978	0.990092	0.109537	21	0.271	370.5
0.005082	0.005964	0.004145	0.005974	0.149763	0.989549	0.106922	21	0.272	378.9
0.005101	0.005968	0.004371	0.005982	0.149792	0.990825	0.107457	21	0.275	389.1
0.005162	0.005975	0.004802	0.005966	0.149795	0.992255	0.091574	21	0.276	392.6
0.005135	0.005927	0.005313	0.005995	0.149863	0.996455	0.098999	20	0.277	405.5
0.005188	0.005995	0.005002	0.005997	0.149973	0.99419	0.102897	21	0.283	412.4
0.005138	0.005988	0.004775	0.005964	0.149969	0.990486	0.109521	22	0.285	422.1
0.00516	0.005991	0.005228	0.005996	0.14999	0.990537	0.103728	22	0.290	436.5
0.005208	0.005999	0.005843	0.005989	0.149894	0.993413	0.085497	22	0.291	445.8
0.005193	0.005998	0.005797	0.006	0.149975	0.999406	0.093772	22	0.294	452.4
0.005208	0.005999	0.005843	0.005971	0.149894	0.993413	0.10595	22	0.297	465.2
0.005216	0.005999	0.005918	0.005994	0.149964	0.999761	0.104246	22	0.298	467.8
0.005232	0.006	0.006	0.005999	0.15	1	0.1113	22	0.300	478.4

PROJECT TECHNICAL COMMITTEE MEMBERS

The following persons were members of the committee that represented the Ship Structure Committee to the Contractor as resident subject matter experts. As such they performed technical review of the initial proposals to select the contractor, advised the contractor in cognizant matters pertaining to the contract of which the agencies were aware, performed technical review of the work in progress and edited the final report.

Chairman: Paul Cojeen, US Coast Guard

Members
Contracting Officer's Technical Representative:

Marine Board Liaison:

Executive Director Ship Structure Committee: LCDR Jason E. Smith,   US Coast Guard

Pramod Dash	BIT Mesra
William Caliendo	US Merchant Marine Academy
Jeom Paik	Pusan National University
Yoo Sang Choo	National University of Singapore
Roshdy Barsoum	Office of Naval Research
Richard Fonda	Naval Research Lab
Robert Sielski	US Navy (retired)
Dhiren Marjadi	Altair
Debu Ghosh	U.S. Coast Guard Electronic Logistic Center (ELC)
Lothar Birk	University of New Orleans
Chris Barry	US Coast Guard ELC / SNAME
Daniel Woods	Germanischer Lloyd
Rong Huang	Chevron (retired)

RECENT SHIP STRUCTURE COMMITTEE PUBLICATIONS

Ship Structure Committee Publications on the Web - All reports from SSC 1 to current are available to be downloaded from the Ship Structure Committee Web Site at URL:
http://www.shipstructure.org
SSC 445 – SSC 393 are available on the SSC CD-ROM Library. Visit the National Technical Information Service (NTIS) Web Site for ordering hard copies of all SSC research reports at URL: http://www.ntis.gov

SSC Report Number	Report Bibliography
SSC 453	Welding Distortion Analysis Of Hull Blocks Using Equivalent Load Method Based On Inherent Strain, Jang C.D. 2008
SSC 452	Aluminum Structure Design and Fabrication Guide, Sielski R.A. 2007
SSC 451	Mechanical Collapse Testing on Aluminum Stiffened Panels for Marine Applications, Paik J.K. 2007
SSC 450	Ship Structure Committee: Effectiveness Survey, Phillips M.L., Buck R., Jones L.M. 2007
SSC 449	Hydrodynamic Pressures and Impact Loads for High Speed Catamaran / SES, Vorus W. 2007
SSC 448	Fracture Mechanics Characterization of Aluminum Alloys for Marine Structural Applications, Donald J.K., Blair A. 2007
SSC 447	Fatigue and Fracture Behavior of Fusion and Friction Stir Welded Aluminum Components, Kramer R. 2007
SSC 446	Comparative Study of Naval and Commercial Ship Structure Design Standards, Kendrick A., Daley C. 2007
SSC 445	Structural Survivability of Modern Liners, Iversen R. 2005
SSC 444	In-Service Non-Destructive Estimation of the Remaining Fatigue Life of Welded Joints, Dexter R.J., Swanson K.M., Shield C.K. 2005
SSC 443	Design Guidelines for Doubler Plate Repairs on Ship Structures Sensharma P.K., Dinovitzer A., Traynham Y. 2005
SSC 442	Labor-Saving Passive Fire Protection Systems For Aluminum And Composite Construction E. Greene, 2005